GAMMA RAY SPECTROSCOPY STUDIES OF THE EXCITED STATES OF ODD PROTON (ODD MASS) NUCLEI IN THE Z=50-62, *N*=64-82 REGION

By

Dwight Beecher Beery

A THESIS

Submitted to
Michigan State University
in partial fulfillment of the requirements
for the degree of

DOCTOR OF PHILOSOPHY

Department of Physics

1969

ABSTRACT

GAMMA RAY SPECTROSCOPY STUDIES OF THE EXCITED STATES OF ODD PROTON (ODD MASS) NUCLEI IN THE Z=50-62, *N*=64-82 REGION

By

Dwight Beecher Beery

The beta, gamma decay schemes of Nd^{141m+g}, Nd^{139m+g}, Ce^{137m+g}, Ba^{133m}, and Ba^{131m} have been studied in an effort to acquire information about the energy level systematics in this region of the table of nuclides. Ge(Li) singles and Ge(Li)-NaI(Tl) coincidence spectrometers were employed to identify and establish the sequence of many new gamma ray transitions. Some significant additions to and changes from previously proposed schemes are suggested by the data.

Excited levels accommodating 10 gamma rays have been located at 145.4, 1126.8, 1292.5, 1298.4, 1580.0, 1607.9, and 1657.2 keV in Pr^{141} following the decay of 2.6-h Nd^{141g}. States in Pr^{139} at 113.8, 405.0, 589.2, 916.8, 1074.4, 1311.8, 1328.2, 1405.5, 1449.5, and 1501.2 keV are populated by 30 min Nd^{139g}, while the decay of 5.5-h Nd^{139m} populates levels at 113.8, 821.9, 828.1, 851.9, 1024.0, 1369.6, 1523.2, 1624.5, 1834.1, 1927.1, 2048.8, 2174.3, and 2196.7 keV. These two sets of states incorporate 17 and 38 transitions, respectively. The 19 gamma rays seen in the decay of 34.4-h Ce^{137m} in equilibrium with 9.0-h Ce^{137g} depopulate excited states of La^{137} at 10.5, 447.1, 493.1,

709.1, 762.2, 781.5, 835.4, 926.6, 1004.8, and 1171.9 keV. Of these levels, only those at 762.2, 835.4, and 1004.8 keV are populated directly by Ce^{137m} and none of these states is populated by both isomers. Only one state of Cs^{133} was seen to be directly populated by 38.9-h Ba^{133m} and an upper limit of 0.1% of the 14.6-min Ba^{131m} disintegrations is placed on the direct feeding to high spin states of Cs^{131} with energies >60 keV.

Limits on the possible spin assignments of the states investigated have been placed from calculated log *ft* values and from the presence of transitions to states with known spins. A multiplet of six high-spin, odd parity states near 2 MeV in Pr^{139} is interpreted as a set of three-quasiparticle states. The multiplet decay pattern suggests the possibility that information can be extracted from these states that is normally available only for lower-lying levels.

A survey has been made of all of the energy state systematics of the low energy levels of odd proton (odd mass) nuclides in the Z=50-62, N=64-82 region. From these observations, some predictions and suggestions for future experiments have been made. The detailed nature of these and the higher-lying states can only be determined after further experimental data become available.

ACKNOWLEDGEMENTS

I wish to thank Dr. W. H. Kelly for the suggestion of this region of study. His readily available aid and skillful guidance during the experimental work and the preparation of this thesis are sincerely appreciated. I also thank Dr. Wm. C. McHarris for his very significant help with many aspects of these investigations.

Dr. H. G. Blosser, Mr. H. Hilbert, and Dr. W. P. Johnson assisted with the operation of the Michigan State University sector-focused cyclotron. The variable energy and high proton beam flux has facilitated the irradiation of the isotopes used in this thesis project.

Dr. C. R. Gruhn directed the detector development program at Michigan State University. The fabrication of high quality Ge(Li) detectors has been a prerequisite for the sucess of the experiments performed in this study.

Dr. R. L. Auble, Dr. G. Berzins, Dr. L. M. Beyer, Mr. J. Black, Mr. W. B. Chaffee, Mr. R. E. Doebler, Mr. R. E. Eppley, Dr. R. C. Etherton, Mr. G. C. Geisler, Mr. R. Goles, Dr. J. J. Kolata, Mr. K. Kosanke, and Mr. R. Todd have aided greatly in useful discussions and in the acquisition of data.

Mr. N. R. Mercer and his machine shop staff were of assistance in the fabrication of some of the apparatus used in this

investigation.

Mr. R. Belgard helped with the drafting of figures.

Miss T. Arnette, Mr. and Mrs. W. Merritt, and the Michigan State cyclotron computer staff have been helpful in clarifying the unique characteristics of the M. S. U. Computer.

The willingness of each of the M.S.U. cyclotron faculty and staff members to answer questions relating to their individual fields of interest has been of considerable value.

Mrs. Ina Samra cheerfully and accurately typed this thesis and the various publications which emerged from the investigations described here.

I acknowledge the financial assistance of the National Science Foundation, U. S. Atomic Energy Commission, and Michigan State University.

Finally, I thank my wife Helen for her understanding, inspiration, and support throughout the course of this study.

TABLE OF CONTENTS

Chapter

LIST OF TABLES

LIST OF FIGURES

CHAPTER I

INTRODUCTION

A significant measure of our understanding of nuclear structure is given by the capability of current nuclear models to predict previously unobserved properties of nuclei. These models, in part, are based on experimental observations of the same nuclear state properties. Therefore, an increase in the quality and quantity of experimental results can aid both in the testing of available models and in the development of improved models.

Comparisons of the experimental results reported here have been made with the currently available models. The latter include the Kisslinger - Sorensen model with a short-ranged pairing force and a long-ranged quadrupole interaction (1), Wildenthal's calculations using the shell model with selected configuration mixing (2), and qualitative concepts from the weak-coupling particle-core model (3).

Past studies of radioactive decay, in conjunction with nuclear reaction work, have played basic and complementary roles in advancing our current understanding of nuclear structure. The investigations included in this thesis are intended to extend and improve some of the information acquired from radioactive decay by means of beta and gamma ray spectroscopy.

During the past several years, many experimental studies have been undertaken of the beta and gamma ray decay schemes of odd proton odd mass neutron deficient nuclei lying in the $50 \leq Z \leq 62$, $64 \leq N \leq 82$ region of the table of nuclides (4-6). In general, these studies characterize the daughter states as fully as possible by combining their decay schemes with the results of available reaction studies and other experimental results and theoretical predictions from the literature.

The "magic numbers" of 50 protons and 82 neutrons correspond to tightly bound or spherical nuclei. In this region the available shell model states in the approximate order of filling are $g_{7/2}$, $d_{5/2}$, $s_{1/2}$, $h_{11/2}$, and $d_{3/2}$. Far from these inert nucleon cores a permanently deformed region is expected. The transitional region between the spherical and deformed regions appears to be characterized by more and lower energy states which suggest a softer nucleus. Within this region the line of β-stability runs roughly through ${}_{51}Sb^{121}_{70}$, ${}_{53}I^{127}_{74}$, ${}_{55}Cs^{133}_{78}$, ${}_{57}La^{139}_{82}$ and ${}_{59}Pr^{141}_{82}$. These stable nuclei have a nearly ideal location for probing this transitional region with radioactive nuclei produced by the (p,xn) and (He^3,xn) reactions employed in this study.

Evidence of considerable experimental and theoretical interest in the region selected for this investigation is seen in current reference compilations (4-6). Recent beta and gamma ray spectroscopy studies performed at Michigan State University (7-15) have played a central role in the acquisition of the currently

accepted experimental data on odd mass antimony and iodine energy level structure. One curious result of these investigations has been the observation of a very smooth systematic trend (i.e. quadratic) in energy of four low-lying states of spins $7/2^+$, $5/2^+$, $3/2^+$, and $1/2^+$ in both the odd mass antimony and iodine isotopes (7,15). It is of interest to see if this smooth trend exists in the odd mass neutron deficient cesium, lathanum, and praseodymium nuclides.

Just below the 82 neutron shell are seen many systematic examples of $h_{11/2} \rightarrow d_{3/2}$ neutron isomerism. Some of these isomers and ground state decays might be expected to populate levels with spins ranging from 1/2 to 15/2. These many levels near a closed shell might then be interpreted in relatively tractable shell model terms.

The selection of specific nuclides within the region of interest was initiated by sufficiency requirements for available energy for electron-capture, half-life, and feasibility of source production and chemical separation. A determination of the current state of experimental and theoretical studies from available publications was also an important early stage of the selection process.

In this study, the investigations of the beta and gamma ray decays of Ba^{131m}, Ba^{133m}, Ce^{137m+g}, Nd^{141m+g}, and Nd^{139m+g} by means of gamma ray spectroscopy are reported. A brief study of systematic trends in this region of the periodic table suggests

several patterns which will be interesting to compare with predictions of future nuclear models.

During the course of this study, other decay schemes (e.g. Pr^{139} and Pr^{140}) were investigated in detail in order to verify that the low intensity gamma rays were assigned to the correct nuclide. The results of these studies are published elsewhere (16,17) and are not included in this thesis.

Chapter II describes in a general way some of the experimental apparatus and several of the methods of gamma ray spectroscopy employed in the present investigation. Emphasis is placed on methods used most recently to significantly increase the amounts and quality of data which can be obtained and analyzed in a given time interval. Also, a sequence of 14 steps used to establish important features of positron and electron capture decay schemes is outlined.

Chapter III describes the experimental results obtained. Following Nd^{141g} decay, six new gamma rays were discovered and placed in a decay scheme containing three new Pr^{141} excited states. From the Nd^{139m+g} decay scheme study, 72 gamma rays were observed and 22 excited states (14 new) were placed in Pr^{139}. A set of six states between 1.6 and 2.2 MeV are interpreted as members of a high spin odd-parity three-quasiparticle multiplet having the $(\pi d_{5/2})(\nu d_{3/2})^{-1}(\nu h_{11/2})^{-1}$ configuration. Gamma ray studies of the decays of Ba^{133m}, Ba^{131m}, and Ce^{137m+g}, are also described. A new high-spin state of Cs^{133}, the first measurement

of two intense gamma rays following Ba^{131m} with a Ge(Li) detector, and an energy level scheme for La^{137} which includes ten excited states are among the results obtained.

In Chapter IV the systematic behavior of some of the nuclear properties in the region are discussed. Here also, some characteristic properties of the interesting three-quasiparticle multiplets in Pr^{139} are summarized.

CHAPTER II

EXPERIMENTAL APPARATUS AND METHODS

The β^+/ε decay schemes constructed during this investigation used both standard and new techniques of gamma ray spectroscopy. Section 2.1 describes in a general way the apparatus in current use at Michigan State University for gamma ray measurements, including a somewhat more detailed description of a multiparameter coincidence system developed during the course of the present study. In section 2.2 some general methods used to analyze data are outlined. Section 2.3 outlines the pattern of operations used in the present study to construct parts of each nuclear decay scheme with the aid of the analyzed data. The descriptions of the production and chemical separations that were used for the several different nuclides are deferred to Chapter III where they are included with a discussion of experimental results.

2.1. The Gamma Ray Spectrometer

The process of data accumulation by gamma ray spectrometers is becoming increasingly efficient, and at the same time the quality of the data is improving. This progress is aided by the rapidly improving technology involved in the manufacture of larger Ge(Li) detectors, amplifier-preamplifier systems with improved performance characteristics (e.g., higher resolution),

faster and more stable analog-to-digital converters (ADC), analyzers with larger memories, more flexible and more sophisticated ADC-computer interfacing, and increasing computer memory. This section describes some significant general characteristics of the gamma ray spectrometers employed in this study for singles and coincidence experiments. Special purpose applications of the apparatus are discussed in Chapter III.

2.1.1. Singles Experiments

The basic components of the singles gamma ray spectrometer used in the present study were: a) A 7-cm^3 Ge(Li) detector (18) cooled to liquid nitrogen temperature (77°K), b) a room temperature FET preamplifier and high-voltage supply, c) a pulse shaping amplifier with pole-zero compensation, d) an analog-to-digital converter (ADC) and multi-channel analyzer (MCA), and e) a data readout system. The performance of a given spectrometer was limited by its weakest link, which could not be isolated to a single component in all cases but depended upon each experiment and its objectives. For example, where gamma ray energies $\geq$2-MeV were measured, the number of channels in the MCA was sometimes the weakest link. Or, low detector efficiency would obscure the full-energy peaks corresponding to gamma rays with very low intensity. A common limitation on gamma ray energy resolution was introduced by the performance of the preamplifier-amplifier system.

For a given set of available components, a balance normally was required between competing parameters to optimize spectrometer

performance. A few of the many typical examples of competing parameters are listed below. If the potential difference applied to the Ge(Li) detector was too low, incomplete charge collection would occur, but too high a potential led to breakdown and increased noise. Too low a counting rate could sometimes produce widened peaks because of long term instability of the electronics, but too high a counting rate could cause pulse pileup, again broadening the peak. This balance was especially important for the detection of weak photons in the presence of a continuous background. Other optimizations employed included those between small and large numbers of MCA channels, short and long shaping amplifier time constants, high and low amplifier gains, and between a large and small number of measurements of gamma ray energies and intensities.

The gamma ray singles spectrometer resolution achieved with Ge(Li) detectors exceeded that obtained with NaI(Tl) scintillation counters by factors of $\gtrsim$10. During the present study, the Ge(Li) detectors were used exclusively for singles gamma ray energy and intensity measurements.

2.1.2. Coincidence Experiments

All but one of 41 excited nuclear states seen to be populated by β^+,ε decay in the course of this study are suggested to have lifetimes $<<$100 nanoseconds (ns). It was thus found useful to employ two or three singles spectrometers in different coincidence configurations to perform anti-coincidence, prompt-coin-

cidence, and delayed-coincidence experiments. The standard pattern of experiments employed in the course of the decay scheme studies described in Chapter III was: a) singles spectrum, b) anti-coincidence spectrum, and c) coincidence spectra. Within these three very general categories of experiments, many special purpose experiments were suggested by unique features of each particular decay scheme under investigation. The study of Nd^{141m+g} decay described in section 3.1 illustrates the "classical" pattern of experiments, whereas the Nd^{139m} study in section 3.2 represents a study with many unexpected features and a wider range of different experiments.

Anti-coincidence and many prompt-coincidence experiments were performed with Ge(Li) detectors inside a split-ring NaI(Tl) annulus as described below in section 2.1.2.A. Other prompt and delayed coincidence experiments were performed with Ge(Li) detectors oriented at 90° from a 3-in. × 3-in. NaI(Tl) detector with the radioactive source under investigation at the apex of the angle. These experiments are outlined in section 2.1.2.B.

During the study of Nd^{139m} decay, the cyclotron and coincidence photon spectrometer were required on ten separate occasions between March, 1968, and September, 1968, for intervals of ≈24 hours. This large expenditure of time for coincidence measurements, which essentially differed only in the energy regions gated by the NaI(Tl) detector spectrometers, suggested the development of a multiparameter coincidence system. This system stores on magnetic tape the

pair of channel numbers corresponding to each coincidence event in each detector. The tapes are later scanned with the aid of a computer program in order to extract the coincidence data. A multiparameter coincidence apparatus that was developed during the course of these investigations is described in section 2.1.2.C.

2.1.2.A. --Split-Ring NaI(Tl) Annulus -- Ge(Li) Spectrometer--

Several specific applications of the split-ring 8-in. × 8-in. NaI(Tl) annulus vs. Ge(Li) gamma ray spectrometer are described and suggested in reference 19. In the present study, the anti-coincidence application with the radioactive sources placed inside the annulus tunnel and on top of the Ge(Li) detector was found to be the most useful of the configurations suggested in reference 19. In this configuration it was possible to obtain convenient and significant reductions of the Compton edges caused by backscattering in the active region of the Ge(Li) detector. This was done with the aid of an additional 3-in. × 3-in. NaI(Tl) anti-coincidence detector placed in the annulus tunnel opposite the Ge(Li) detector.

An essential feature of spectra taken with the anti-coincidence spectrometer was the enhancement of the primarily electron-capture-fed gamma ray transitions to the ground states of nuclei. That is, gamma rays which are not detected by one detector of the coincidence spectrometer within the coincidence resolving time (usually $\lesssim$100 ns) of the detection of a photon in the other detector were enhanced typically by factors of 2 to 10 over ratios seen in singles experiments with respect to other photons.

One might suspect that the anti-coincidence spectrometer would necessarily make the gamma rays involved in cascades difficult to detect. However, the effect of Compton background reduction can sometimes outweigh the cascading photon full-energy peak intensity reduction. For example, compare the 145.4- and 981.3-keV full-energy peaks in Figure 1 (singles) with the corresponding peaks in Figure 2 (anti-coincidence with the configuration described above). A definite "peak/background" enhancement is seen in Figure 2 even though the 145.4- and 981.3-keV gamma rays of Nd^{141} are in cascade. A quantitative explanation of this enhancement would require consideration of the numbers and kinds of contributions to the Compton background. However, the presence of a scattered photon associated with each count in the Compton distribution of the spectrum taken with the Ge(Li) detector suggests a partial explanation. The Compton scattered photon of even a primarily electron-capture-fed ground state transition gamma ray can be picked up by a NaI(Tl) detector, and, undistinguished from a coincident photon, trigger the anti-coincidence circuit. Thus a background count can be removed by a process which is not associated with the production of a full-energy peak.

Both integral- and gated-coincidence experiments were also performed with this spectrometer. The effects of summing of coincident photon pulses in the annulus were removed to first approximation by comparing spectra taken with adjacent gates.

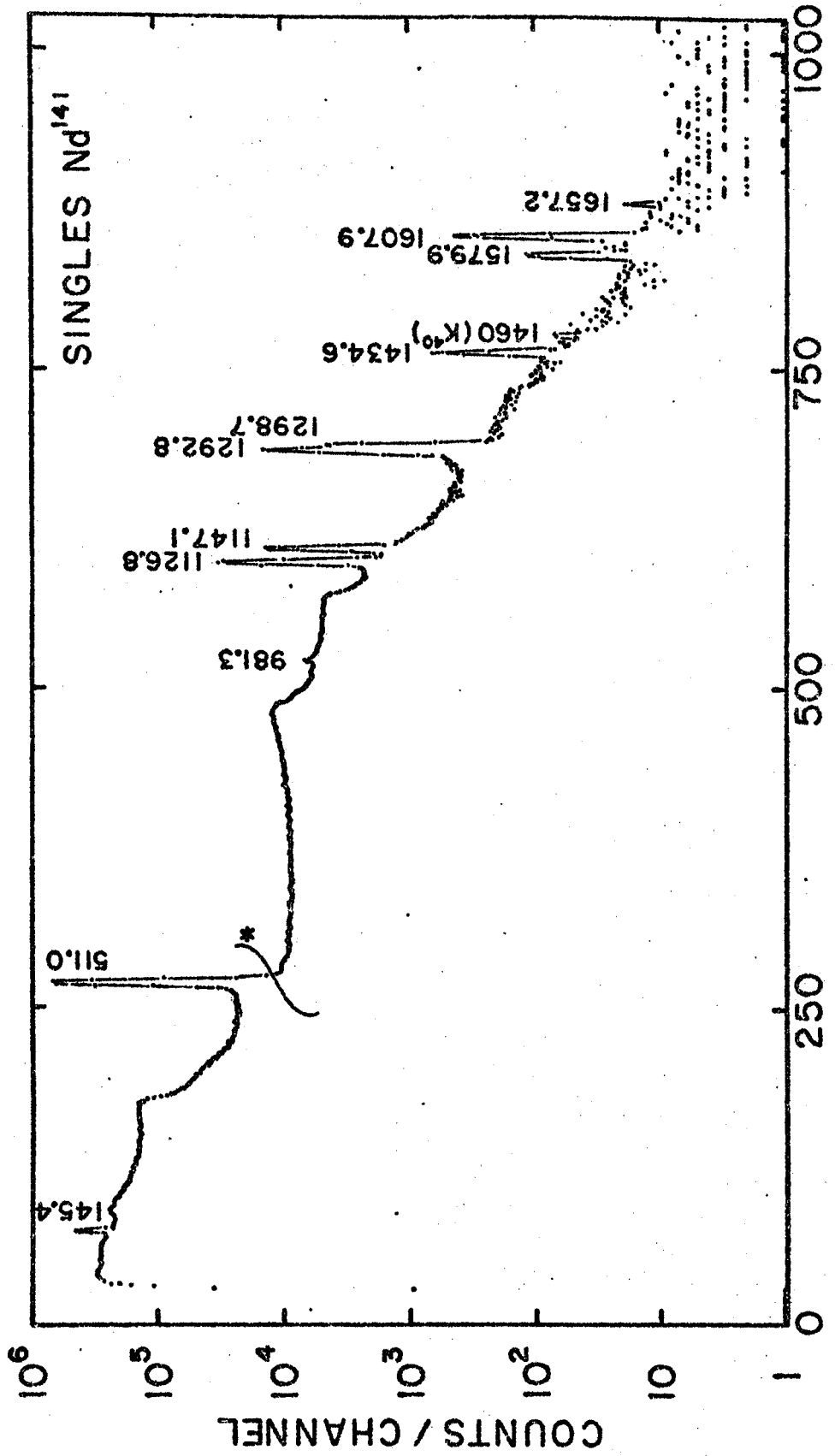

Fig. 1. Singles γ-ray spectrum from the decay of Nd^{141} taken with a 7-cm^3 Ge(Li) detector. Because of analyzer spillover, the portion of the spectrum to the left of the asterisk (*) was recorded for a shorter period of time and then normalized to the remainder of the spectrum.

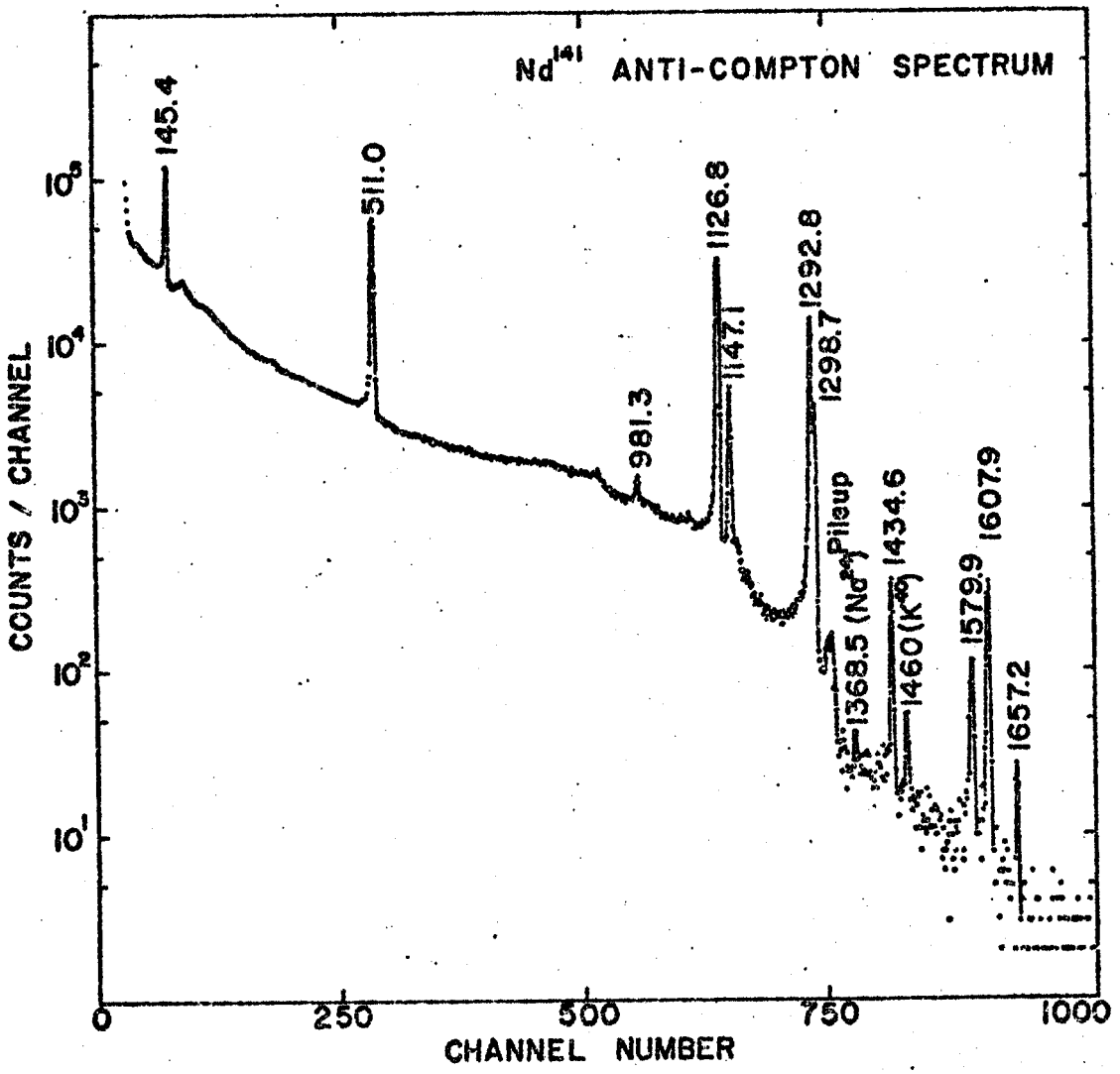

Fig. 2. Nd^{141} anti-coincidence spectrum. Note the larger peak/background ratios for the 145.4- and 981.3-keV full-energy peaks here as compared with the corresponding ratios in Figure 1. The text explains qualitatively how this can happen even though the 145.4- and 981.3-keV gammas are in cascade with each other. It is noted that "anti-Compton" usually implies placement of the radioactive source outside the annulus and "anti-coincidence" most commonly suggests an internal location of the source. This distinction is not employed here.

2.1.2.B.--3-in. × 3-in. NaI(Tl)-Ge(Li) Spectrometer--Somewhat cleaner coincidence spectra were obtained by the use of a 3-in. × 3-in. NaI(Tl) detector gated gamma ray spectrometer. The smaller NaI(Tl) detector has the advantages of higher resolution (8% rather than 10% for the 661-keV gamma ray of Cs^{137}) and reduced summing.

This photon coincidence spectrometer was employed for a very useful delayed-coincidence run described in section 3.2.3.C. A 200-ns delay in one branch of the coincidence circuit enhanced several full energy peaks by two orders of magnitude with respect to peaks involved in prompt coincidences. The enhancement is due to the fact the gamma rays populated a state that was found to decay with a 40-ns half-life.

In addition to its use in prompt coincidences where source intensity was not a significant limitation, the 3-in. × 3-in. NaI(Tl)-7-cm^3 Ge(Li) spectrometer was used for multiparameter coincidence experiments as described in the following section.

2.1.2.C.--Multiparameter Ge(Li)-NaI(Tl) Spectrometer--In the conventional coincidence experiments described in the previous section, signals from the Ge(Li) detector (only) are recorded if certain coincidence requirements are satisfied. Separate coincidence experiments are required for each set of pulse height requirements placed on output signals from the NaI(Tl) electronics which trigger the coincidence circuit. Each conventional coincidence experiment employs two detectors, a considerable collec-

tion of electronics, and many man-hours in order to assemble and operate the apparatus and analyze the data. The only basic parameter change from one prompt coincidence experiment to the next in the study of a particular decay scheme is the single channel pulse height analyzer window chosen. However, since the experiments were usually conducted at intervals of one week or more, the spectrum energy calibrations changed and each analysis of data had to be conducted independently. In addition, each coincidence experiment required additional accelerator time to prepare the radioactivity.

One way to remove the massive duplication involved in these experiments is to record the signals from both detectors following each fast-coincidence event. It would not be practical to store each ordered-pair of channel numbers in separate computer locations since $>10^6$ locations would be required for even an array of 1024×1024 channels. However, if each ordered pair of channel numbers would be written on magnetic tape with the aid of dedicated buffer storage of ≈240 events, ≤2000 events/sec could be recorded with no deadtime beyond the ADC (20).

Near the end of the present study, such a system was developed with the aid of a dual 4096-channel ADC interfaced to an SDS SIGMA-7 computer and magnetic tape readout. Typically, 20 coincidence events/sec are recorded for 15 hours whereupon one 2400 foot tape is filled with 1.1×10^6 events. A computer pro-

gram, EVENT RECORDER, was written in order to extract coincidence data from the magnetic tape. Only ten minutes is required to scan the entire tape, punch-out and print-out one to five 4096-channel spectra of data, and rewind the tape.

The sequence of operations at the end of a multiparameter coincidence experiment was: a) Scan the tape for the integral coincidence spectrum obtained from each detector, b) choose gates from each spectrum judiciously with or without background subtraction, c) scan the tape for the gated coincidence spectra, and d) analyze the data, noting that each spectrum displaying the Ge(Li) detector data has the same gain. An application of this powerful tool was employed, in the present study, only to the 30-min Nd^{139g} decay. The results are described in section 3.2.6.B.

Future applications and development of the multiparameter coincidence spectrometer may be expected to increase the efficiency of decay scheme studies at Michigan State significantly. A Ge(Li)-Ge(Li) multiparameter spectrometer is presently in use, and future developments may include triple-coincidence and anti-coincidence-coincidence experiments, delayed-coincidence experiments with time as one of three parameters, and experiments with other combinations of three or more parameters which would be recorded on magnetic tape and removed later. A primary weakness of the current system is that it is not easily monitored. Monitoring has been accomplished to date with a separate MCA and scaler to count all of the coincident events.

2.2. Data Analysis

Rapid advances in many aspects of experimental nuclear spectroscopy have resulted in a significant increase in the rate of data accumulation during the course of this study. For example, long-lived sources from Oak Ridge have been replaced by short-lived sources from the Michigan State University sector-focused cyclotron, 4-keV FWHM resolution of Ge(Li) detector systems have been replaced by spectrometers with 2-keV FWHM resolution, and 1024 channel analyzers have been replaced in our gamma ray spectrometers with 4096 channel analyzers and 8092 channel ADC's coupled to the Sigma-7 and PDP-9 computers.

Most of the data analysis in the present study was carried out on the Michigan State University Cyclotron Laboratory SDS SIGMA-7 computer with FORTRAN programs written or adapted for this computer. Brief and general descriptions of the gamma ray energy and intensity measurements, x-ray and annihilation photon measurements, and the analysis of the gamma-gamma coincidence spectra are given below. Discussions related to the special characteristics of individual experiments are given in Chapter III.

2.2.1. Gamma Energy and Intensity Measurements

The centroids and areas of photon spectra peaks were determined following the subtraction of linear or cubic interpolated backgrounds. The computations were performed with the aid of the MOIRAE program, written in machine language for the

SIGMA-7 computer by R. Au. The major functions of this program are found in the MIKIMAUS program originally written by G. Berzins and outlined in Appendix D of reference 21.

A significant feature of the MOIRAE program is that it is operated on-line with the SIGMA-7 computer and allows a more rapid analysis than did earlier methods.

Gamma ray energy measurements were made by first computing least squares quadratic calibration equations from centroid channel numbers of well-known standard energies and then computing the energies of "unknown" gammas from their measured centroids. Rough energy approximations (±1 keV) were made from "external" calibrations taken in successive measurements of calibration, unknown, and calibration sources. Serious energy measurements (±≈0.2 keV) were made from "internal" calibrations taken by simultaneously counting the unknown and standard calibration sources.

The choice of standard calibration sources and how they are employed are significant factors in gamma energy measurements. Ideally one would like standards that emit only the gamma rays actually used as standards and a small number of them because the spectral distribution of the calibration photons often obscures other photon peaks of interest. On the other hand, many good calibration points are useful in order to establish a reliable calibration curve.

Gamma ray relative intensities were established with the aid of a detector efficiency versus photon energy curve for energies

ranging from 30-keV to 3-MeV. A linear relationship between the log of the $i^{\underline{th}}$ full energy peak efficiency (eff_i) and the log of the $i^{\underline{th}}$ photon energy (E_i) between ≈150-keV and ≈3-MeV was observed for each detector to within experimental uncertainties. This dependence ($eff_i/eff_j = (E_j/E_i)^{1.64}$ for the 7-cm^3 detector) was employed in the "MOIRAE E(I)" computer program.

2.2.2. Double and Single Escape Peaks

Double and single escape peaks were used to check the energies of full-energy peaks and their intensities. Their energies are 1022.0- and 511.0-keV respectively below the corresponding full-energy peak, and the intensities were derived from empirical efficiency curves. Recent evidence (22) suggests that the energy differences may need to be corrected by a "field increment effect" factor depending on the detector-source geometry and the electric field in the detector created by the diode bias voltage. This correction was negligible (<0.1-keV) for the experimental conditions of the present study. In particular, the electric fields produced by the detector biases were relatively low. Both double and single escape peaks are depressed by anti-coincidence runs, enhanced in 511-keV annihilation photon gated coincidence experiments, and characterized in singles spectra by the lack of Compton edges. A careful consideration of these characteristics was necessary and useful in the process of data analysis.

2.2.3. X-Ray and Annihilation Photon Measurements

K x-rays accompanied 84 to 90% of the decay processes of electron capture and internal conversion in nuclei with $50 \leq Z \leq 60$ (23). With measured *K* x-ray intensities and measured *K*-fluorescent yields (the latter are tabulated on page 570 of reference 6 as a function of daughter Z), a rough check can be obtained on proposed decay schemes and elements present in a given spectrum.

Since almost every positron emission event is followed by an annihilation process involving two 511.0-keV annihilation photons, it is commonly feasible to determine ground state beta branching ratios with the aid of the intensity of the annihilation photons, as described in section 2.3. To eliminate the possibility of the positrons penetrating into the detectors and to allow studies to be made on the total positron annihilation, copper absorbers were placed around the samples during some of the counting intervals.

2.2.4. Gamma-Gamma Coincidence Spectra

Chance coincidence rates were maintained below 1/10 of the rate of true coincidences at all times. The Compton distribution underlying the full energy peaks of interest in a coincidence gate can contribute significantly to coincidence spectra. To remove this effect to first order, spectra in coincidence with the Compton background in adjacent gates were compared. In the multiparameter coincidence experiments referred to in section 2.1.2.C the subtraction of weighted spectra taken with adjacent gates can be performed as the magnetic tape is scanned.

A major weakness of Ge(Li)-NaI(Tl) photon coincidence spectrometers is the poor resolution of the NaI(Tl) detector. The use of Ge(Li)-Ge(Li) coincidence spectrometers has been severely restricted because of the limitations introduced by low detector efficiency. However, this restriction is decreasing in this laboratory as the large Ge(Li) detectors required for adequate full-energy peak efficiency become more readily available.

2.3. Decay Scheme Construction

A nuclear decay scheme presents significant results of experimental studies. In the present investigation these results include the energies, spins, parities, and half-lives of the states, the disintegration energy for electron-capture, the gamma and beta transition intensities, the gamma decay multipolarities, and the log *ft* values for beta decay to each state. The methods used to construct decay schemes are so varied that a new pattern must be devised in the process of studying each individual decay. Abundant evidence of this is seen in Chapter III as eight decay schemes are described in eight quite different sequences.

The location of states may be suggested initially by gamma energy sums, anti-coincidence data, prompt coincidence data, delayed coincidence data, gamma ray relative intensities, or other parameters. These parameters become more difficult to translate into a consistent system of energy levels as the number of gamma rays increases.

After the energy levels are established, the determination

of the gamma and beta transition intensities and the log *ft* values is a fairly routine operation involving a rather long sequence of operations. Thus, it lends itself readily to computer analysis. Tentative values of these latter parameters were commonly useful in the process of updating partial decay schemes. For these reasons and in order to reduce decay scheme construction time and numerical errors, a computer program called DECAY SCHEME has been written.

The sequence of operations used to perform these "routine" aspects of the decay scheme construction was suggested by data derived from many different experiments. It was independent of the order in which the experiments were performed. Therefore, an understanding of this sequence is a prerequisite to an understanding of the calculation of gamma and beta transition intensities and lot *ft* values. This sequence, described below, is not entirely incorporated into the current version of the DECAY SCHEME computer program, but it was employed in full as part of the construction of each of the decay schemes discussed in Chapter III. For these reasons, this chapter concludes with a list of steps which outlines briefly the pattern of operations used in the present study to derive the gamma and beta transition intensities and the log *ft* values from the remainder of each decay scheme and the full-energy peak areas after the energy levels had been established.

1) Calculate the relative photon intensities I from $I \equiv A/(\text{eff})$
   where $A \equiv$ net full-energy peak area in a singles run and
   eff $\equiv$ relative efficiency of the Ge(Li) detector employed at

the energy of the photon of interest. If absorbers are employed for special purpose runs, eff is reduced by a factor given by reference 23 as a function of the energy of the photon, and of the thickness, density, and atomic number (Z) of the absorber.

2) If reliable direct measurements are not available, calculate the internal conversion coefficients by least-squares fits of calculated conversion coefficients tabulated in the current literature (24) as a function of gamma ray energy, Z of the nucleus in question, and a measured or assumed multipolarity.

3) Calculate the total transition relative intensities $I_t \equiv I(1+\alpha_{tot})$, where $\alpha_{tot} \equiv$ total internal conversion coefficient.

4) Calculate the total beta-feeding relative intensity $I_\beta \equiv \Sigma(I_t)_{out} - \Sigma(I_t)_{in}$ for decay to each excited daughter state, where $\Sigma(I_t)_{out(in)} \equiv$ sum of all total transition intensities depopulating (populating) the excited state.

5) Tabulate ε_K/β^+ ratios for decay to each daughter state (from Figure 3 on page 575 of reference 6) as a function of the parent nucleus Z and the positron endpoint energy. $\varepsilon_K \equiv K$ electron-capture transition probability and $\beta^+ \equiv$ positron emission transition probability for the competing modes of beta decay to each daughter state.

6) Calculate $\varepsilon_K/\varepsilon_{tot}$ for the decay to each daughter state as a function of Z of the daughter nucleus, the total energy of

the capture transition, and the binding energies of the K and L_I shells of the daughter nucleus, where $\varepsilon_{tot} \equiv$ total electron-capture transition probability. The theoretical values for the ratios of the relative intensities of K, L_I, L_{II}, L_{III}, and $M+N+\cdots$ capture are given in the formulas and graph of page 576 of reference 6.

7) Calculate $\varepsilon_{tot}/\beta^+$ for decay to each daughter state from the results of steps 5 and 6 above.

8) Calculate $\Sigma I_{\beta^+} = \frac{1}{2} I_{511}$, where $\Sigma I_{\beta^+} \equiv$ sum of all positron relative intensities and $I_{511} \equiv$ relative intensity of the 511.0-keV annihilation photons measured with total annihilation.

9) Calculate $\Sigma I_{KEC} = (I_{KX}/\omega_K) - \Sigma I_{KIC}$, where $\Sigma I_{KEC} \equiv$ sum of all K electron-capture relative intensities, $I_{KX} \equiv K$ x-ray relative intensity (see step 1), $\Sigma I_{KIC} \equiv$ sum of all K internal-conversion relative intensities (see steps 1 and 2), and $\omega_K \equiv$ K-fluorescent yield, or fraction of K-vacancies which give rise to K x-rays, as listed on page 570 of reference 6 as a function of Z of the parent isotope.

10) Calculate the total beta-feeding relative intensity to the ground state of the daughter from $I_\beta = I_{\beta+} (1+\varepsilon_{tot}/\beta^+)$, where each quantity refers here to the ground state beta-decay alone.

11) Set $N \equiv 100/(\Sigma I_\beta + I_m)$, where $\Sigma I_\beta \equiv$ sum of all beta-decay relative intensities of the parent decay and $I_m \equiv$ total

transition relative intensity of an isomeric parent to (a) lower state(s) of the parent. $N \equiv$ normalization constant which converts each of the above relative intensities into percent of the total parent disintegrations.

12) Apply steps 7 and 11 to steps 4 and 10 in order to determine the percent of parent beta decay populating each daughter state by β^+ and ε_{tot} decay individually.

13) Calculate $Q_{Ki} = Q_{K\varepsilon} - E_i$ for each daughter state, where $Q_{Ki} \equiv$ available energy for K electron capture to the i^{th} daughter state, $Q_{K\varepsilon} \equiv$ available energy for K electron capture to the daughter ground state (tabulated in reference 6), and E_i is the energy of the i^{th} state.

14) Calculate $\log (ft) = \log (f_o t) + \log C + \Delta \log (ft)$ for beta decay to each daughter state, where $\log f_o t$ is a function of Q_i and the partial half-life of the decay, $\log C$ is a function of Z of the parent, and $\Delta \log ft$ is a function of the fraction of parent disintegrations which proceed by K electron capture decay to the daughter state of interest. This calculation is clearly described on page 574 of reference 6 which includes graphs of each of these functions.

CHAPTER III

EXPERIMENTAL RESULTS

3.1. Decay Schemes of Nd^{141g} and Nd^{141m}

3.1.1. Introduction

Since the first production of Nd^{141} in 1937 by Pool and Quill (25), who used fast neutrons to induce the $Nd^{142}(n,2n)$ Nd^{141} reaction, this nuclide has been produced by a number of reactions involving the use of protons, deuterons, alpha particles, and photons as projectiles (4-6). Similarly, there have been various more or less successful studies of its decay scheme (4-6). Among the more complete gamma ray spectroscopic studies that utilized only NaI(Tl) detectors (26-29), however, there exist some serious discrepancies. Also, in none of these studies are more than three Pr^{141} excited states reported, whereas, as a result of the study of inelastically scattered deuterons on Pr^{141}, Cohen and Price (30) have reported levels at 140, 1140, 1300, 1500, and 1630 keV, with additional levels at 1800 keV and higher energies. Some studies on inelastically scattered neutrons (31) and N^{14}-induced Coulomb excitation (32), although with poorer resolution, have also indicated the existence of a number of levels starting in the vicinity of 1 MeV. In the only previous published

work on Nd^{141} decay utilizing Ge(Li) detectors, Koehler and Grissom (33), using a very small detector, report only four gamma rays, depopulating the first three of the excited states reported by Cohen and Price.

Since the energy for Nd^{141} electron-capture decay is 1800 keV (28,34), one might expect some of the other higher-lying Pr^{141} levels also to be populated from its decay. For this reason and because of the discrepancies among the earlier studies, it was felt that a re-investigation of Nd^{141} decay was in order. Nd^{141} has been produced by the relatively clean $Pr^{141}(p,n)Nd^{141}$ reaction. Ge(Li) and NaI(Tl) detectors were used in singles, coincidence, and anti-coincidence configurations to study its gamma rays. Additionally, as no specific rare-earth chemical separations had been performed on the targets in any of the previous work, Nd was separated chemically from the other rare earths in order to insure that the activities which were observed came from a Nd isotope. Six new gamma rays were found as a result of these studies. These can be fitted into a decay scheme that includes the population of three additional excited states in Pr^{141}. The decay of the short-lived Nd^{141m} isomer (35,36) was also investigated to see if it might decay directly to high-spin states in Pr^{141}; the results allow an upper limit of 0.1% of the total Nd^{141m} disintegrations to be placed on any direct population of such levels.

3.1.2. Source Preparation

The Nd^{141} sources were prepared by bombarding 99.97% pure

Pr_2O_3 with 9 MeV protons from the Michigan State University sector-focused cyclotron. Typically, ≈100-mg targets were bombarded with a ≈1-μamp beam for 1 hour. Sources were normally allowed to decay for at least one hour to let any short-lived contaminants decay away, and then they were counted for two to four half-lives, more source being added with the passage of time in order to retain a relatively constant counting rate. It was found that no competing gamma rays with different half-lives were observed for approximately four half-lives of the Nd^{141}. Most of the coincidence experiments, which required several days' counting time, were performed with multiple bombardments.

To insure that only radiations from Nd were observed, the singles gamma ray spectrum was confirmed with a chemically-separated source. In this source the Nd was separated from the Pr target and any other contaminating rare earths by eluting it from a Dowex-50 cation-exchange column with α-hydroxy-isobutyrate (37).

The Nd^{141m} sources were produced by bombarding similar Pr_2O_3 targets for ≈10 sec. No chemical separations were performed on these sources.

3.1.3. Nd^{141g} Gamma Ray Spectrum

3.1.3.A. --Singles Spectra-- A 7-cm^3 five sided coaxial Ge(Li) detector was used to determine the energies and intensities of the Nd^{141} gamma rays. It was mounted in a dip-stick cryostat. The wall thickness of the evacuated aluminum can covering the detector was 0.16 cm. Typical resolution obtained with this de-

tector was ≈4.3 keV FWHM for the 661.6-keV gamma ray of Cs^{137}, using a room temperature FET preamplifier, a low-noise RC linear amplifier with pole-zero compensation, and a 1024-channel analyzer. A 3-cm^3 planar Ge(Li) detector mounted in a similar fashion was used to confirm the energy values and intensity ratios of the gamma rays observed. Both of these detectors were manufactured in this laboratory (18,38).

The energies of the gamma rays were measured by counting the Nd^{141} sources simultaneously with a number of well-known calibration sources, which are listed in Table 1. In order that activities decaying with different half-lives could be identified, spectra were recorded periodically as the sources aged. A background correction was made for each peak by fitting a cubic equation to several channels above and below the peak and then subtracting. The centroid of each calibration peak was then determined and a least-squares fit made to a quadratic calibration curve. The centroids of unknown peaks were similarly determined and the corresponding energies calculated from the calibration curve. The energies of weak Nd^{141} gamma rays, which would be obscured by the calibration standards, were determined by using the now-well-determined stronger gamma rays as internal standards. A gamma ray spectrum taken with the 7-cm^3 detector is shown in Figure 3.

A list of gamma ray energies and relative intensities is given in Table 2. The energies assigned are mean values taken from a number of different measurements recorded at different

Table 1. Gamma rays used as energy standards for $Nd^{141m,g}$ decay.

Nuclide	γ-ray energy (keV)	Reference
Co^{57}	121.97±0.05	a
Co^{57}	136.33±0.04	a
Ce^{139}	165.84±0.03	b
Cs^{134}	644.744±0.027	c
Cs^{137}	661.632±0.069	d
Cs^{134}	795.806±0.050	c
Mn^{54}	834.84±0.07	e
Y^{88}	898.01±0.07	e
Sc^{46}	1120.50±0.07	e
Co^{60}	1173.226±0.040	f
Co^{60}	1332.483±0.046	f
Na^{24}	1368.526±0.044	f
Tl^{208}(D.E.)	1592.46±0.10	f
Na^{24}(D.E.)	1731.91±0.012	f
Y^{88}	1836.08±0.07	e

[a]Reference 39.

[b]Reference 40.

[c]Reference 41.

[d]Reference 42.

[e]Reference 43.

[f]Reference 44.

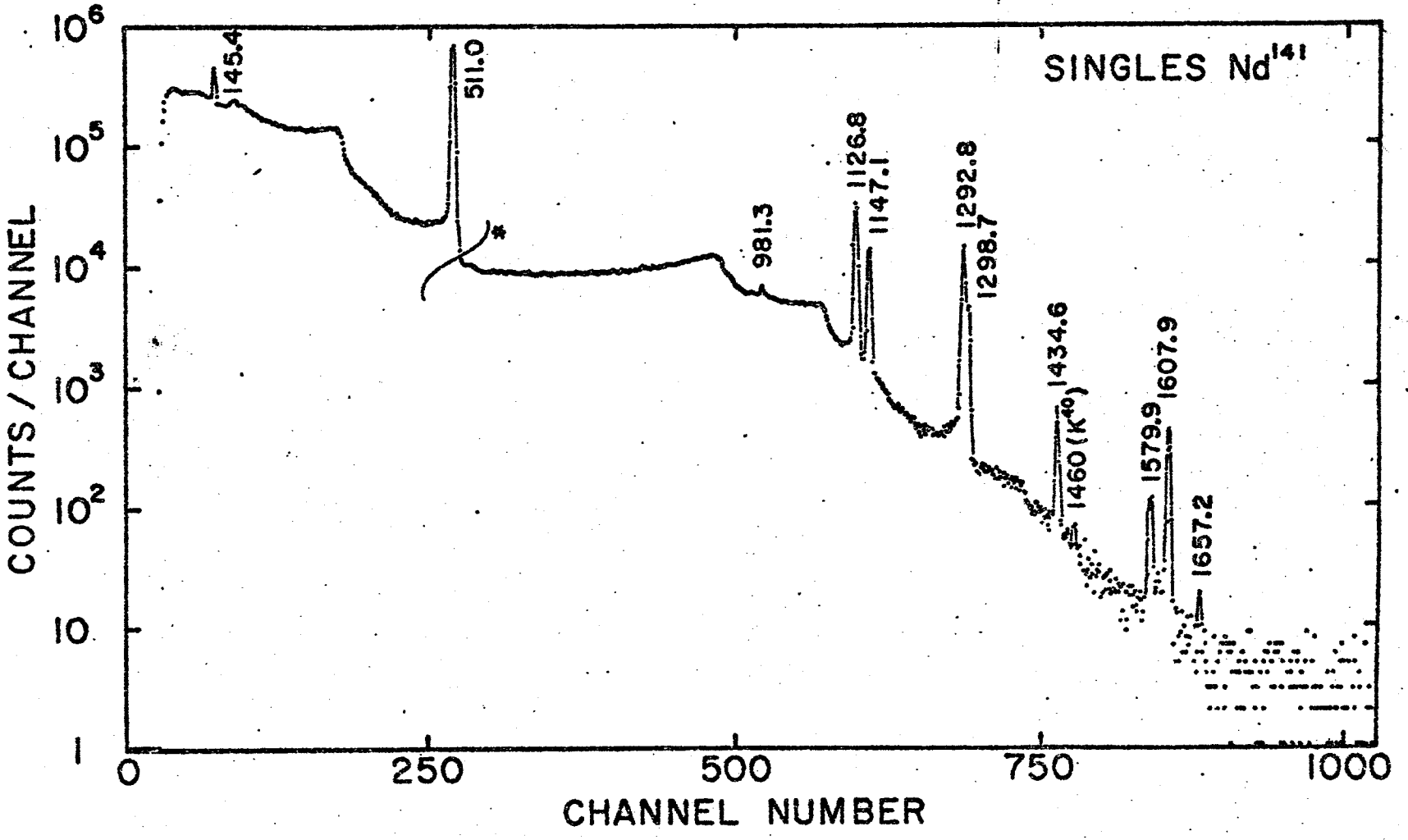

Fig. 3. Singles γ-ray spectrum from the decay of Nd^{141} taken with a 7-cm^3 Ge(Li) detector. Because of analyzer spillover, the portion of the spectrum to the left of the asterisk (*) was recorded for a shorter period of time and then normalized to the remainder of the spectrum.

Table 2. Energies and relative intensities of gamma rays from the decay of Nd^{141}.

Measured γ-ray energy (keV)	Relative intensity			
	Singles spectra[a]	145.4-keV γ-γ coincidence spectrum[b]	Integral γ-γ coincidence spectrum[b]	Anticoincidence spectrum
K x-rays	(8.0±2.0)×10	---	---	---
145.4±0.3	30.3±3.0	46±5 (16±6)	81±10 (51±11)	11.1±1.1
511.006 (annih.)	832±83[c]	955±300	1340±150	60±6
981.3±0.6	3.0±0.3	147±30 (144±30)	90±25 (87±25)	1.1±0.3
1126.8±0.4	≡100	≡100 (0)	≡100 (0)	≡100
1147.1±0.4	38.2±3.8	1810±200 (1770±200)	720±70 (680±70)	14.3±1.4
1292.8±0.6	61.2±6.1	67±12	87±12	58.7±5.9
1298.7±0.7	16.3±2.0	(0)	(0)	15.5±2.0
1434.6±0.5	3.0±0.3	107±40 (104±40)	27±9 (24±9)	1.6±0.2
1579.9±1.0	0.74±0.12	---	---	0.83±0.15[d]
1607.9±0.6	2.3±0.2	---	---	2.2±0.2
1657.2±1.0	0.12±0.04	---	---	0.15±0.05

[a] A total electron conversion coefficient of α=0.46 has been reported (40) for the 145.4-keV transition. This indicates a total transition intensity of 44.2±4.4 on the above scale. Although all the intensities in the table are photon intensities, the conversion coefficients for the higher-energy transitions should be small enough such that the photon and transition intensities should be nearly the same.

[b] The intensities given in parentheses are those corrected for chance coincidences.

[c] Two 0.32-cm Cu absorbers forming a sandwich around the Nd^{141} source were used for the determination of the intensity of 511-keV photons in total annihilation.

[d] After subtraction of the 1575-keV Pr^{142} contaminant peak produced by a $Pr^{141}(n,\gamma)Pr^{142}$ reaction, where the neutrons were produced predominantly in the degrading foils.

times, different system gains, and with each of the two Ge(Li) detectors. The corresponding uncertainties in energies are based on the reproducibilities both of the standard energies and the Nd^{141} energies from the calibration curves, the sizes of the Nd^{141} photopeaks above the background, and the quoted errors of the standard energies listed in Table 1.

The relative peak areas obtained are also averages from a number of runs, and the associated statistical uncertainties include estimated uncertainties in the backgrounds. Relative photopeak efficiency curves for the Ge(Li) detectors were obtained in two ways: First, a set of standard gamma ray sources whose relative intensities had been measured with NaI(Tl) detectors was used. Second, a set of points was obtained from sources emitting several gamma rays whose relative intensities were known from well-established decay schemes. The efficiency curves resulting from the separate methods were in very good agreement.

The *K* x-ray intensity was obtained by comparing the low-energy portion of the spectrum directly with the gamma ray spectrum of Ce^{141}; the comparison was made using the 3-cm^3 detector. Ce^{141} also decays to Pr^{141}, with 70% of its decay populating the 145.4-keV state. Its ratio of *K* x-rays to 145.4-keV gamma rays has been measured (45) to be 0.341±0.010, and, using this value, the corresponding ratio for Nd^{141} decay was found to be 264±71.

3.1.3.B. --Coincidence Spectra-- From the Nd^{141} disintegration energy (28,34) of 1800 keV and the measured gamma ray

energies listed in Table 2, it is evident that only coincidences involving the 145.4-keV gamma ray are energetically allowed. Thus, a 3-in × 3-in. NaI(Tl) detector was gated on the 145.4-keV photopeak and the resultant coincidence spectrum seen by the 7-cm^3 Ge(Li) detector was displayed; the resolving time of the system was ≈50 ns. Figure 4 shows this coincidence spectrum. In Table 2 the relative intensities from this experiment are also included; these have been corrected for chance coincidences. Comparison of the relative intensities of the 145.4-keV gamma-gamma coincidence spectrum with those of the singles spectra clearly indicate that the 981.3-, 1147.1-, and 1434.6-keV gamma rays are in coincidence with the 145.4 keV gamma, whereas the 1126.8-, 1292.8-, and 1298.7-keV gamma rays are not.

In order to search for additional weak gamma rays that might have passed unobserved in the other measurements, an experiment was also performed in which the NaI(Tl) gate was set to accept all transitions greater than 130 keV in energy. This "integral" gamma-gamma coincidence spectrum is shown in Figure 5, and the relative intensities from it are listed in Table 2. They verify the results of the 145.4-keV gamma-gamma coincidence experiment, but no new, weak gamma rays are indicated.

To complement these experiments and confirm which gamma rays appeared in cascades and which came from primarily electron-capture-fed ground-state transitions, an 8-in. × 8-in. NaI(Tl) split annulus detector was employed (19) in an anti-coincidence experiment with

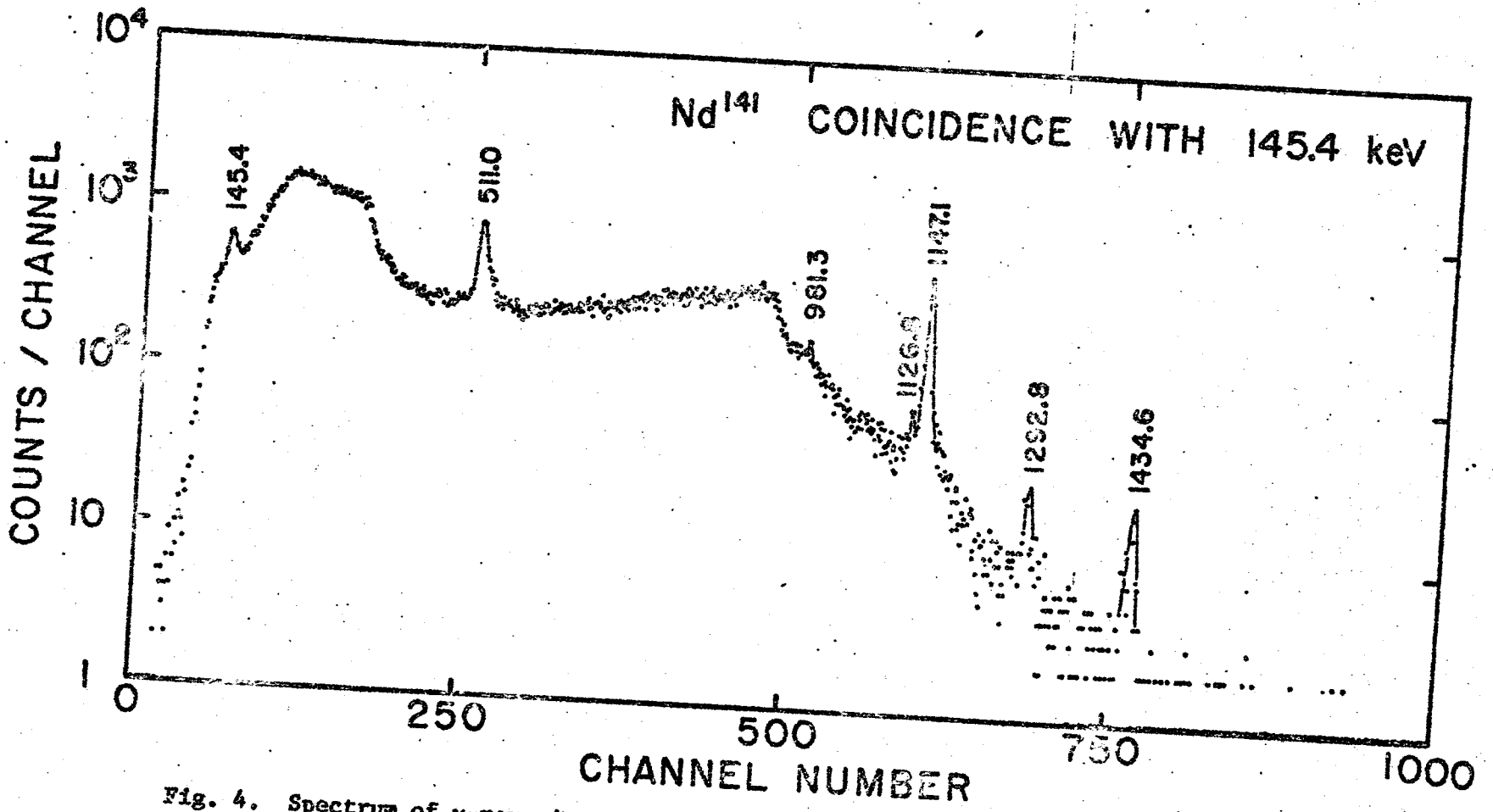

Fig. 4. Spectrum of γ-rays in coincidence with the 145.4-keV γ. The gate detector was a 3-in. × 3-in. NaI(Tl) scintillator, while the signal detector was the 7-cm^3 Ge(Li) crystal.

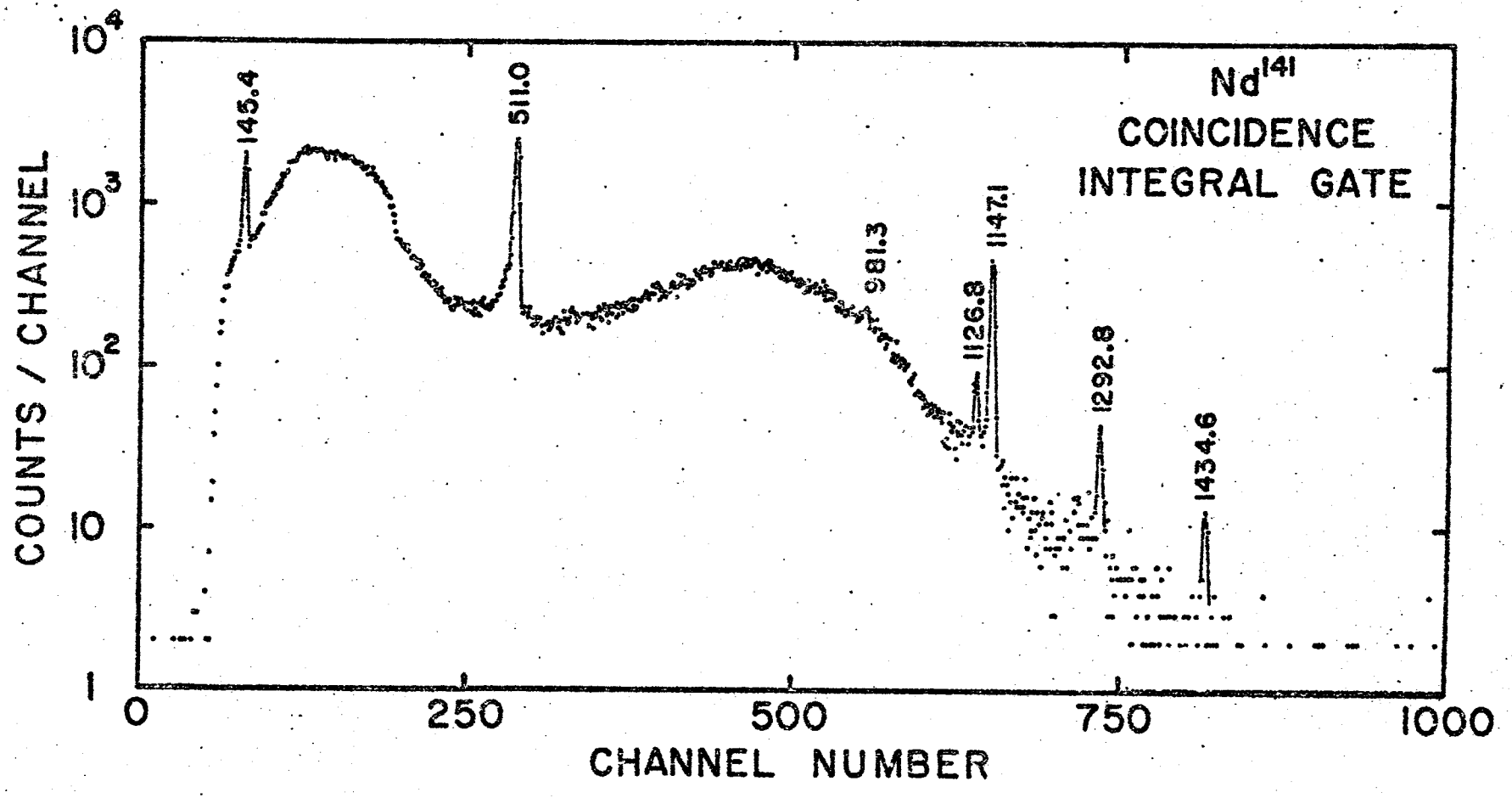

Fig. 5. Integral γ-ray coincidence spectrum. This spectrum was recorded by the 7-cm^3 Ge(Li) detector in coincidence with a 3-in. × 3-in. NaI(Tl) scintillator that was set to accept all γ-rays above 120 keV.

the 7-cm^3 Ge(Li) detector. The single-channel analyzer on the annulus gate was set so that the gate would be active for all gamma rays above 80 keV. The Nd^{141} sources were placed inside the annulus tunnel and on top of the Ge(Li) detector. An additional 3-in. × 3-in. NaI(Tl) anti-coincidence detector was placed in the tunnel above the sources and the Ge(Li) detector to reduce further the sharp Compton edges formed by backscattering in the Ge(Li) detector. The resulting anti-coincidence spectrum is shown in Figure 6. The intensities of all ten of the Nd^{141} gamma rays, which were seen in this spectrum, are included in Table 2. Only four of these gamma rays, the same four indicated by the other coincidence experiments, appear to be in coincidence with another gamma ray because of the large reductions in their intensities as compared with the intensities from the singles spectra.

3.1.4. Nd^{141m} Gamma Ray Spectra

The energy of the 60-sec Nd^{141m} isomeric transition to the ground state was measured to be 756.5±0.3 keV, in excellent agreement with the recent work of Geiger and Graham (46), who obtained 756.8±1.3 keV. A search was also conducted for gamma rays resulting from direct electron-capture transitions from Nd^{141m} to states of Pr^{141} and/or from alternate transitions depopulating Nd^{141m} to Nd^{141g}. Approximately 1 min after a 10-sec bombardment of Pr_2O_3 with the 9-MeV protons, a 59-sec count of the Nd^{141m} ($+Nd^{141g}$) spectrum was stored in the first quadrant of an analyzer having 4096 channels of memory. The Nd^{141m} ($+Nd^{141g}$) source was gradually moved toward the Ge(Li) detector during this time in order to maintain the

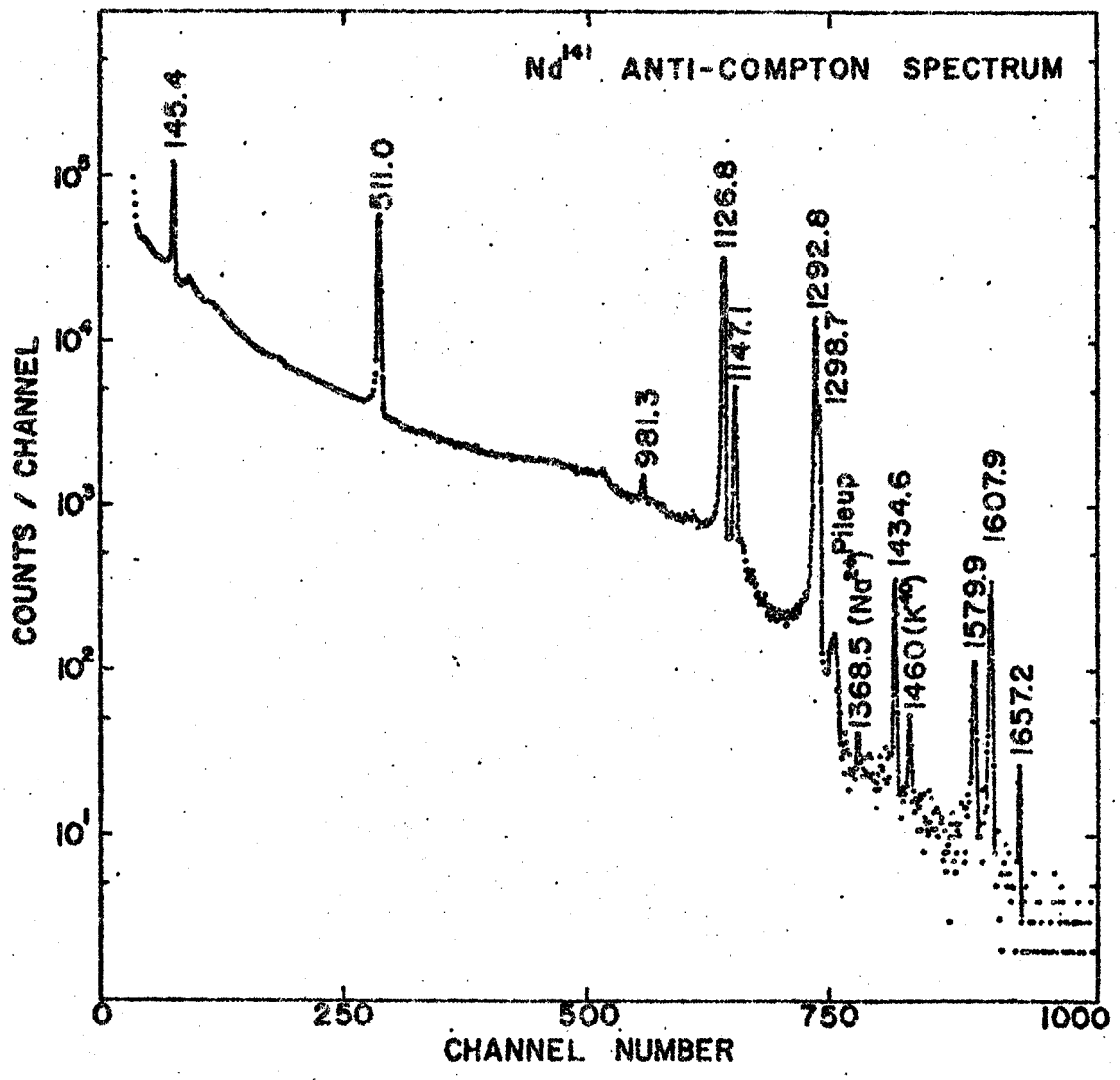

Fig. 6. Anti-coincidence spectrum recorded by the 7-cm^3 Ge(Li) detector when placed inside the tunnel of an 8-in. × 8-in. NaI(Tl) split annulus with a 3-in. × 3-in. NaI(Tl) detector at the other end of the tunnel. For details, see the text or reference 19.

analyzer dead time at approximately a constant 12%; this procedure allowed the data to be collected more rapidly than with a fixed source position. Following intervals of ~1 sec for switching analyzer quadrants, 59-sec counts were stored successively in the three remaining quadrants. The entire process was performed 60 times to reduce statistical errors and to search carefully for weak gamma rays.

The resulting four spectra, each representing 59 min of counting time, are shown in Figure 7. The 756.5-keV gamma is clearly the only observable gamma ray that decays with a 60-sec half-life. The other gamma rays in Figure 7 are the three most intense Nd^{141g} decay transitions. From these spectra, an upper limit of 0.1% of the 756.5-keV gamma intensity was placed on any gamma ray with an energy between 130 and 2600 keV following direct electron-capture transitions from 11/2- Nd^{141m} to high-spin states in Pr^{141}; the same limit applies to alternate transitions to lower-lying states in Nd^{141}.

3.1.5. Decay Scheme and Discussion

The decay scheme that was deduced from the foregoing measurements is shown in Figure 8. Transition energies and excited state energies are given in keV, the β^+ energy coming from the work of Biryukov and Shimanskaya (28). The β^+/ε ratio for decay to the Pr^{141} ground state (also the limits placed for decay to the 145.4-keV state) is a calculated value, using the method of Zweifel (47). The other transition intensities, both for electron-capture and for the (total) electromagnetic transitions, are adjusted to this value and read in percent of the total Nd^{141} disintegrations. Using the measured value

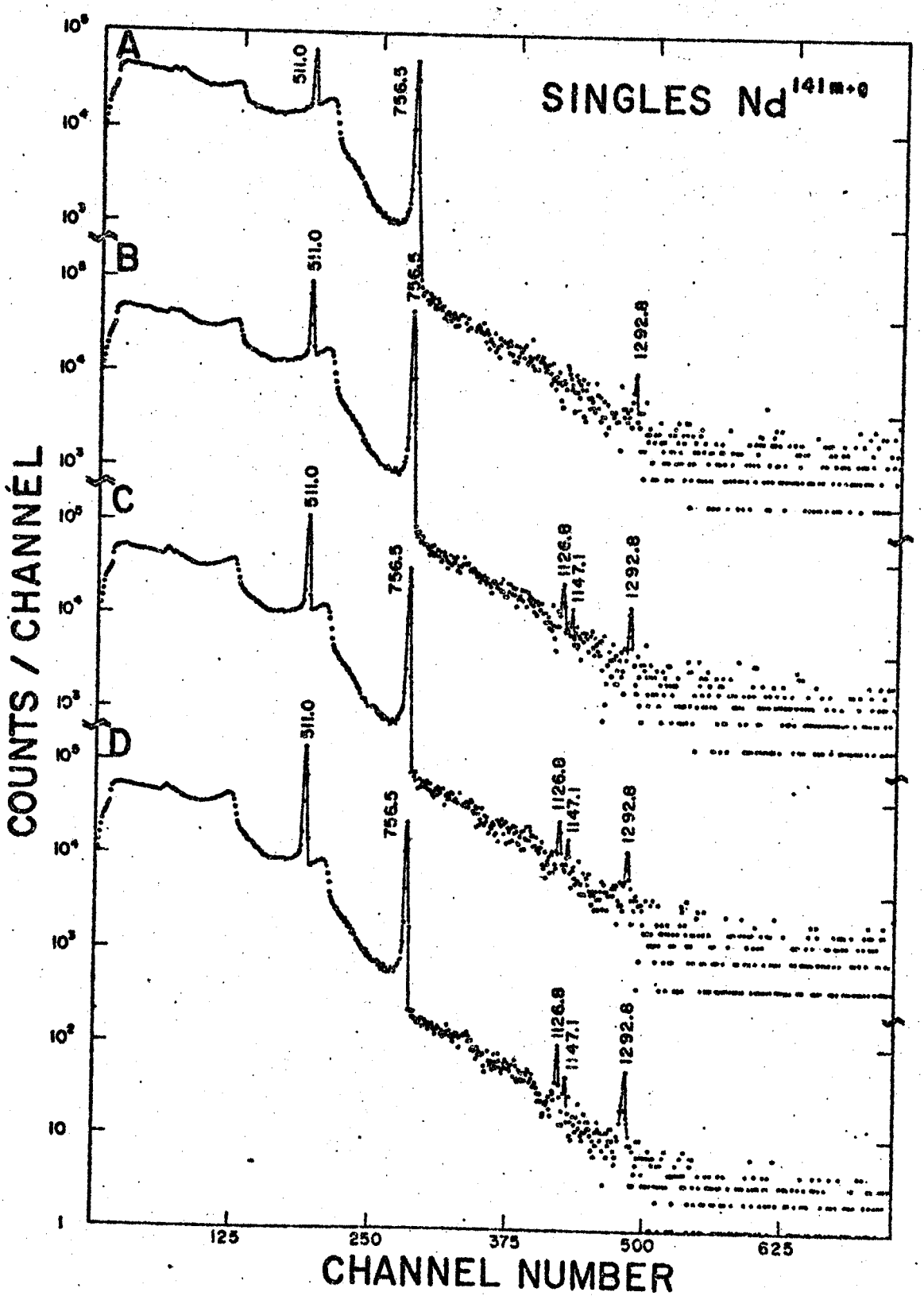

Fig. 7. Singles γ-ray spectra of Nd^{141m} + Nd^{141g}. A) The spectrum from the sum of 60 runs, each started ≈1 min after a 10 sec activation and lasting 59 sec. B) Same, except started 60 sec later. C) 120 sec later. D) 180 sec later.

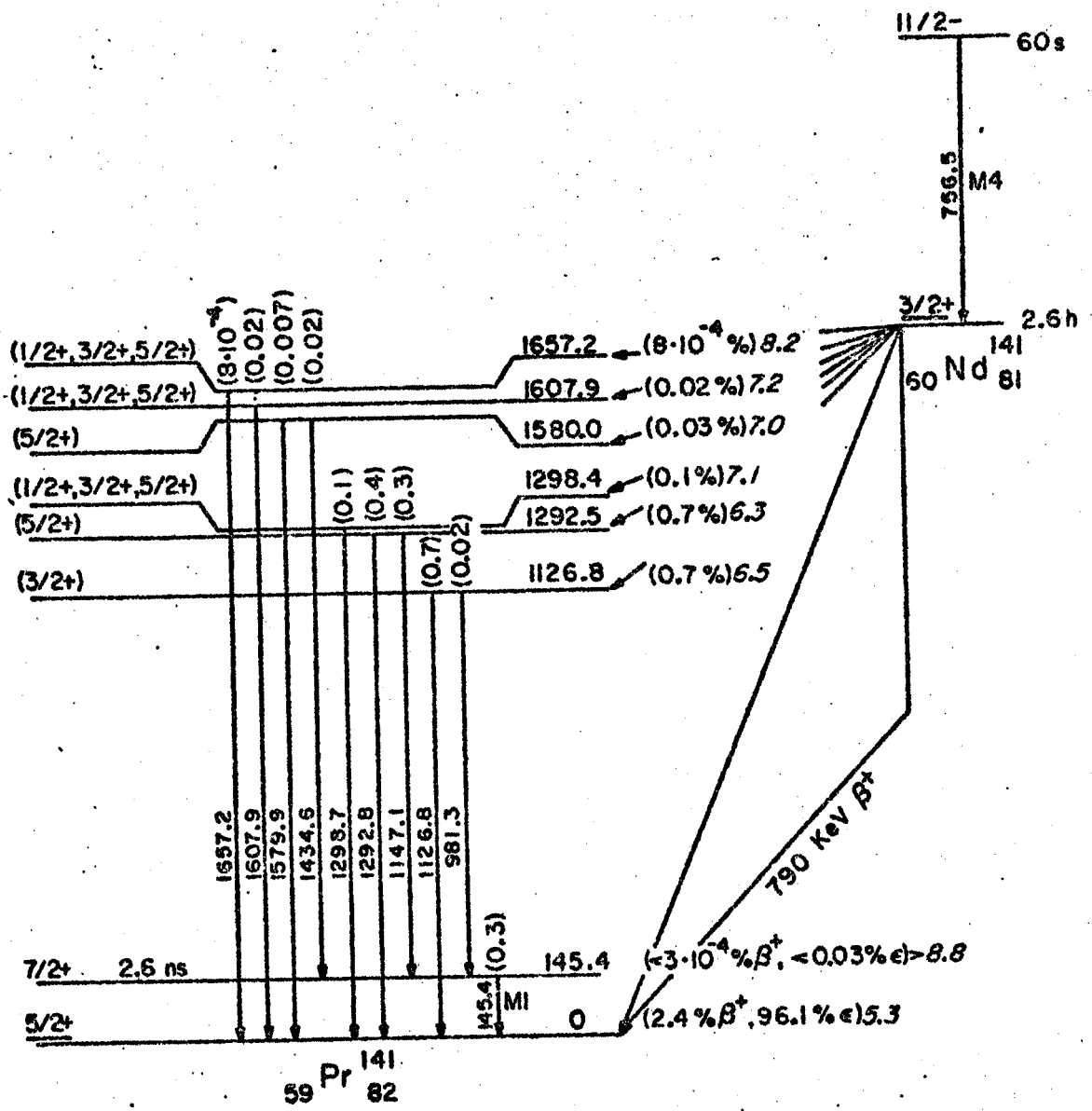

Fig. 8. Decay scheme of Nd^{141g+m}. Excited-state and γ-ray energies are given in keV. The intensities of all transitions are total transition intensities and are given in per cent of the total Nd^{141g} disintegrations. Log *ft* values are based on a 2.6-hr half-life. The spin and parity assignments to the upper six states in Pr^{141} are tentative; see text.

of 9.6 for the intensity ratio of K x-rays to 511-keV gamma rays, which is in good agreement with that measured by Biryukov and Shimanskaya (28), and making reasonable assumptions about the K fluoresence yield and the ratio of K capture to capture from higher shells (see, e.g., reference 23), values of 4.3% β^+ and 94.3% ε were obtained. However, since this is quite clearly an allowed transition, there appears to be at least as much uncertainty in the experimental value as in the theoretical value of β^+/ε. The theoretical value was adopted since any needed future adjustments could be made more easily with respect to it. The log ft values were calculated on the basis of a 2.6-hr half-life (28) for Nd^{141}.

The 981.3-, 1298.7-, 1434.6-, 1579.9-, 1607.9-, and 1657.2-keV transitions have not been previously reported in decay schemes. The energy of the 145.4-keV state in Pr^{141} has been well calibrated from Ce^{141} decay (40), the photon energy being given as 145.43-keV. The evidence for the 1126.8- and 1292.5-keV states, as well as the new state at 1580.0 keV, is based both on the coincidence results with the 145.4-keV gamma and the enhancement of the 1126.8-, 1292.8-, and 1579.9-keV gamma rays in the anti-coincidence experiment, indicating that they are ground-state transitions. The energies of these states were chosen on the basis of the best-defined gamma rays depopulating them, although it can be seen that the cascade energy sum gives excellent agreement with the crossover energy in each case. The placement of states at 1298.4, 1607.9, and 1657.2 keV is based on the enhancement of the respective gamma rays in the anti-coin-

cidence experiment and the fact that these gamma rays were suppressed in both coincidence experiments. No evidence was seen for the state at 880 keV reported by Cybulska and Marquez (27).

The ground-state spins of both Nd^{141} and Pr^{141} have been measured by atomic beam methods, that of the former (48) being 3/2 and of the latter (49) being 5/2. In shell-model terms, Nd^{141} is predicted to be a $(d_{3/2})^{-1}$ neutron state, while the ground state of Pr^{141} should be a $d_{5/2}$ proton state outside a closed $g_{7/2}$ proton subshell. Thus, 98.5% of the Nd^{141} disintegrations consist of its 3/2+ ground state populating the Pr^{141} 5/2+ ground state directly, and the log ft value of 5.3 is about what one would expect for an allowed transition between such similar states.

Now, the 145.4-keV transition in Pr^{141} has been well characterized (40) from Ce^{141} decay as an ℓ-forbidden $M1$ with an $E2$ admixture of 0.4±0.3% having a mean life of 2.63±0.10 ns. The state itself is presumed to have a $(g_{7/2})^{-3}(d_{5/2})^{6}$ configuration. This configuration forms the ground state of Pr^{143} and the 5/2+ state in this nucleus (50,51) is placed at 57 keV, so the 5/2+ and 7/2+ states cross over between Pr^{143} and Pr^{141}. The 7/2+ 145.4-keV state in Pr^{141} would not be expected to receive observable direct population from $3/2^{+}$ Nd^{141g}, again in accord with the measurements reported here.

Considering that Pr^{141} is a single closed shell nucleus one encounters unexpected difficulties in characterizing its higher-lying states. Basically, the problem is as follows: Pr^{141} can be considered to be a single proton outside a Ce^{140} even-even core, so

one is tempted to use the core-coupling model in describing the Pr^{141} higher-lying states. Ce^{140}, with a closed neutron shell and a closed $g_{7/2}$ proton subshell, is expected to be rather rigid and not subject to low-lying vibrations. This appears to be true, for its first excited state is a 2+ state at 1.596 MeV that decays via a non-enhanced $E2$ transition (52). Currie (53), in trying to account for the retardation of the $E2$ transition from a 4+ level at 2.083 MeV to this level, applied a quasi-particle representation for both states, but his best numerical results implied a $[(g_{7/2})(d_{5/2})]_{2+}$ configuration instead of the anticipated (and probably more likely) $[(g_{7/2})^2]_{2+}$ or perhaps $[(d_{5/2})^2]_{2+}$. This means that, although the Ce^{140} 2+ state does appear to be a two quasi-particle state, its exact structure is not clear.

On the other hand, the first excited state of Ce^{142}, having only two additional neutrons, lies at 0.65 MeV and appears to be a 2+ quadrupole vibrational state (54). The first few Pr^{143} excited states, which lie much lower than those in Pr^{141}, can probably be explained by a coupling of the 7/2+ ground state and the 5/2+ 57-keV state to this Ce^{142} 2+ collective state (50,55).

The known Pr^{141} states lie at an intermediate energy, so one cannot decide without further evidence whether they are three quasi-particle states, one quasi-particle states coupled to a vibrational core, or perhaps a mixture of the two. Although the two neutrons of Ce^{142} are probably more effective in softening the Ce^{140} core than is the single proton (outside only a subshell) of Pr^{141}, the $E2$ transition probabilities may or may not be enhanced

over the single-particle estimates. In the following, keeping in mind the different kinds of states possible, tentative predictions are made for the spins and parities of the six upper states on the basis of beta and gamma decay systematics. It must be kept in mind, however, that these are only tentative, and for quite definite assignments one needs more information about the levels. High-resolution scattering reactions of various kinds that populate these states are particularly valuable. A summary of results from some recently published (β,γ), $(n,n'\gamma)$, (n,n'), (He^3,d), and (d,He^3) studies are included in the following subsection.

The log ft values are all more or less in the range expected for allowed transitions. First-forbidden decay cannot be excluded, especially to the highest-lying states, on the basis of the log ft values, but then the only negative parity states would be those resulting from the $h_{11/2}$ shell-model state or from octupole vibrations. The $d_{3/2}$ ground state of Nd^{141} should not populate the former, although the $h_{11/2}$ Nd^{141m} might. The latter have not been reported near this excitation in any of the neighboring even-even nuclei. Thus, all six states are probably 1/2+, 3/2+, or 5/2+. This set is consistent with either interpretation of the states -- by coupling the 5/2+ or 7/2+ single quasi-particle states to a 2+ vibrational core, one can get 1/2+ through 11/2+, with two sets of 3/2+ through 9/2+, and on the basis of three quasi-particles, the range is even broader.

Assignments for the three states that exhibit gamma ray

branching can be narrowed down from the above limits. The intensity ratio of the 1126.8-keV gamma ray to the 981.3-keV gamma from the 1126.8-keV state is 35. The mere existence of the 981.3-keV gamma rules out a 1/2+ assignment, for this would require the 981.3-keV transition to be *M*3. For a 5/2+ assignment, the single-particle estimate (23) yields a ratio (both *M*1's) of less than 2, while for a 3/2+ it predicts a ratio (*M*1/*E*2) of about 200. Even a slight *E*2 enhancement or *M*1 retardation would therefore favor a 3/2+ assignment.

For the 1292.5- and 1580.0-keV states, which have ground-state to cascade transition ratios of 1.33 and 0.35, respectively, the 1/2+ assignment can similarily be eliminated. Unless there is some quite unusual *M*1 retardation or *E*2 enhancement, the 3/2+ spin can also be eliminated, so a 5/2+ assignment is preferred.

The 756.5-keV excited state of Nd^{141} has been shown to have a half-life of 60.3±1.0 sec (46). It is one of the series of $h_{11/2}$ isomers found just below the *N*=82 shell. Since the 11/2- (presumably single quasi-particle $h_{11/2}$) state lies (56) at 822 keV in Pr^{139}, it is possible that the same state lies in the 1-MeV vicinity in Pr^{141} and that there could be come direct population of it from Nd^{141m}. From Figure 5, however, it can be seen that such population must be less than 0.1% of the intensity of the 756.5-keV isomeric gamma ray. Depending on the exact location of the $h_{11/2}$ state in Pr^{141}, this upper limit means simply that the log *ft* for electron capture has to be greater than approximately 6.0. The same upper limit can be placed on any branching gamma

decay to lower states in Nd^{141} itself, if at least one gamma ray having an energy greater than 130-keV is involved.

3.1.6. Comparison with Recent Investigations

After the completion of the present work, some additional publications became available (88,89,90,118). The energy levels and spins proposed in these studies are summarized in Table 2a. A (γ,n) reaction on Nd_2O_3 (enriched to 95% Nd^{142}) was employed to obtain the Nd^{141} parent for the (β,γ) study described in reference 118. The essential features of the Nd^{141} decay scheme proposed there (118) confirm the corresponding features of the decay scheme proposed here. No interpretations were made of the properties of the states.

Although the experimental uncertainties of the reaction energy measurements were relatively large, some common levels are suggested in Table 2a. Probably the 1657.2-keV state corresponds to the 1160 (1645) keV state proposed in reference 90 (88). By incorporating the results of the (He^3,d) study (88), the spins proposed in the present study can be narrowed down for the 1298.4, 1607.9, and 1657.2 keV states to 1/2+, (3/2,5/2)+, and 1/2+, respectively.

Table 2a. Experimentally determined levels and spins of Pr^{141}.

Present Study	Hesse and Wien[a]	van der Merwe et al.[b]		Wildenthal, Auble, Newman and Nolen[c]	Baer and Bardwick[d]
(β,γ)	(β,γ)	$(n,n'\gamma)$	(n,n')	(He^3,d)	(d,He^3)
0[e] [$5/2^+$]	0 [$5/2^+$]	0	0	0[$5/2^+$]	0
145.4[$7/2^+$]	145.4[$7/2^+$]	145	145	145[$7/2^+$]	145
---	---	1118[($7/2^+$,$9/2^+$)]	---	1114[$11/2^-$]	---
1126.8[($3/2^+$)]	1126.8[($5/2^+$)]	1127	1131	---	1130
1292.5[($5/2^+$)]	1292.8[($5/2^+$)]	1293[($5/2^+$)]	---	---	---
1298.4[($1/2^+$,$3/2^+$,$5/2^+$)]	1298.5[($1/2^+$,$3/2^+$)]	1300	1302	1298[$1/2^+$]	1310
---	---	1436	---	---	---
---	---	1452	---	---	---
---	---	1456	1459	---	---
---	---	1493	1498	---	---
---	---	1521	1525	---	---
1580.0[($5/2^+$)]	1579.8	1578	1589	---	---
1607.9[($1/2^+$,$3/2^+$,$5/2^+$)]	1608.7	1607	---	1600[($3/2$,$5/2$)$^+$]	1620
---	---	1650	---	---	---
1657.2[($1/2^+$,$3/2^+$,$5/2^+$)]	---	---	1660	1645[$1/2^+$]	---
---	---	(1695)	---	---	---
---	---	(1705)	---	---	---
---	---	1782	1790	---	---
---	---	1808	---	---	---
---	---	1823	1820	---	---
---	---	1844	1854	---	---

[a]Reference 118.
[b]Reference 90.
[c]Reference 88.
[d]Reference 89.
[e]All energies are listed in keV.

3.2. Decay Schemes of Nd^{139m} and Nd^{139g}

3.2.1. Introduction

One of the most interesting regions of the nuclidic chart for current study is the region just below N=82, for here many systematic examples of rather extreme isomerism can be observed. The neutron-deficient side of the A=139 decay chain extends into this region, and its members are well suited for probing the region because nuclei rather far removed from β-stability are reached not too far below the closed shell. Thus, many interesting states should be populated by their decay, and these states should still be amenable to explanation in relatively straightforward shell-model terms -- the number of nucleons making substantial contributions to a given configuration should not be so large as to be completely unmanageable.

$_{58}Ce^{139}_{81}$ is the first radioactive member on this side of the chain, and it decays directly to stable La^{139} with a Q_ε of only 270 keV and a half-life of 140 d; it has a very simple decay scheme that has been known for a long time (57). It does, however, have an interesting $h_{11/2}$ isomeric state (746 keV; $t_{\frac{1}{2}}$ = 55 sec), a member of the extensive N=81 series. The decay of the second radioactive member, 4.5-h $_{59}Pr^{139}_{80}$, to Ce^{139} is considerably more complex; the results on this decay scheme are published elsewhere (16).

$_{60}Nd^{139}_{79}$ is three beta decays from stable La^{139} and has a rather large amount of energy available for β-decay (Q_ε = 2.8 MeV; cf. below). As in other N=79 odd-mass isobars, the $h_{11/2}$-$d_{3/2}$

(metastable-ground state) separation is fairly small, making the *M4* isomeric transition quite slow. This means that here one is presented with two dissimilar isomers decaying almost independently, and because each can populate reasonably high-lying states in Pr^{139}, a wealth of information about many quite different states in this daughter nucleus is available from the study of these decays.

Nd^{139m} was first observed by Stover (58) in 1950 as part of an investigation of the products of bombardment of Pr^{141} with 40- and 50-MeV protons. Chemical identification was performed by ion exchange, and the mass number was established with reference to the granddaughter, Ce^{139}. The half-life was measured to be 5.5±0.2 h.

Later studies (59,60) of conversion electron intensities and energy differences for a 231-keV transition accompanying this decay indicated it to be an *M4* and to originate in Nd not Pr. Four neighboring odd-mass isobars with 79 neutrons were known (6) to have isomeric states involving an 11/2- → 3/2+ transition. From the trends in the isomeric level energies and in the reduced transition probabilities, Gromov and his co-workers concluded that here we have a like pair of states (59) and that the 5.5-h activity was the 11/2- metastable state.

The 3/2+ ground state was not seen so easily, and its half-life was only recently measured (61) to be 29.7±0.5 min. For that experiment it was produced by bombarding Pr^{141} with 30- and 33-MeV deuterons.

The only previous studies of Nd^{139m} decay (56,60) resulted in rather sketchy decay schemes containing serious disagreements.

Because of this and the absence of any decay scheme for Nd^{139g}, it was felt that this would make a good system for investigation. This study has indicated the presence of 51 gamma rays accompanying Nd^{139m} decay and 21 that follow Nd^{139g} decay. Of these gamma-rays, 56 have been placed in decay schemes containing a total of 22 excited states. Fourteen of these states have not been seen before.

The decay scheme of Nd^{139g} turns out to be unexceptional, having much in parallel with the decay scheme of Nd^{141} (seen in Figure 8) and some other nuclei in this region below N=82. The low-spin states that it populates in Pr^{139} can be characterized reasonably well and follow expected systematics. On the other hand, the decay scheme of Nd^{139m} is anything but standard. This high-spin isomer decays only 12.7% by the 231.2-keV isomeric transition, the rest being by β^+/ε to mostly high-spin, high-lying states in Pr^{139}. Six of these, between 1624.5 and 2196.7 keV, are populated by decay that is less hindered (log ft's between 5.5 and 6.3) than the decay to an $h_{11/2}$ isomeric state at 821.9 keV in Pr^{139} (log ft=7.0), which is almost certainly an allowed transition. This would seem to indicate that the transitions to these six states are also allowed, which would imply odd-parity states.

This is interpreted as the configuration of Nd^{139m} being peculiarly suited for populating a multiplet of three-quasiparticle states. During the explanation, the problem associated with multiple particle rearrangements in beta and gamma decay is discussed.

3.2.2. Source Preparation

The 5.5-h Nd^{139m} activity was produced for most of the experiments by the relatively clean $(p,3n)$ reaction on 100% abundant Pr^{141}. Targets of 99.999% pure (62) Pr_2O_3 were bombarded typically for ≈1 h with ≈2-μA of 29-MeV protons from the Michigan State University sector-focused cyclotron. Sources were allowed to decay for about five hours to let the 30-min Nd^{139g} produced by the bombardments reach transient equilibrium with Nd^{139m}. Experiments were then performed with the sources for approximately twenty hours, until the Pr^{140} produced by the 3.3-d decay of Nd^{140} became a significant contaminant.

From crude excitation function studies of reactions following the bombardment of Pr^{141} with protons of various energies, it was possible to distinguish the Nd^{139m+g} activities from weak contaminant activities. Following each bombardment with 29-MeV protons, it was possible to identify every contaminant peak observed in spectra recorded between 20 min and 40 h after the end of the bombardment. These weak contaminants, roughly in decreasing order of importance, were Pr^{140}, Pr^{139}, Ce^{139}, Nd^{141}, and Pr^{142}. It is significant that no 22-min Nd^{138} was produced, for its daughter, 2.1-h Pr^{138}, could prove a troublesome contaminant.

Nd^{139m} sources were also produced following the bombardments of Nd^{142} with 36-MeV τ's (He^3 ions) and of Pr^{141} by 48- and 60- MeV τ's, all from the MSU cyclotron. These reactions were not so clean as the $(p,3n)$ reaction on Pr^{141}, but they confirmed the relative intensities of the Nd^{139m} gamma rays.

Most of the Nd^{139g} sources were produced by bombarding similar Pr_2O_3 targets with 29-MeV protons for ≈45 sec. Experiments were carried out immediately upon concluding each of the bombardments, and the gamma rays resulting specifically from Nd^{139g} decay were followed as their intensities dropped from their initial values to those when Nd^{139g} was in transient equilibrium with Nd^{139m}.

The relative intensities of all the Nd^{139g} gamma rays which were observed were confirmed by measurements of the activity produced by 48- and 60- MeV τ's on Pr^{141}. These reactions would produce Pm^{139}, which, were it a low-spin nucleus as anticipated, would populate Nd^{139g} by β-decay much more strongly than Nd^{139m}. They did in fact yield Nd^{139g}/Nd^{139m} isomer ratios some 30 times as large as the $(p,3n)$ reaction Pr^{141}, but they yielded many more interfering short-lived activities as well.

3.2.3. Experimental Results for Nd^{139m}

3.2.3.A. --Gamma Ray Singles Spectra-- A 7-cm^3 five-sided coaxial Ge(Li) detector manufactured (18) in this laboratory was employed to determine the energies and intensities of the Nd^{139m} gamma rays. The wall thickness of the evacuated aluminum can enclosing the detector was 0.16 cm. Under typical operating conditions, a resolution of ≈2.5 keV FWHM for the 661.6-keV gamma of Cs^{137} was obtained, using a room temperature FET preamplifier, a low-noise RC linear amplifier with pole-zero compensation, and a 4096-channel analyzer or ADC coupled to a computer.

Energies of the prominent Nd^{139m} gamma rays were measured by

counting the Nd^{139m} sources simultaneously with several well-known calibration sources. To determine the energy calibration curve, a least-squares fit of the photopeak centroids of the calibration transitions to a quadratic equation was used after the background had been subtracted from under the peaks. The background correction for each peak was made by fitting a linear equation to several channels adjacent to both sides of the peak and then subtracting. The energies of the lower-intensity Nd^{139m} gamma rays, which were obscured by the calibration standards, were then determined similarly by using the stronger Nd^{139m} gamma rays as the standards. Some gamma ray singles spectra are shown in Figures 9a and 9b.

The spectrum shown in Figure 9b was used to place an upper limit of 0.1% of the disintegrations of Nd^{139m} on any gamma transition with an energy above 2300 keV. This would appear to rule out the 2350- and 2500-keV gamma rays proposed earlier (6,56) to have intensities ≈50 times as large as the present upper limit. The events observed above 2300 keV in Figure 9b come from long-lived room backgrounds that were not subtracted out.

The contaminant peaks seen in Figure 9a accompany the reaction, $Pr^{141}(p,2n)Nd^{140}\xrightarrow{\varepsilon}Pr^{140}$, and Pr^{139} and Ce^{139} disintegrations following Nd^{139m+g} decay. Their energies, relative intensities, and intensity changes as functions of time were seen to be consistent with the properties of the associated decay schemes established in this study and elsewhere (6,63-67).

A summary of the Nd^{139m} gamma ray energies and relative in-

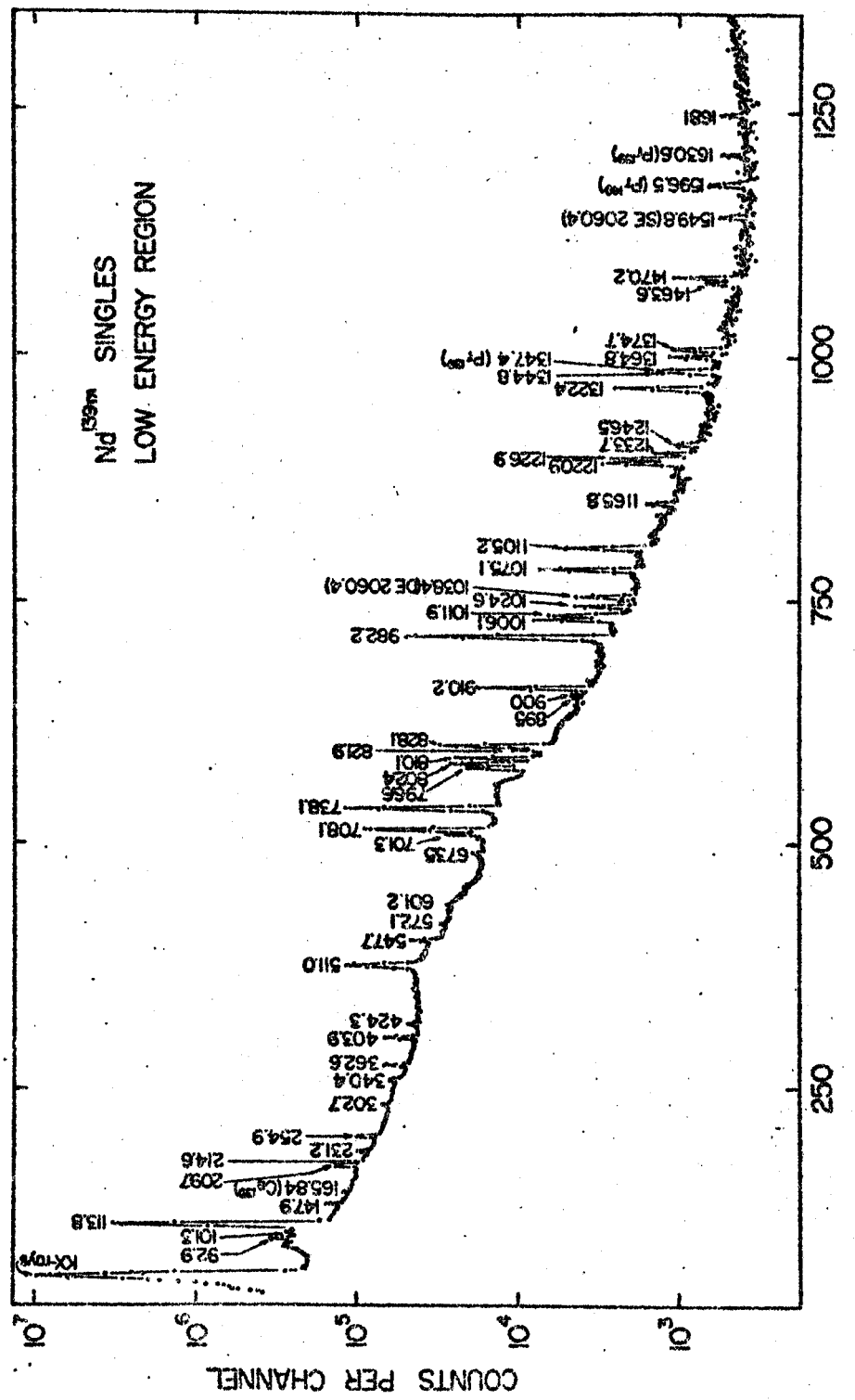

Fig. 9a. Nd^{139m} singles γ-ray spectrum taken with a 7-cm^3 Ge(Li) detector — low-energy portion. This spectrum was accumulated for a 1-day period, using multiple bombardments to obtain optimum sources. Because of analyzer spillover, the portion of the spectrum below ≈120 keV was recorded for a shorter period of time and then normalized to the remainder of the spectrum.

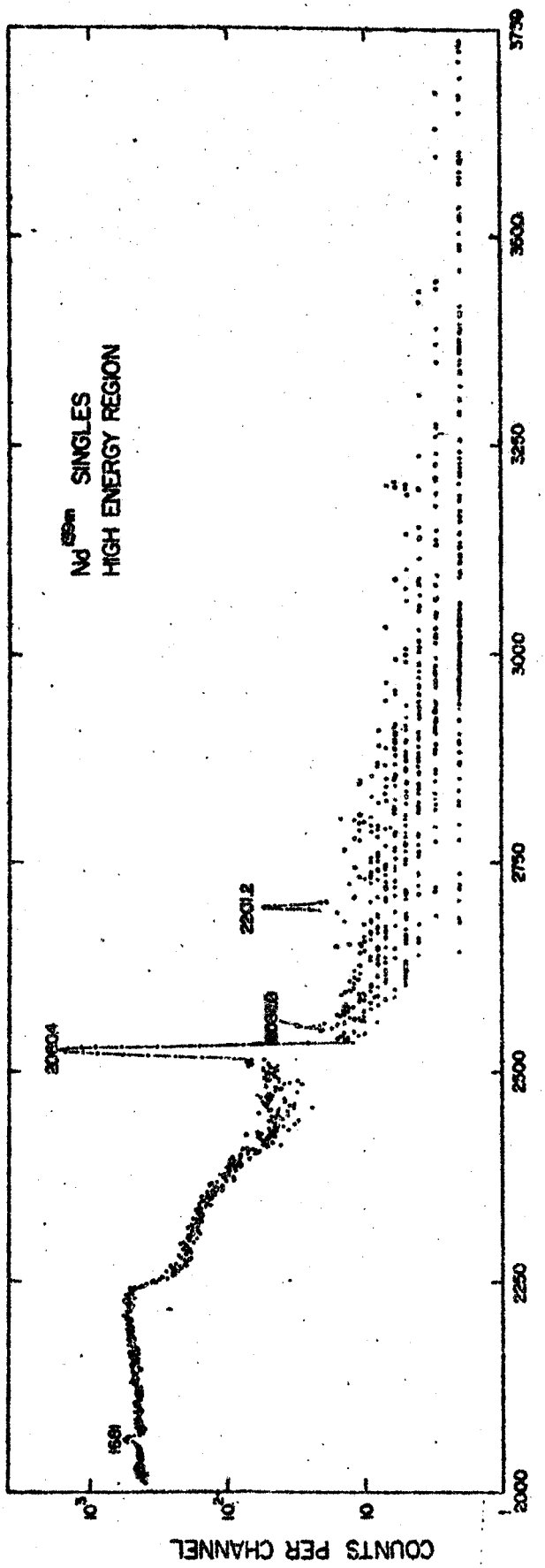

Fig. 9b. Nd^{139m} singles γ-ray spectrum taken with a 7-cm^3 Ge(Li) detector — high-energy portion. The events above 2300 keV come primarily from room background. From this spectrum an upper limit of 0.1% was placed on any transition with an energy greater than 2300 keV.

tensities is given in Table 3. The energies assigned are mean values taken from a number of different measurements recorded at different times, different locations, with different system components, and with different parameters. Corresponding energy uncertainties are based on the reproducibilities of the Nd^{139m} energies from the calibration curves, the sizes of the Nd^{139m} photopeaks both before and after background subtraction, and the quoted errors on the standard energies (68). The relative gamma ray intensities listed in Table 3 are also averages from a number of runs and were obtained using experimentally determined efficiency curves (cf. section 3.1.3.A). Associated with these intensities are statistical uncertainties that include estimated uncertainties in the underlying backgrounds.

3.2.3.B. --Gamma Gamma Coincidence Studies-- Coincidence and anti-coincidence experiments were performed using Ge(Li)-NaI(Tl) spectrometers. For the first experiment, in order to determine which gamma rays appear in cascades and which come primarily from ε-fed ground-state transitions, and 8-in. × 8-in. NaI(Tl) split annulus detector was employed in an anti-coincidence experiment with the 7-cm^3 Ge(Li) detector (19). The Nd^{139m} source was inserted into the center of the annulus tunnel, which was then blocked by a 3-in × 3-in. NaI(Tl) detector at one end and by the Ge(Li) detector at the other end. By including the 3-in. × 3-in. NaI(Tl) detector in anti-coincidence with the Ge(Li) detector, the Compton edges from backscattering in the Ge(Li) detector were reduced over what they would have been with only the annulus in anti-coincidence.

Table 3. Energies and relative intensities of gamma rays present in the decay of Nd^{139m}.

Measured γ-ray energy (keV)	Relative intensity	Measured γ-ray energy (keV)	Relative intensity
92.9±0.2	3.2± 0.6	828.1±0.2	29 ± 2
101.3±0.8	0.7± 0.2	851.9±0.5[b]	1.4± 0.4[b]
113.8±0.1	133 ±25	895.1±0.6	0.8± 0.2
147.9±0.1	2.5± 0.5	900.3±0.6	1.1± 0.3
209.7±0.1	6.2± 0.6	910.2±0.2	21.6± 2
214.6±0.2	1.4± 0.4	982.2±0.2	79 ± 2
231.2±0.2	2.4± 0.2	1006.1±0.2	9.5± 0.7
254.9±0.3	3.7± 0.6	1011.9±0.2	8.0± 0.6
302.7±0.3	1.4± 0.2	1024.6±0.3	3.6± 0.4
340.4±0.5	2.7± 0.5	1075.1±0.2	9.6± 1
362.6±0.2	6.2± 0.5	1105.2±0.2	7.4± 0.4
403.9±0.3	8.0± 1.0	1165.8±0.5	1.0± 0.5
424.3±0.3	2.0± 0.4	1220.9±0.3	5.0± 0.5
511.0(γ±)	3.2± 2.8[a]	1226.9±0.3	4.0± 0.4
547.7±0.3	7.5± 0.7	1233.7±0.5	0.8± 0.4
572.1±0.5	1.7± 0.4	1246.5±1.0	0.9± 0.4
601.2±0.8	1.3± 0.4	1322.4±0.3	7.0± 0.9
673.5±0.5	2.5± 0.7	1344.8±0.6	1.3± 0.4
701.3±0.3	13 ± 2	1364.8±0.6	1.7± 0.6
708.1±0.1	72 ± 2	1374.7±0.5	1.8± 0.5
733 ±1 [b]	1.0± 0.6[b]	1463.6±0.5	1.0± 0.3
738.1±0.2	≡100	1470.2±0.3	2.0± 0.5
796.6±0.3	13 ± 2	1680.7±0.8	0.8± 0.2
802.4±0.3	21 ± 2	2060.4±0.2	15.5± 1.0
810.1±0.3	18 ± 2	2085.0±0.5	0.1± 0.05
821.9±0.3	3.7± 0.4	2201.2±0.8	0.3± 0.1

[a]Calculated from the decay scheme proposed later in the present study. Components of the observed annihilation photon intensity from Nd^{139g} and/or Pr^{139} decay always exceed the Nd^{139m} component.

[b]Seen in coincidence spectra only. The intensities given here are inferred from the completed decay scheme and the behavior of these photons in the coincidence spectra.

The single-channel analyzers associated with the NaI(Tl) detectors were set to accept all gamma rays above 80 keV. A resolving time (2τ) of ≈100 ns was used, and the true-to-chance ratio was usually ≈100/1. The resulting spectrum is shown in Figure 10.

The 231.2- and 821.9-keV gamma ray peaks seen here were enhanced in the anti-coincidence experiments (relative to their singles intensities) far more than were any of the other Nd^{139m} transitions, as indicated in Table 4. Thus, each of the other Nd^{139m} gamma rays appeared to be involved in one or more coincidences with ≥80-keV photons. The following coincidence experiments elucidated most of these cascades.

A coincidence spectrum gated by the split annulus detector on the 113.8-keV gamma is shown in Figure 11. The gamma ray intensities seen in this experiment, normalized to 100 for the 738.1-keV gamma intensity, are listed in Table 4. Four gamma intensities are reduced by factors of about 10, viz., the 796.6-, 828.1-, 1006.1-, and 1220.9-keV gamma rays, whereas several other prominent peaks appear to be in coincidence with the intense 113.8-keV gamma. These results are indicated in Table 5.

Figures 12 and 13 show the spectra resulting from gating this same spectrometer on two adjacent energy intervals, 680-720 and 720-760 keV. Because the resolution of the annulus in these experiments was only ≈13%, there was considerable overlap between these gated regions; however, as can be seen in Figure 9a a single gamma ray dominates each region, so a comparison of the intensities observed in coincidence with these adjacent gated regions was quite

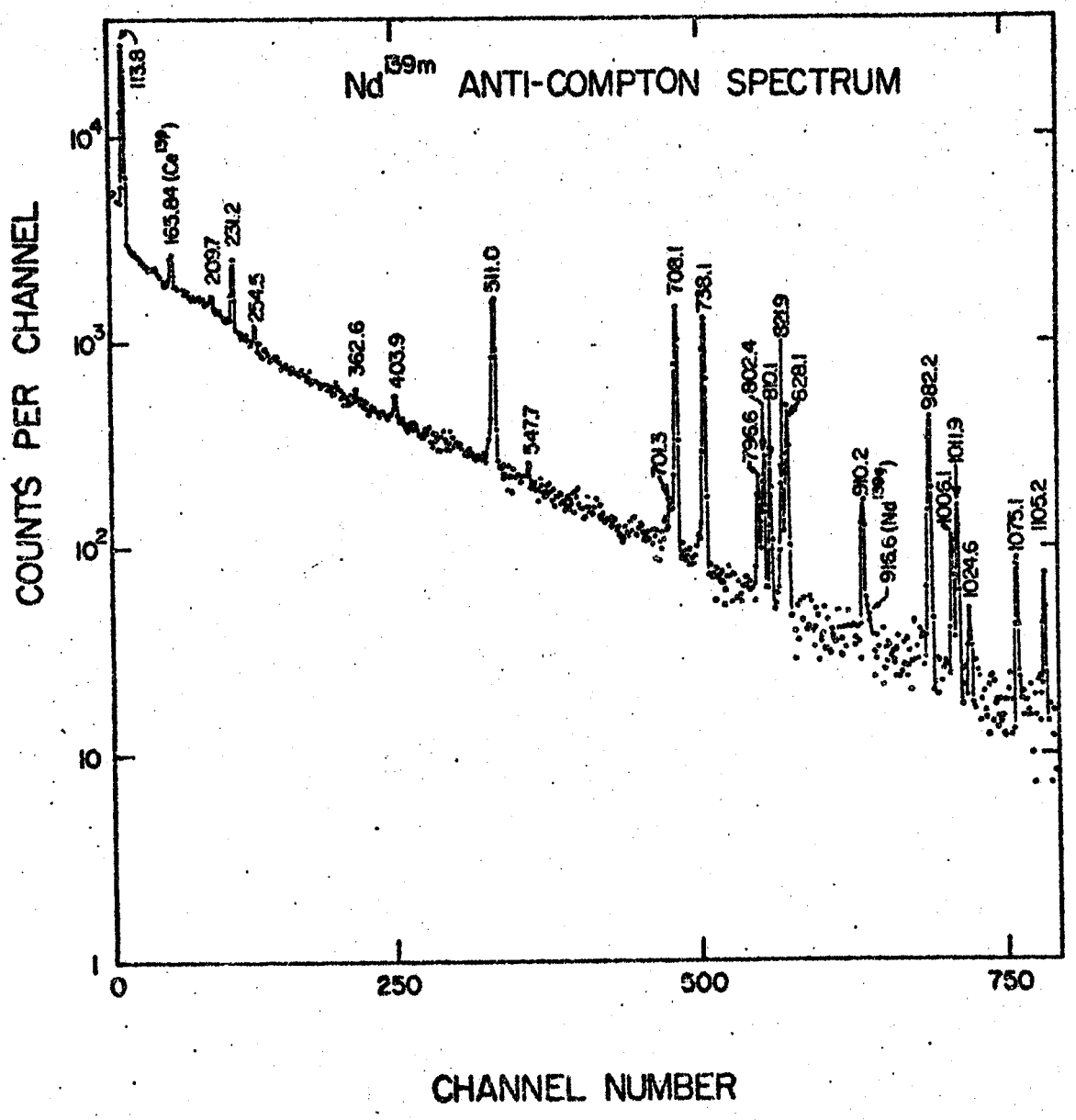

Fig. 10. Nd^{139m} anti-coincidence spectrum recorded by the 7-cm^3 Ge(Li) detector when placed inside the tunnel of an 8-in. × 8-in. NaI(Tl) split annulus, with a 3-in. × 3-in. NaI(Tl) detector at the other end of the tunnel. For details, see the text or reference 19. Characteristic of this type of spectrum is the noticeable absence of Compton edges. The 231.2-keV γ is the only γ-ray enhanced over its singles intensity.

Table 4. Relative intensities of photons in the decay of Nd^{139m} observed in coincidence experiments.

Energy (keV)	Relative intensity[a]					
	Singles spectra	Anti-coincidence spectrum	113.8-keV γ-γ coinc. spectrum	113.8-keV γ-γ delayed coinc. spectrum	662-722 keV γ-γ coinc. spectrum	722-780 keV γ-γ coinc. spectrum
92.9	3.2	---	---	0.4	---	---
113.8	133	13	---	40	---	---
147.9	2.5	---	---	5	---	---
209.7	6.2	0.3	---	14	---	---
214.6	1.4	---	---	3	1.6	3.4
231.2	2.4	≡2.4[b]	---	<1.5	<1	<1
254.9	3.7	0.5	---	8.0	12	6.1
302.7	1.4	---	---	1.8	6.4	9.7
340.4	2.7	---	---	<0.6	<10	12
362.6	6.2	0.3	8	1.3	24	36
403.9	8.0	1.1	6	9.4	62	34
424.3	2.0	---	1	1.8	5.5	15
547.7	7.5	1.0	4	≡7.5	33	18
572.1	1.7	---	1	1.1	<4	16
601.2	1.3	---	2	<0.7	<6	<6
673.5	2.5	---	2	2.0	20	8
701.3	13	0.8	10	11	56	43
708.1	72	13	70	0.6	51	70
733	1.0	---	---	---	---	4
738.1	≡100	13	≡100	1.3	≡100	≡100
796.6	13	1.7	2	<1	18	48
802.4	21	2.3	14	18	98	60
810.1	18	2.4	17	<1	19	9.7
821.9	3.7	2.2	0.8	<1	<8	<8

Table 4. (continued)

828.1	29	5.7	3	0.9	35	103
851.9	1.4	.4	---	<1	---	---
895.1	0.8	---	---	---	6	3
900.3	1.1	---	---	---	8	6
910.2	21.6	2.2	22	---	22	81
982.2	79	6.9	78	<1	285	461
1006.1	9.5	2.0	1	<1	11	40
1011.9	8.0	2.3	7	7.8	54	24
1024.6	3.6	0.5	4	<0.8	6.1	3
1075.1	9.6	1.8	9	<1	34	54
1105.2	7.4	1.4	4	6.6	43	27
1220.9	5.0	1.4	<1	<1	5.5	22
1226.9	4.0	0.6	2	4.7	21	12
1233.7	0.8	---	---	---	5	---
1322.4	7.0	1.6	5	<1	25	34
1344.8	1.3	---	0.8	<0.6	11	11
1364.8	1.7	---	1	0.9	10	6
1374.7	1.8	---	---	1.4	10	<8
2060.4	15.5	---	22	<5[c]	---	---
2085.5	0.1	---	0.2[d]	---	---	---

[a]All relative intensities from the coincidence runs are normalized with the aid of the singles spectra relative intensities listed here.

[b]This isomeric transition in Nd^{139} was the only transition seen which was not seen in coincidence with at least one other photon, thus it was used for normalization here.

[c]Limit placed on basis of absence of double excape peak and Compton background from the 2060.4-keV γ-ray.

[d]Only two counts observed.

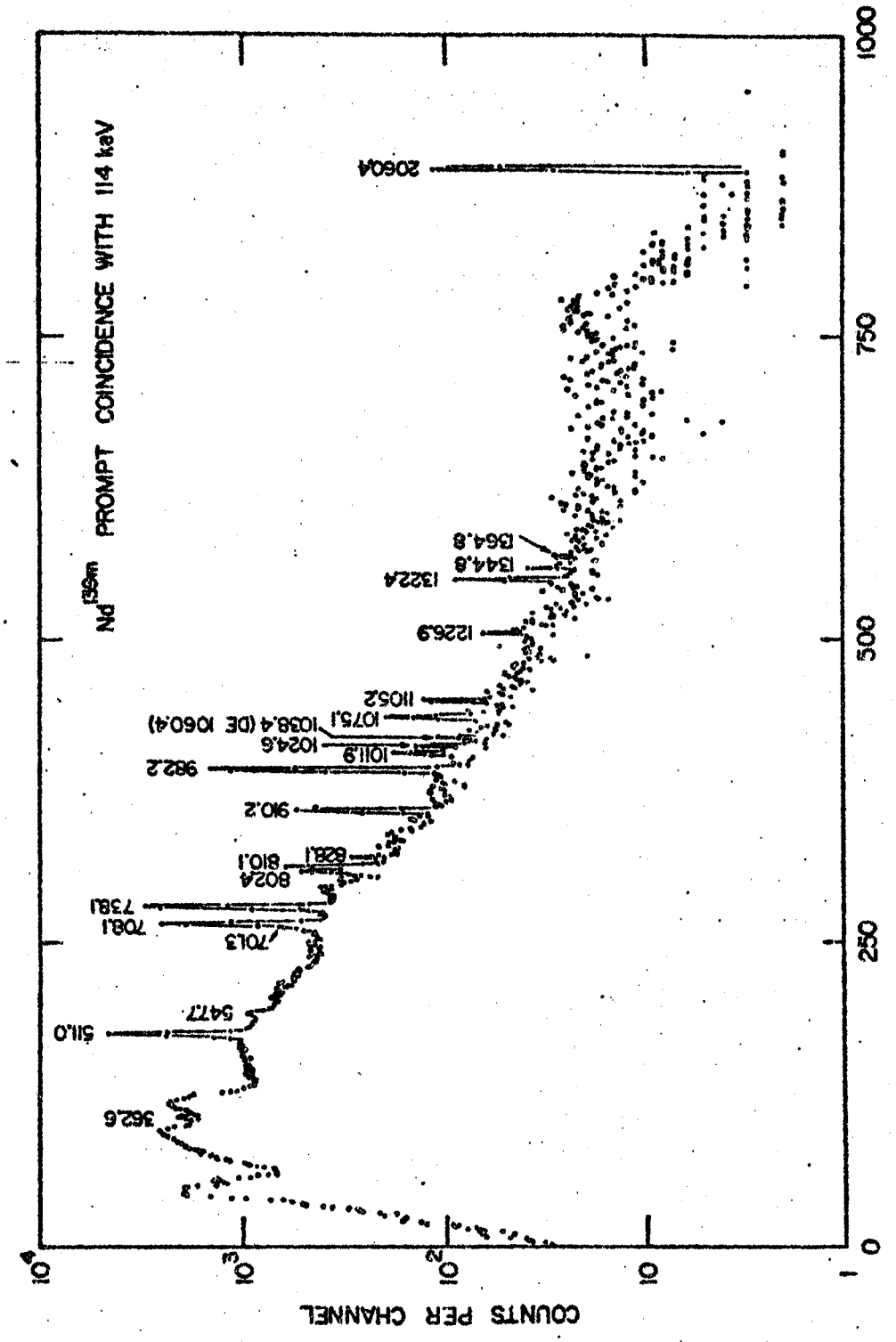

Fig. 11. Spectrum of Nd^{139m} γ-rays in prompt coincidence with the 113.8-keV γ. The gate detector was the 8-in. × 8-in. NaI(Tl) split annulus, while the signal detector was the 7-cm^3 Ge(Li) detector. The results are listed in Table 5.

Table 5. Summary of γ-γ anti-coincidence and coincidence experiment results.

Gate interval[a] (keV)	γ in gate[b] (keV)	γ's enhanced[c] (keV)	Figure No.
Anti-coincidence	≈80-2500	231.2, 821.9[e]	10
110-118	113.8[d]	362.6, 601.2, 708.1[e], 810.1, 910.2, 982.2, 1024.6, 1038DE, 1075.1, 1322.4, 1344.8, 2060.4, 2085.0	11
110-118 delayed display spectrum	113.8[d]	147.9, 209.7, 214.6, 254.9, 302.7, 403.9, 424.3, 547.7, 572.1, 673.5, 701.3, 802.5, 1011.9, 1105.2, 1226.9, 1364.8, 1374.7	22
400-408	403.9	701.3	14
450-550	511.0, 547.7	---	15
500-600	511.0, 547.7	362.6	16
680-720	673.5, 701.3, 708.1[e], 733, 738.1	254.9, 302.7, 403.9, 673.5, 701.3, 802.5, 895.1, 900.3, 1011.9, 1105.2, 1226.9, 1233.7, 1364.8, 1374.7	12
720-760	701.3, 708.1[e], 733, 738.1	214.6, 340.4, 362.6, 733, 982.2, 1075.1, 1322.4	13

Table 5 (continued)

790–840	796.6, 802.4, <u>810.1</u>, 821.9[e] <u>828.1</u>, 851.9	209.7, 302.7, 424.3, 572.1 796.6, 828.1, 910.2, 1006.1, 1220.9	17
840–900	828.1, 851.9, 895.1, 900.3, <u>910.2</u>	601.2, 810.1, 1024.6, 1165.8	18
950–1150	<u>982.2</u>, 1006.1, 1011.9, 1024.6, 1075.1, 1105.2, 1165.8	214.6, 340.4, 362.6, 851.9	19
1180–1300	1165.8, <u>1220.9</u> <u>1220.9</u>, <u>1233.7</u>, <u>1246.5</u>	821.9, 828.1	20
1900–2200	<u>2060.4</u>, 2085.0 <u>2201.2</u>	113.8	21

[a]Prompt coincidence timing except where specified otherwise.

[b]Underlined γ-energies carry the bulk of the γ-intensity in the gates.

[c]I.e., enhanced with respect to spectrum gated on adjacent regions. Conclusions summarized here are based on relative γ-intensities in Table 4, comparisons with results of other coincidence runs (to reduce gated background effects), and consideration of relative γ-intensities within each run (to reduce effect of pulse-heights on timing).

[d]Approximately 1/3 of the population of the 113.8-keV state follows decay of the 821.9-keV state with a 40 nsec $t_{\frac{1}{2}}$.

[e]Delayed γ-ray due to 40 nsec half-life of 821.9-keV state.

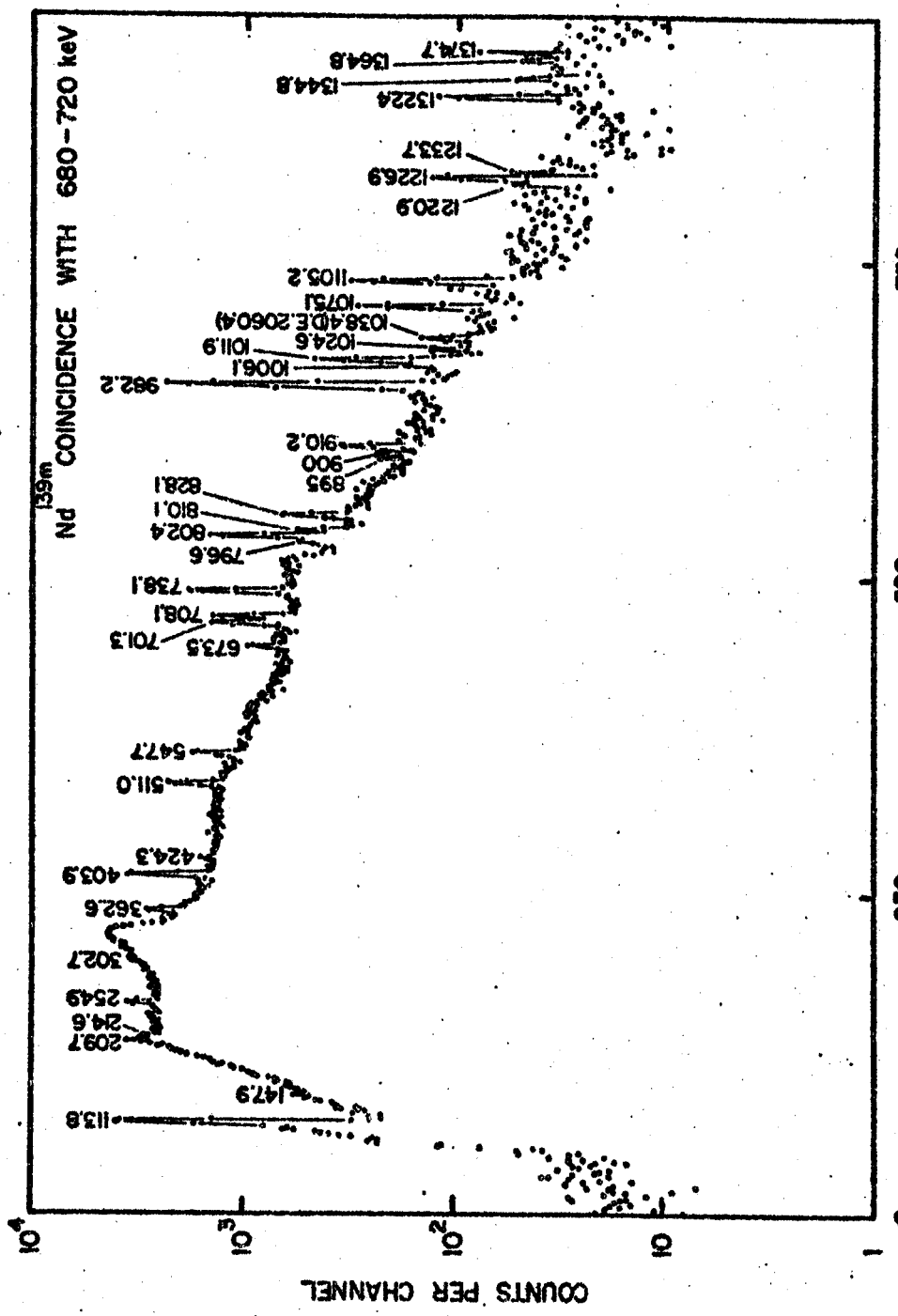

Fig. 12. Spectrum of Nd^{139m} γ-rays in coincidence with the 680–720-keV energy interval. The gate signals came from the 8-in. × 8-in. NaI(Tl) split annulus.

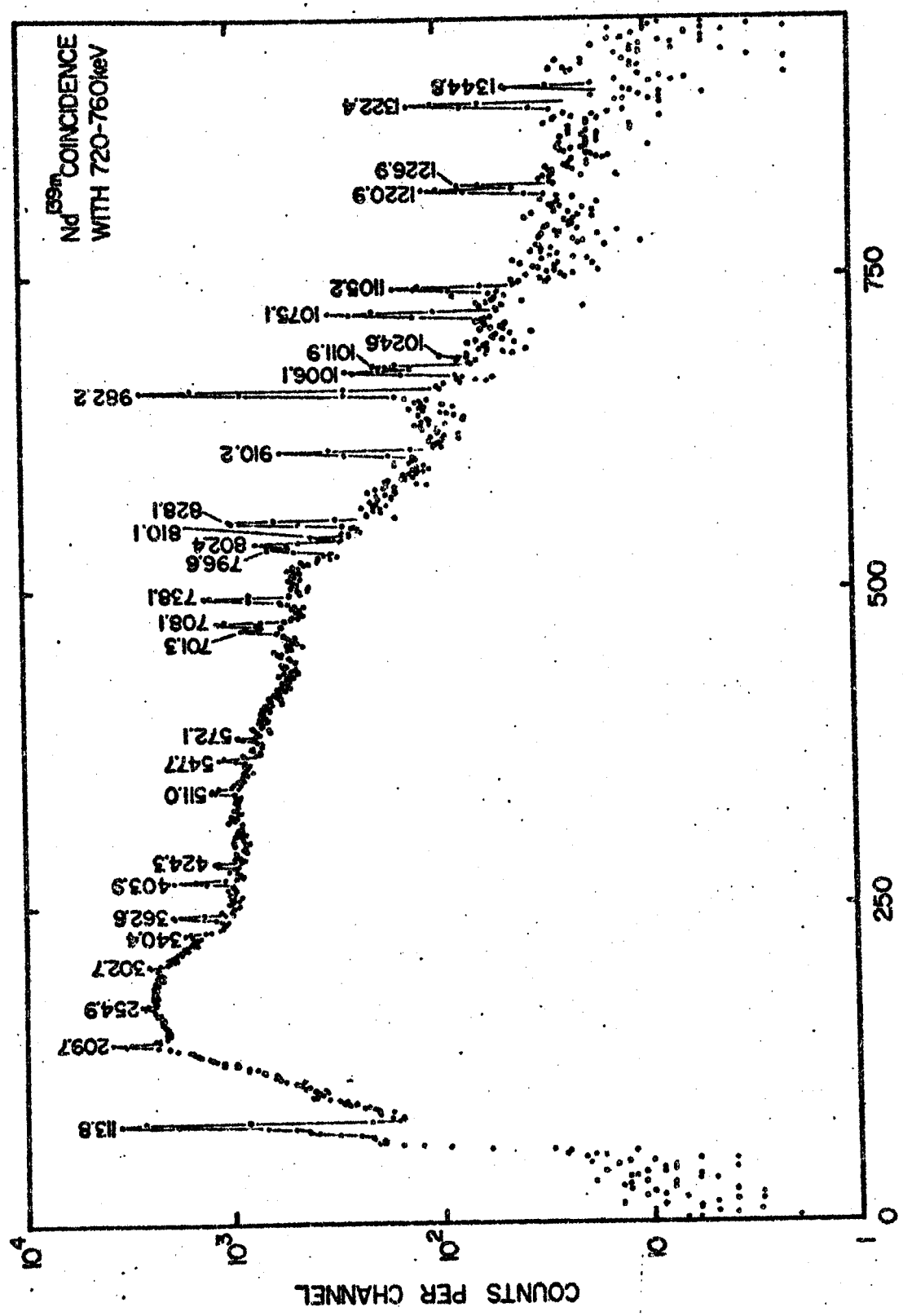

Fig. 13. Same as Figure 12, except that the NaI(Tl) gate was set on the adjoining 720-760-keV energy interval.

useful in constructing the decay scheme.

A comparison of the spectra recorded with adjacent coincidence gates also aided in determining the effects of the underlying Compton backgrounds inevitably in the gates. In all, 12 different gated regions were used to obtain coincidence spectra similar to those of Figures 12 and 13. The results are seen in Figures 14-21 and summarized in Tables 4 and 5.

3.2.3.C. --Delayed Coincidence Experiments-- Possibly the single most useful coincidence experiment was a delayed coincidence experiment using a 3-in. × 3-in. scintillator and the Ge(Li) detector. The 3-in. × 3-in. NaI(Tl) scintillator was gated on the 113.8-keV gamma, the coincidence timing resolution (2τ) was ≈100 ns, and a delay of ≈200 ns was added to the Ge(Li) side of the coincidence circuit. The resulting spectrum is shown in Figure 22. Several peaks are enhanced up to two orders of magnitude relative to the 708.1-, 738.1-, and 910.2-keV peaks, which were seen earlier to be in prompt coincidence with the 113.8-keV gamma. The intensities from this spectrum are listed in Table 4. Later, in section 3.2.4.A, it will be described how this delayed coincidence spectrum confirms the placement of nine states in Pr^{139}.

The state responsible for the delays lies at 821.9 keV, and in order to measure its half-life, a fast-slow coincidence system with two 2-in. × 2-in. NaI(Tl) detectors and a time-to-amplitude converter were used. Now, from the prompt and delayed coincidence data there was no evidence for delays connected with states other

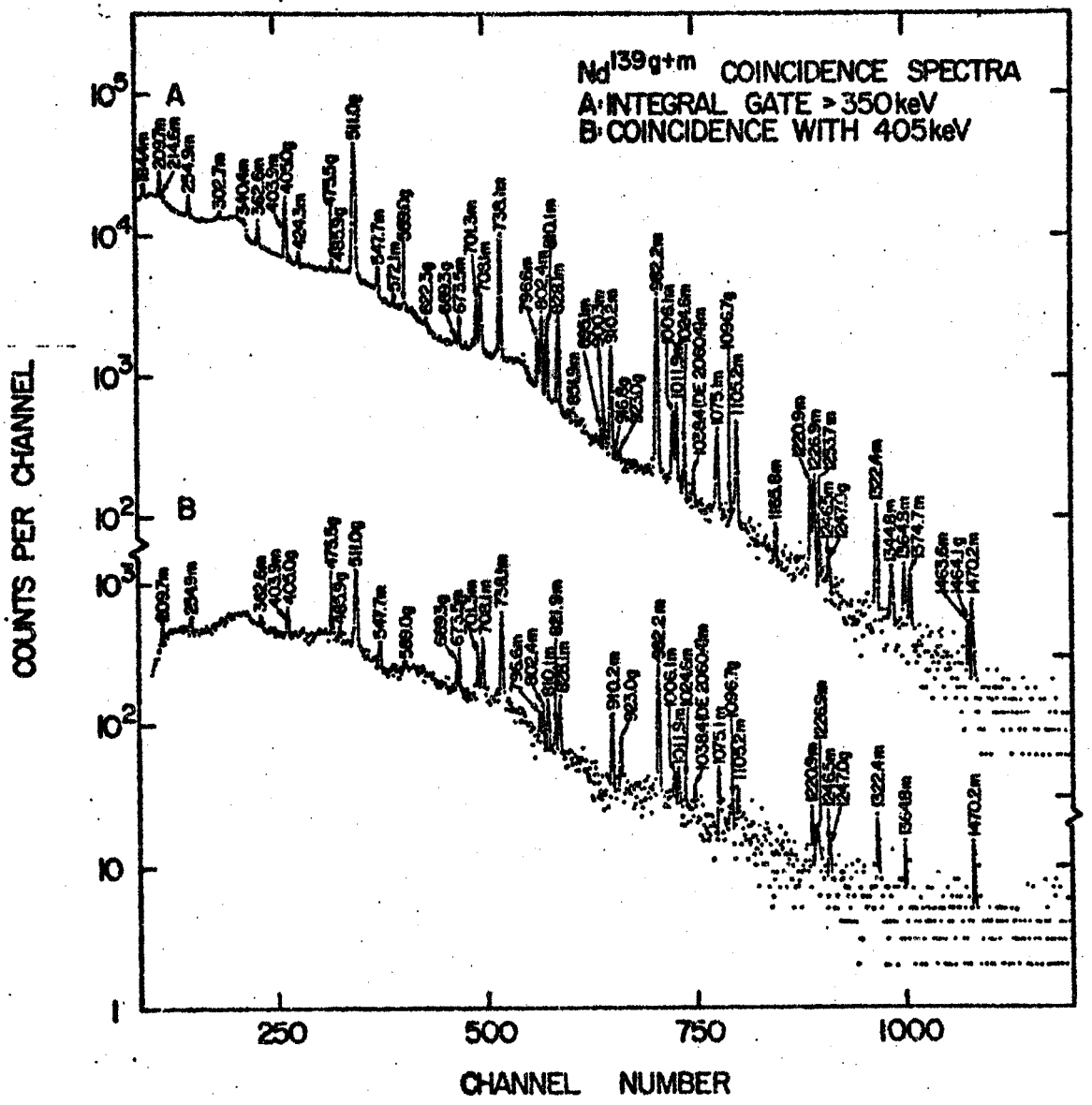

Fig. 14. A) Nd^{139g+m} integral coincidence spectrum. This spectrum was recorded by the 7-cm^3 Ge(Li) detector with the 8-in. × 8-in. NaI(Tl) split annulus set to accept all γ-rays above 350 keV.

B) The annulus gate was set on the 405-keV energy region.

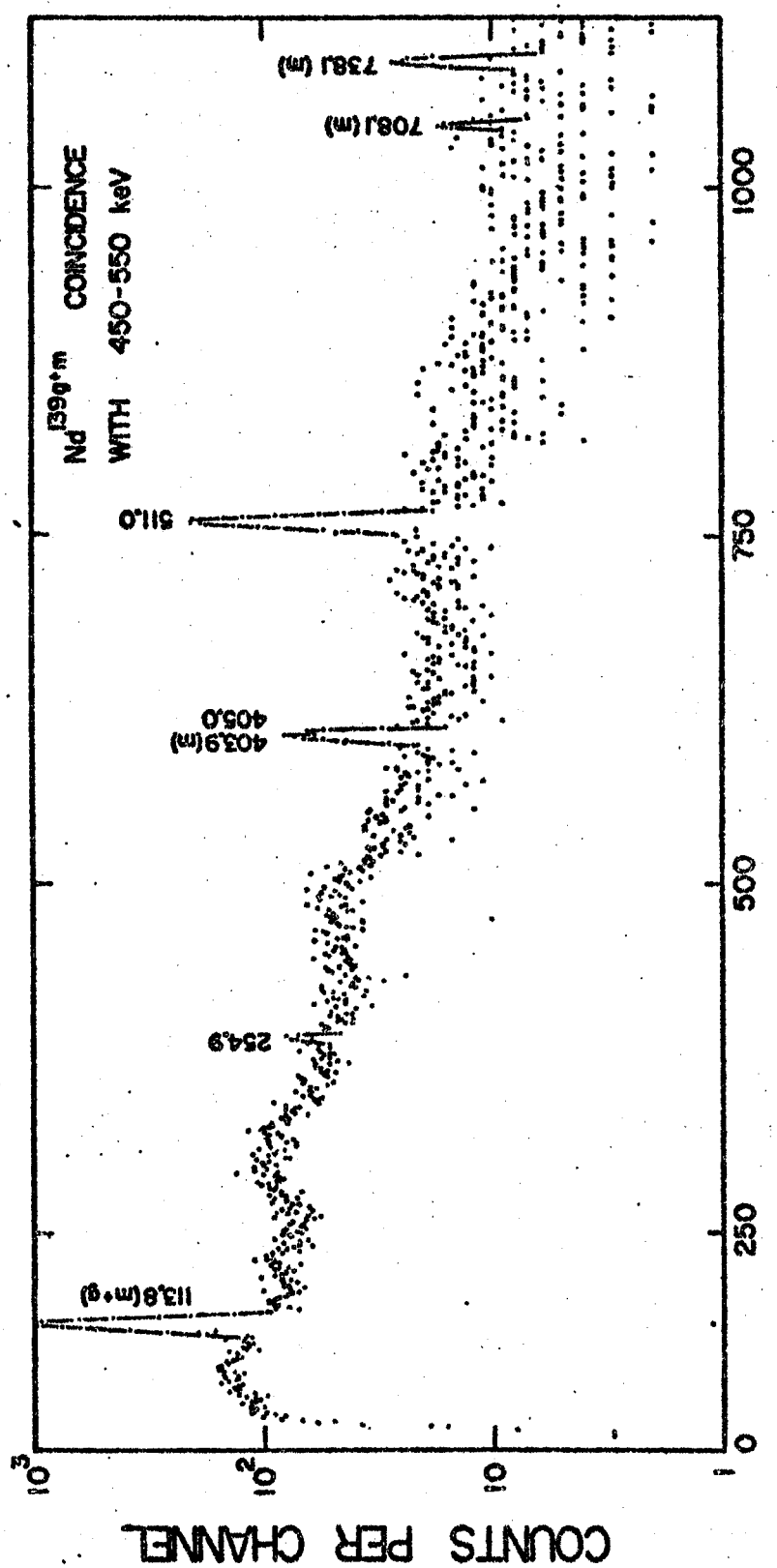

Fig. 15. Spectrum of Nd^{139g+m} γ-rays in coincidence with the 450–550-keV energy interval. The gate signals came from the 3-in × 3-in. NaI(Tl) detector.

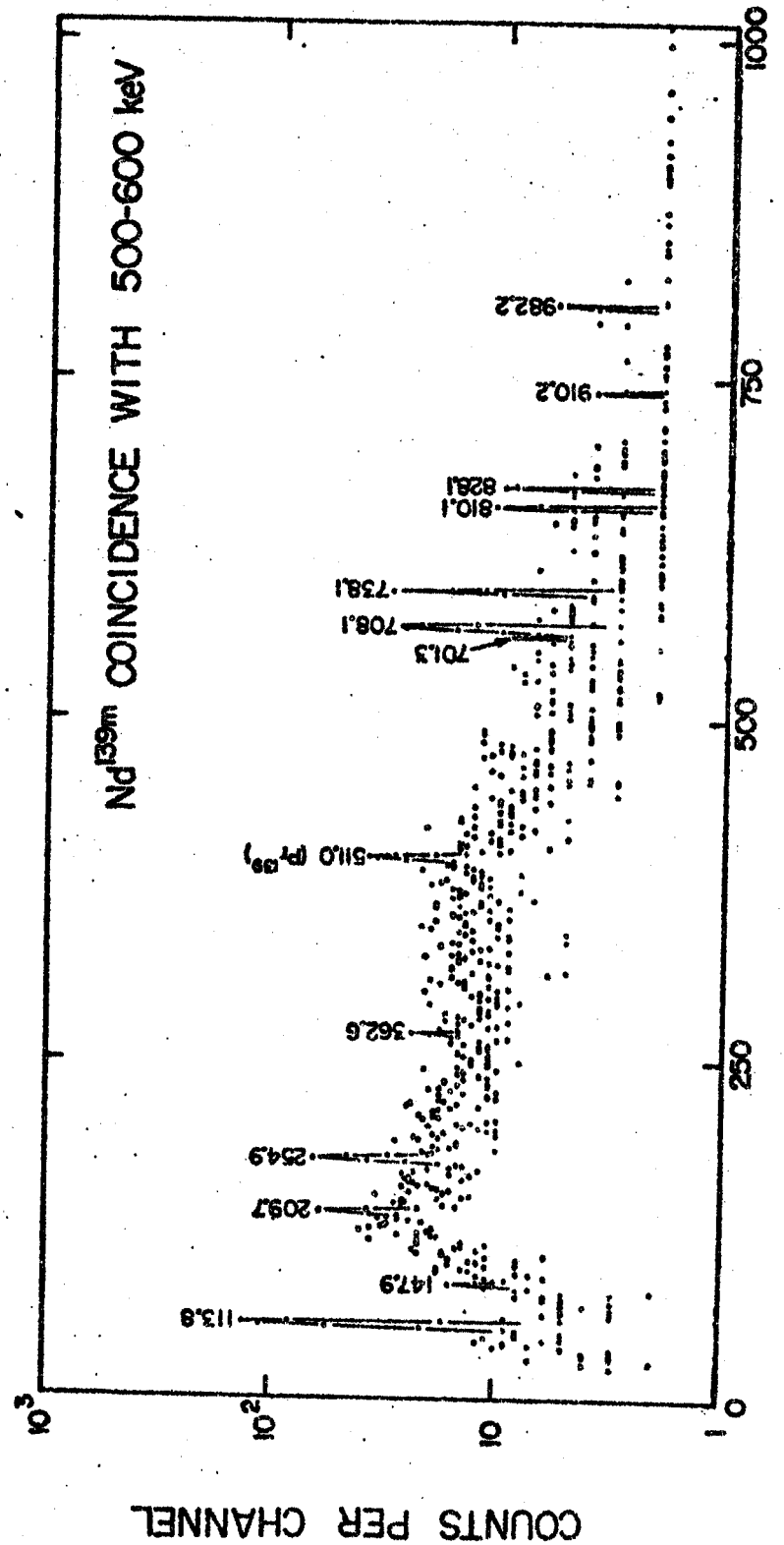

Fig. 16. Spectrum of Nd^{139m} γ-rays in coincidence with the 500-600-keV energy region. This spectrum was recorded by the 7-cm^3 Ge(Li) detector. The gate signals came from the 3-in. × 3-in. NaI(Tl) detector.

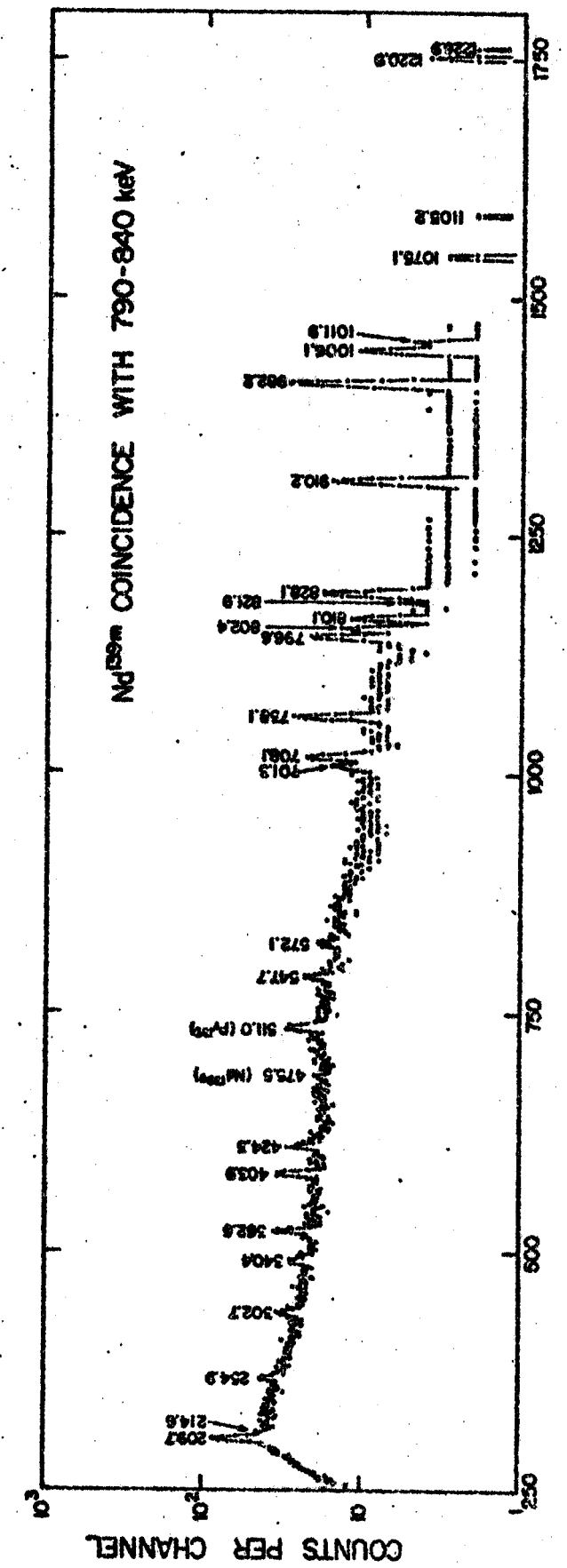

Fig. 17. Spectrum of Nd^{139m} γ-rays in coincidence with the 790-840-keV energy interval. This spectrum was recorded by the 7-cm^3 Ge(Li) detector. The gate signals came from the 8-in. × 8-in. NaI(Tl) split annulus detector.

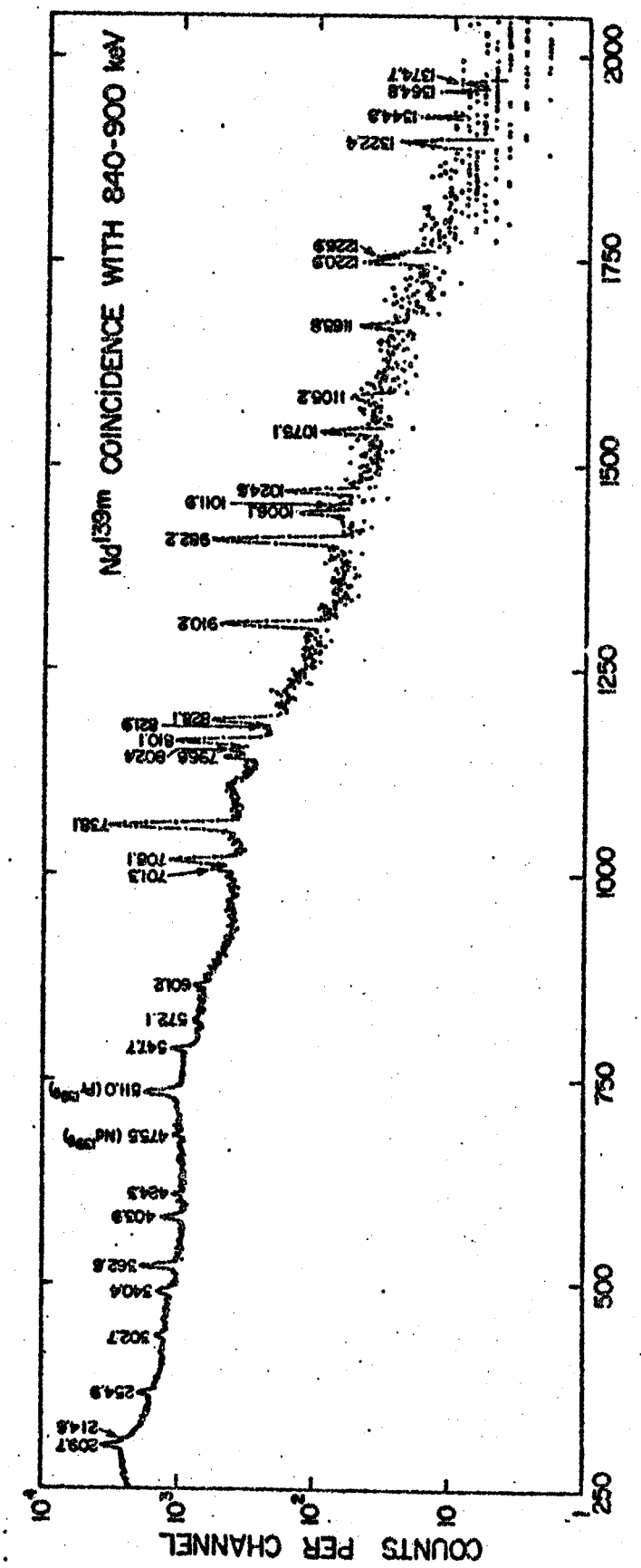

Fig. 18. Same as Figure 17 except that the NaI(Tl) gate was set on the adjoining 840-900-keV energy interval.

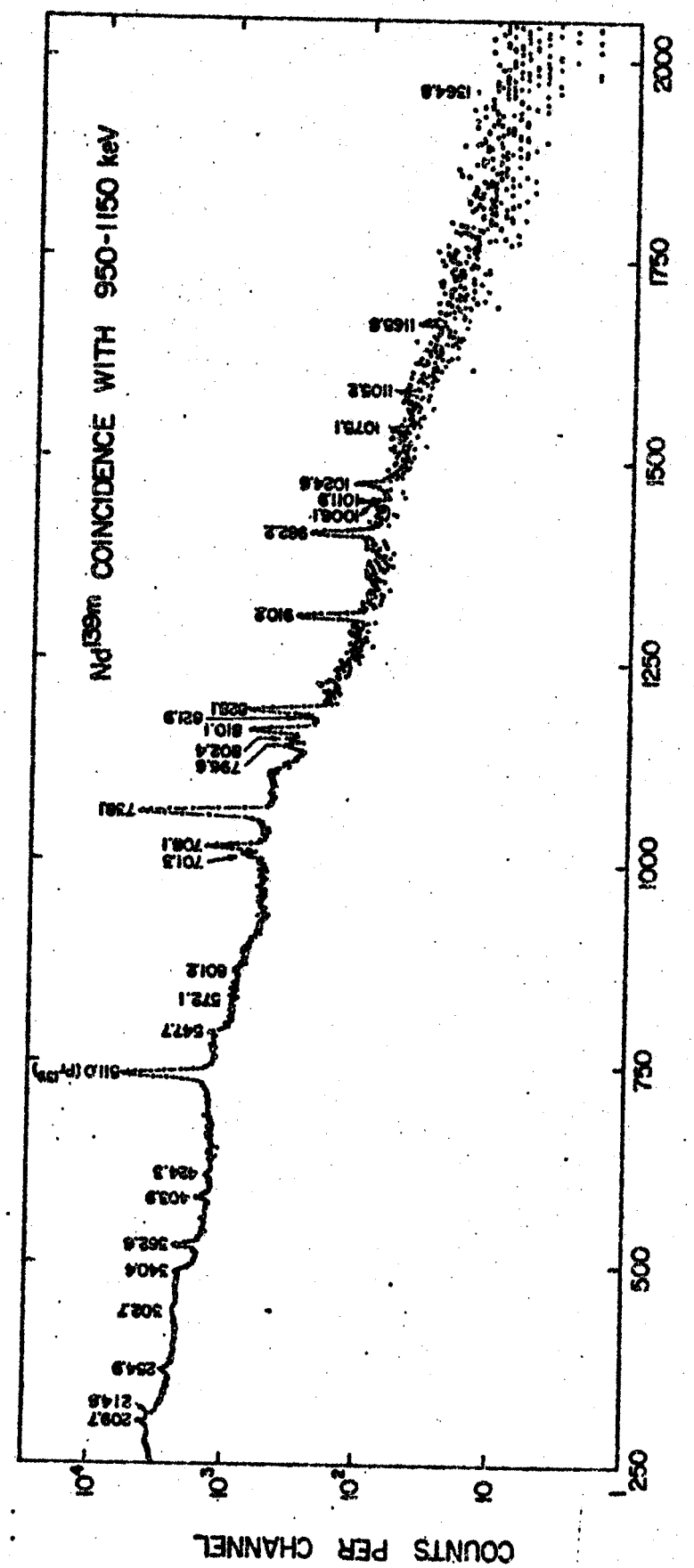

Fig. 19. Same as Figure 17 except that the NaI(Tl) gate was set on the 950-1150-keV energy interval.

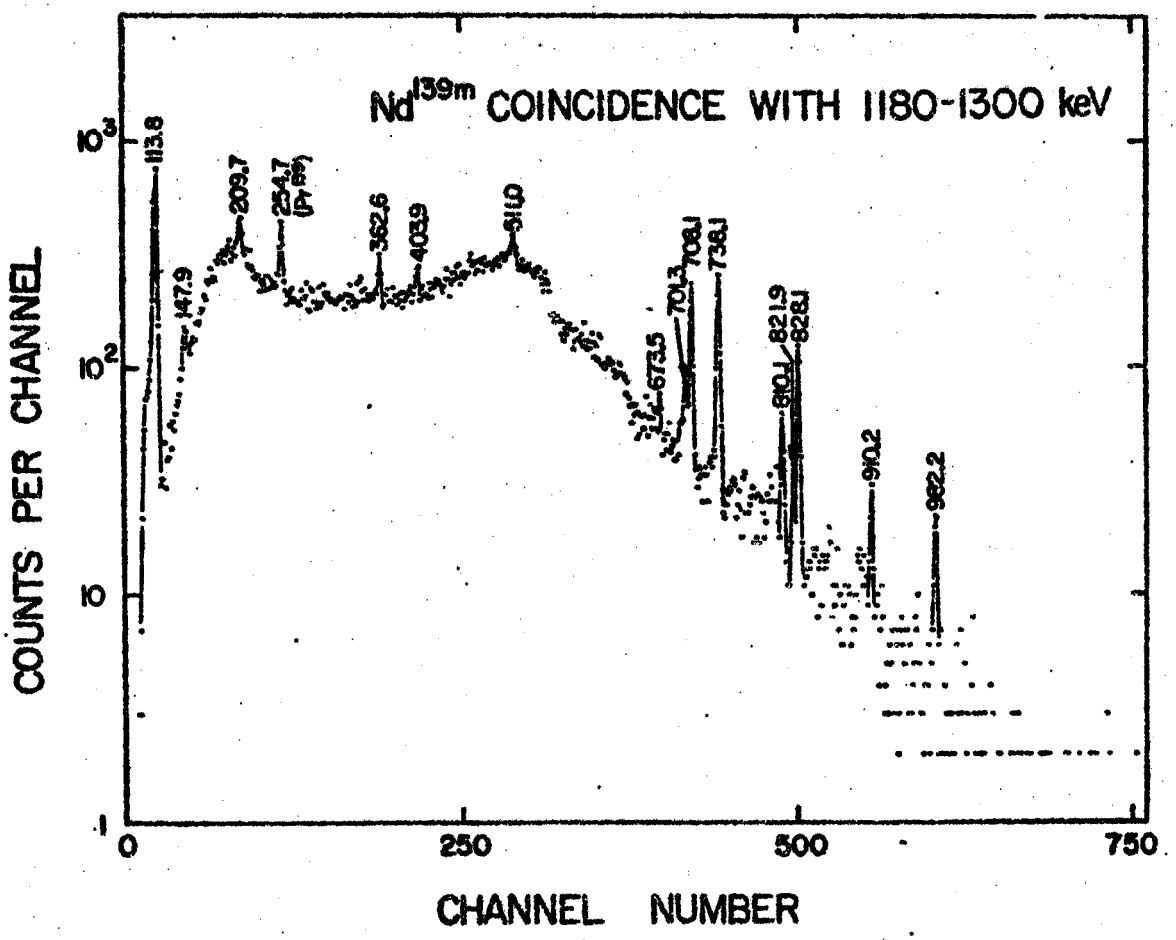

Fig. 20. Same as Figure 17 except that the NaI(Tl) gate was set on the 1180-1300-keV energy interval.

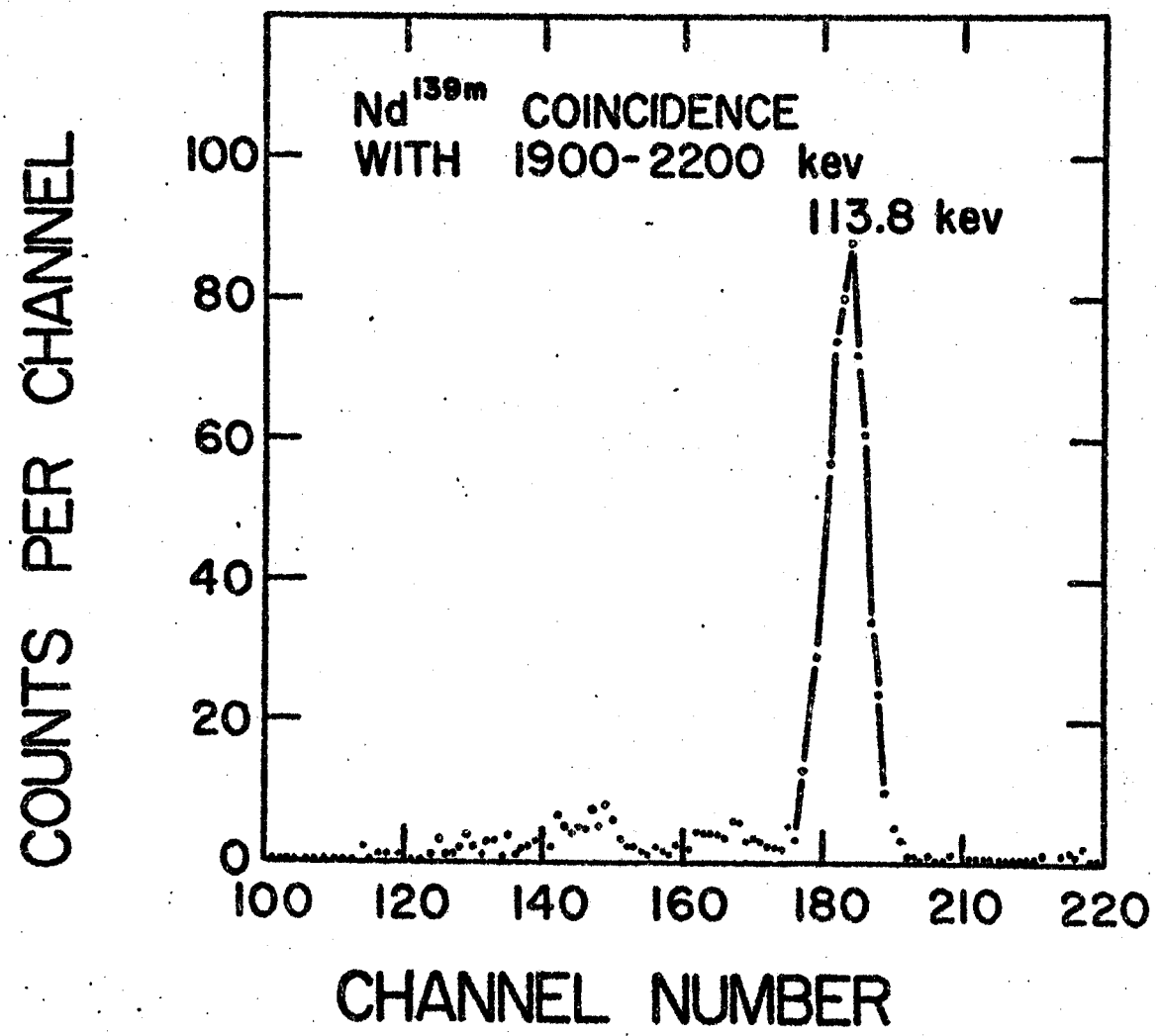

Fig. 21. Spectrum of Nd^{139m} γ-rays in coincidence with the 1900-2200-keV energy interval. The gate signals came from the 3-in. × 3-in. NaI(Tl) detector.

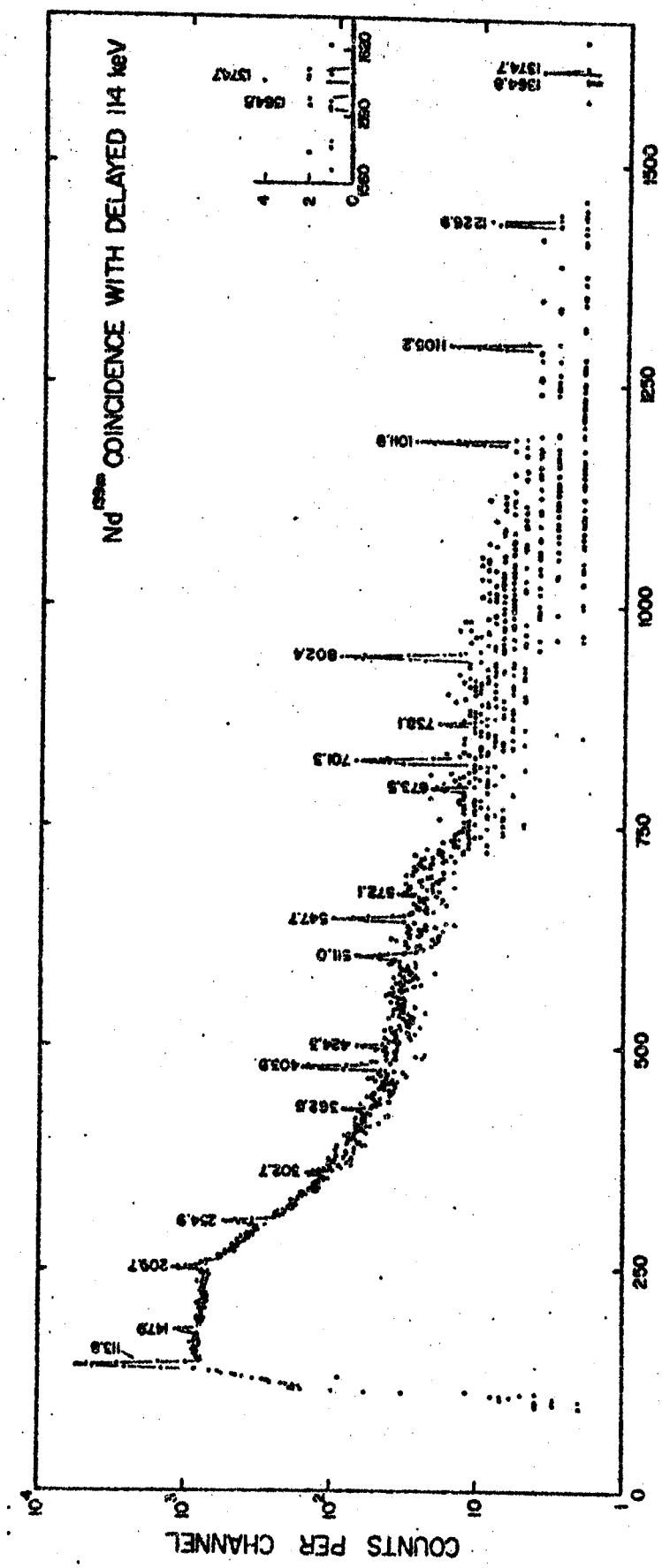

Fig. 22. Spectrum of Nd^{139m} γ-rays in delayed coincidence with the 113.8-keV γ. A 3-in. × 3-in. NaI(Tl) scintillator was gated on the 113.8-keV γ and the timing resolution (2τ) of the coincidence circuit was ≈100 ns, but a delay of ≈200 ns was introduced into the Ge(Li) side of the circuit. Several peaks are enhanced by up to two orders of magnitude relative to the 708.1-, 738.1-, and 910.2-keV peaks, which were seen earlier to be in prompt coincidence with the 113.8-keV γ.

than the 821.9-keV state. For this reason and because of leading-edge walk problems with lower-energy gamma rays, the system was triggered with (prompt and delayed) pulses above 600 keV. The timing was chosen so that the prompt coincidence peak would be centered in the 512-channel analyzer used.

The time spectrum that remained following subtraction of the 17 counts/channel background is shown in Figure 23. The resolution of the system was 3.3 ns FWHM, and the timing calibration was made by inserting precisely measured pieces of delay cable into the circuit. No difficulties connected with channel widths or nonlinearities in the TAC were noted, so no corrections were made for these. The half-life calculated following a least-squares fit of a straight line to the logarithms of the data points in Figure 23 was 40±2 ns. No evidence of decays with different half-lives was observed in this experiment. The ratio of the areas under the prompt peak and the delayed curves are consistent with the decay scheme and the interpretation that the 821.9-keV state decays with a 40-ns half-life.

3.2.4. Nd^{139m} Decay Scheme

A decay scheme has been constructed for Nd^{139m} from the results of the coincidence studies and the energy sums and relative intensities of the transitions. This decay scheme is shown in Figure 24, together with the decay scheme for Nd^{139g}, which will be discussed later. The striking difference between the two decay schemes is worthy of note, with the 113.8-keV gamma being the only

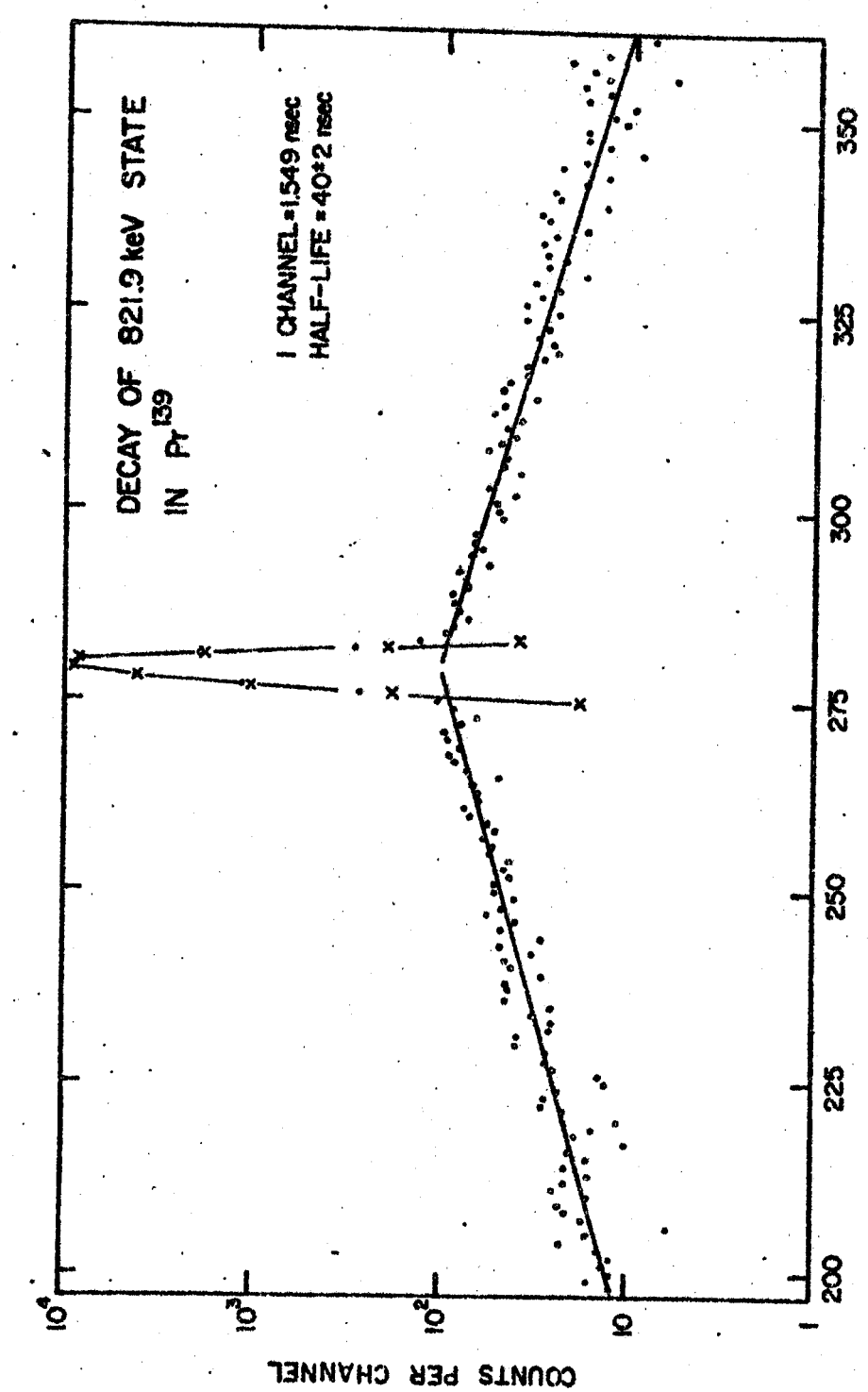

Fig. 23. Time-to-amplitude converter decay curve for the 821.9-keV state in Pr^{139}. The circuit used was symmetrical, with identical 2-in. × 2-in. NaI(Tl) detectors (gated on all pulses above 600 keV) starting and stopping a TAC. The calibration is 1.55 keV/channel, and the measured half-life of the state is 40±2 ns. Subtraction of the least-squared straight-line fit to the points produces the points indicated by X's, which show the resolution of the system to be 3.3 ns FWHM.

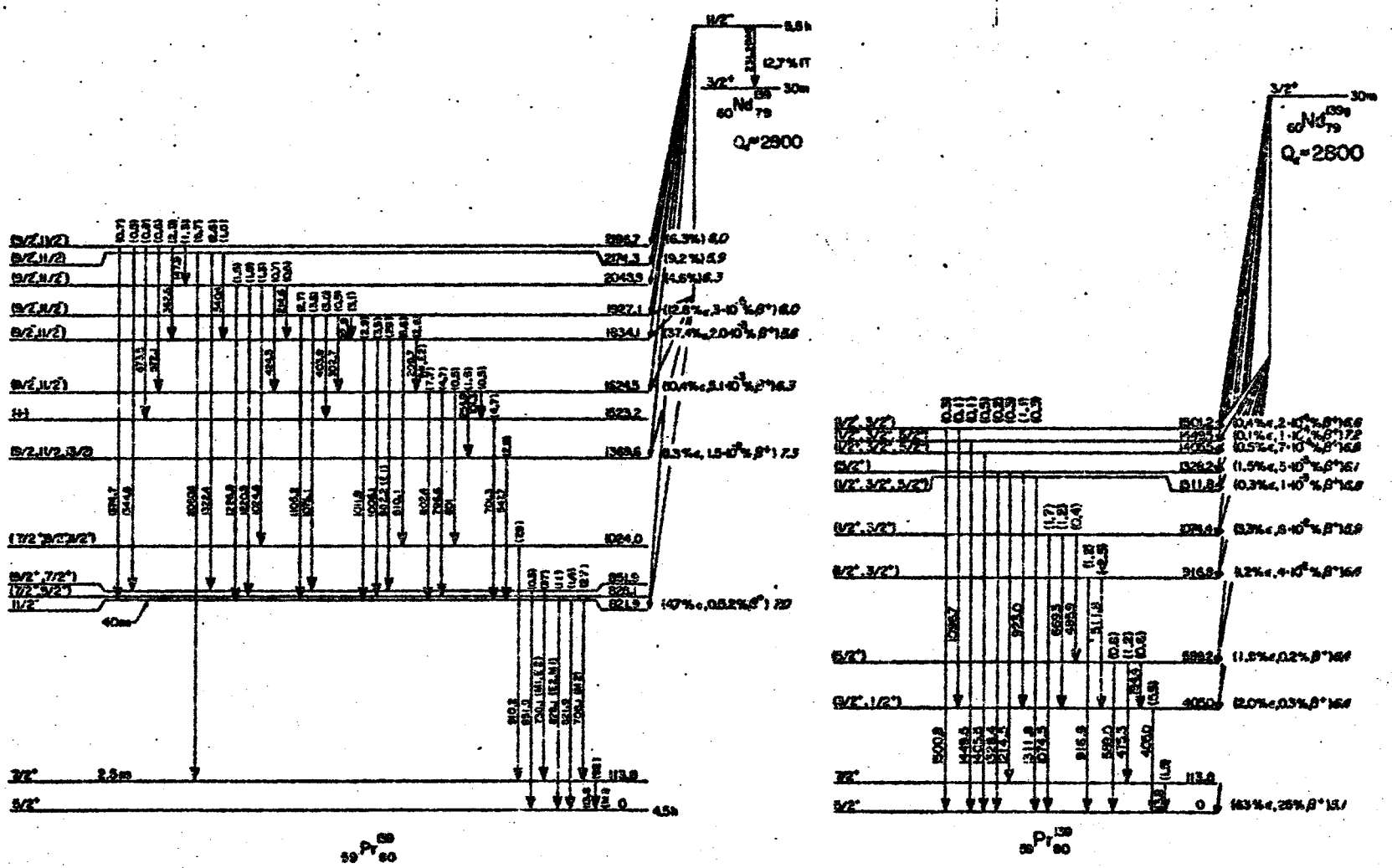

Fig. 24. Decay schemes of Nd^{139m} and Nd^{139g}. All energies are given in keV and (total) transition intensities are given in percent of the disintegrations of the respective parent. The β^+/ε-ratios are calculated values and the log *ft* values (in italics on the right-hand sides of the levels) are calculated on the basis of 5.5-h and 30-min half-lives.

common transition. All energies are given in keV, and the Q_ε is a calculated value (69). Total transition intensities are given in units of percent per disintegration of the parent Nd^{139m}. The β^+/ε ratios are also calculated values, using the method of Zweifel (47). In general, the energy sums of competing crossover and cascade transitions agree to within ±0.2 keV. Because there are so many coincident, cascading transitions in this nucleus, there are many checks as to the energies of most of the levels. The energy assigned for each level is therefore a weighted value based both on the transitions that feed into and out of that level. Both because there are an abnormally large number of gamma ray branchings in this nucleus and because the interpretation of the higher-lying states makes it essential that they be convincingly placed, the relevant sets of sums have been presented in Table 6, where it can be seen that the self-consistency is excellent.

3.2.4.A. --The 113.8-keV Level and Those that Are Depopulated through It-- The large relative intensity of the 113.8-keV gamma combined with its coincidence behavior leads one to place a first-excited state at 113.8 keV, in agreement with earlier studies (56,60).

The isomeric state at 821.9 keV was first placed on the basis of several prompt coincidence experiments having timing resolutions (2τ) of ≈100 ns (see, e.g., Table 5). It was then confirmed by the delayed coincidence experiment of Figure 22, which suggested that seven levels above 821.9 keV are depopulated through the 821.9-keV state. The gamma transitions presumed to originate from these levels

Table 6. Cascade energy relations for Nd^{139m} γ-rays.

γ-Rays in Sum[a]	Sum[a]	State Energy Adopted[a]
821.9	821.9	821.9
113.8 + 708.1	821.9	
851.9	851.9	851.9
113.8 + 738.1	851.9	
802.4 + 821.9	1624.3	1624.5
796.6 + 828.1	1624.7	
601 + 910.2 + 113.8	1625	
254.9 + 547.7 + 821.9	1624.5	
101.3 + 701.3 + 821.9	1624.5	
1011.9 + 821.9	1833.8	1834.1
1006.1 + 828.1	1834.2	
982.2 + 851.9	1834.1	
810.1 + 910.2 + 113.8	1834.1	
209.7 + 802.4 + 821.9	1834.0	
1105.2 + 821.9	1927.1	1927.1
1075.1 + 851.9	1927.0	
403.9 + 701.3 + 821.9	1927.1	
302.7 + (1624.5 state)	1927.2	
92.9 + (1834.1 state)	1927.0	
1226.9 + 821.9	2048.8	2048.8
1220.9 + 828.1	2049.0	
1024.6 + 910.2 + 113.8	2048.6	
424.3 + (1624.5 state)	2048.8	
214.6 + (1834.1 state)	2048.7	
2060.4 + 113.8	2174.2	2174.3
1322.4 + 851.9	2174.3	
340.4 + (1834.1 state)	2174.5	
1374.7 + 821.9	2196.6	2196.7
1344.8 + 851.9	2196.7	
673.5 + 701.3 + 821.9	2196.7	
572.1 + (1624.5 state)	2196.6	
362.6 + (1834.1 state)	2196.7	
147.9 + (2048.8 state)	2196.7	

[a]All energies in keV.

were enhanced by roughly two orders of magnitude over their intensities in prompt coincidence experiments (cf. Table 4), and the ratio of each intensity to that of, say, the 547.7-keV gamma is within ±20% of what it was in the singles spectra. Not only were the direct transitions from these levels to the 821.9-keV state enhanced, but so were many interconnecting transitions. [At gamma ray energies below 300 keV, quantitative comparisons of the delayed gamma ray intensities with the decay scheme were significantly less precise because the earlier crossovers of the lower-energy pulses artificially introduced enhancement factors of >2 into the delayed coincidence spectrum.] The energies of these seven Pr^{139} states, at 1369.6, 1523.2, 1624.5, 1834.1, 1927.1, 2048.8, 2196.7 keV, were assigned from the weighted energy sums listed in Table 6.

3.2.4.B. --The 828.1-, 851.9-, 1024.0-, and 2174.3-keV States-- These four states are suggested by energy sums and relative gamma ray intensities (cf.Table 3), as well as by the prompt coincidence data (Tables 4 and 5). The absence from Figure 22 of all ten of the gamma rays indicated in the decay scheme to feed the 828.1-, 851.9-, and 1024.0-keV states is consistent with the interpretation of these states' positions.

The 828.1-keV state is also confirmed by the suppression of 796.6-, 828.1-, 1006.1-, and 1220.9-keV gamma rays in the prompt coincidence experiments gated on the 113.8-keV gamma; see Figure 11 and Table 4.

3.2.4.C. --Remaining Gamma Rays-- The twelve very weak gamma

rays observed at 733, 895.1, 900.3, 1165.8, 1233.7, 1249.9, 1364.8, 1463.6, 1470.2, 1681, 2085.0, and 2201.2 keV have not been definitely placed in the level scheme. These gamma rays do not fit between any existing states and do not significantly change the interpretation of the level scheme or its comparison with other nuclei or with theoretical calculations. The sum of these gamma ray intensities amounts to only 1.5% of the observed Nd^{139m} gamma ray intensity. Some tentatively suggested placements follow.

The 733-keV gamma ray was seen only in coincidence with the 738.1-keV gamma. The energies of these two sum to 1471.2 keV, within the measured uncertainty of the 1470.2-keV gamma, thus tentatively suggesting a level at 1584.0 keV.

Evidence involving poor statistics indicates that the 2085.0-keV gamma ray is in coincidence with the 113.8-keV gamma, whereas the 2201.2-keV gamma is not. On these grounds alone tentative states at 2198.8 and 2201.2 keV may be inferred.

In order to obtain a lower limit for the log *ft* values of transitions to these "unplaced" states, it was assumed that each unplaced state was fed directly by ε-decay and de-excites entirely by the unplaced gamma rays. It then followed that the corresponding log *ft* values would all be larger than about 7.8.

The properties of a few of the remaining five very weak gamma rays (1165.8, 1233.7, 1249.9, 1463.6, and 1681 keV) can be seen in Table 4. It was not possible to find a unique location for them in the decay scheme. The sum of their intensity is less than 0.7% of the total observed Nd^{139m} gamma rays.

3.2.4.D. --Comparison with Another (β,γ) Study-- After the completion of the present study, a publication became available which describes an investigation of Nd^{139m} decay following the $Nd^{142}(\gamma,3n)$ Nd^{139m} reaction produced by bremsstrahlung on Nd_2O_3 enriched to 95% Nd^{142} (119). The decay of Nd^{139g} was not reported and a competing $Nd^{142}(\gamma,4n)$ reaction produced 5.2-h Nd^{138m} which was distinguished from 5.5-h Nd^{139m} only by coincidence measurements. A number of confirmations are obtained from reference 119 but no additions or corrections to the present study are required. No interpretation was made of the properties of the states.

3.2.5. Spin and Parity Assignments from Nd^{139m} Decay

3.2.5.A. --Electron Data and Multipolarities-- The gamma intensities from the present measurements were compared with the conversion-electron intensity data of Gromov, et al. (56,70) in order to gain multipolarity information about some of the more intense, lower-energy transitions following Nd^{139m} decay. These comparisons and predicted multipolarities are listed in Table 7 and plotted in Figure 25. It was not possible to use the conclusions of Gromov, et al. directly because their gamma intensities were obtained with NaI(Tl) scintillators and differ markedly from our data. However, from *K/L* conversion intensity ratios, the 231.2- and 708.1-keV transitions have been established to be *M4* and *M2*, respectively, by both sets of previous workers (56,60). The theoretical conversion coefficients (71) for these transitions were then used as a basis for determining the remaining coefficients. At lower energies (≤300 keV) it appeared that the coeffi-

Table 7. Multipolarity of γ-transitions.

Transition energy[a] (keV)	K-electron intensity[b]	γ-ray intensity[c]	Experimental α_K	Theoretical α_K				Multipolarity
				*E*1	*E*2	*E*1	*E*3	
209.7	25±14	6.2±0.6	9.7(-2)	3(-2)	1.2(-1)	1.3(-1)	4.6(-1)	*M*1,*E*2
						*M*3	*M*4	
231.2	≡1000	2.4±0.2	≡9.5[d]	---	---	2.4	9.5	*M*4[e]
				*E*3	*M*2	*E*4	*M*3	
708.1	152±8	72 ±2	≡1.74(-2)[d]	9.5(-3)	1.74(-2)	2.0(-2)	4.1(-2)	*M*2[e]
				*E*1	*E*2	*M*1	*E*3	
738.1	≈50±7	≡100	4 (-3)	1.4(-3)	3.6(-3)	5.6(-3)	8.1(-3)	*M*1,*E*2
				*E*1	*E*2	*M*1	*E*3	
828.1	10±3	29 ±2	3 (-3)	1.2(-3)	2.8(-3)	4.4(-3)	6.3(-3)	*E*2,*M*1
				*E*1	*E*2	*M*1	*E*3	
982.2	8±2	79 ±2	8 (-4)	8.3(-4)	2.0(-3)	2.9(-3)	4.2(-3)	*E*1

[a]Energies from present study.

[b]Relative *K*-electron intensities from reference 56.

[c]Relative γ-ray intensities from present work.

[d]The theoretical value (71) was used, as reference 56 and reference 59 agreed on a multipolarity for this transition based on measured *K*/*L* electron intensity ratios.

[e]See reference 56 and reference 60 for descriptions of two independent measurements of this multipolarity.

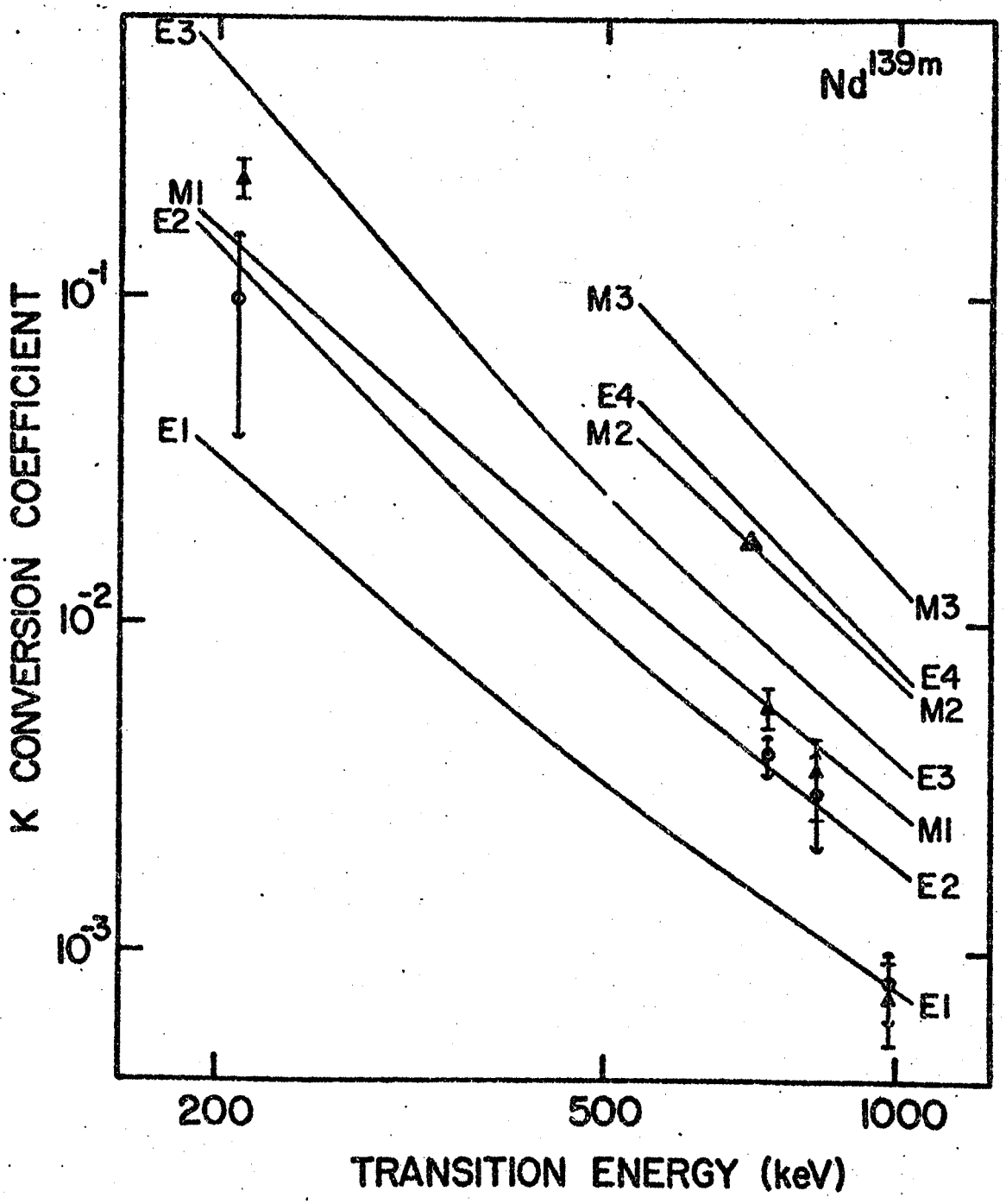

Fig. 25. A comparison of experimental and theoretical *K*-conversion coefficients for some of the γ-transitions following Nd^{139m} decay. The lines are the theoretical values of Sliv and Band (71). The data points were obtained by comparing the electron intensities of Gromov, et al. (56,70) with the γ-ray intensities measured in the present study, assuming the theoretical values of the 231.2-keV (*M4*) and 708.1-keV (*M2*) transitions to be correct for purposes of normalization. Each circle (triangle) refers to reference 56 (70).

cients were affected by absorption in the electron counter window.

3.2.5.B. --Ground and Metastable States of Nd^{139}-- Here at N=79 one ought to consider three-quasiparticle (hole) states, but to a reasonable first approximation the low-lying ones can be thought of as single hole states, so there are some similarities with the N=81 nuclides. Among the latter there are now seven known that have $d_{3/2}$ ground states and $h_{11/2}$ isomeric states connected by $M4$ isomeric transitions (72). Also, the N=79 nuclei Te^{131}, Xe^{133}, Ba^{135}, and Ce^{137} (references 14 and 73,74,75, and 76, respectively) have 3/2+ ground states and 11/2- metastable states. Thus, when K-L conversion electron energy differences suggested that the 231.2-keV transition occurs in Nd rather than in Pr and the conversion line intensity confirmed that the transition was an $M4$, this indicated a similar $d_{3/2}$-$h_{11/2}$ isomer pair. The energies of the N=79 and N=81 isomers have been plotted in Figure 26, including Nd^{139m} and a projection for Sm^{141m} (77).

It is instructive to compare the reduced transition probability of the 231.2-keV gamma with those of the other $M4$ gamma rays, for these isomeric transitions should be among the best examples of true single-particle transitions. In Figure 26 the squares of the radial matrix elements, $|M|^2$, of these transitions are also plotted. These were calculated using Moszkowski's approximations for single-neutron transitions (78,79):

$$T_{SP}^{(ML)} = \frac{0.19(L+1)}{[(2L+1)!!]^2}|M|^2\left(\frac{\hbar\omega}{197\text{MeV}}\right)^{2L+1}(a \text{ in } 10^{-13}\text{cm})^{2L-1} \times S(j_i, L, j_f) \times 10^{21} \text{ sec}^{-1}.$$

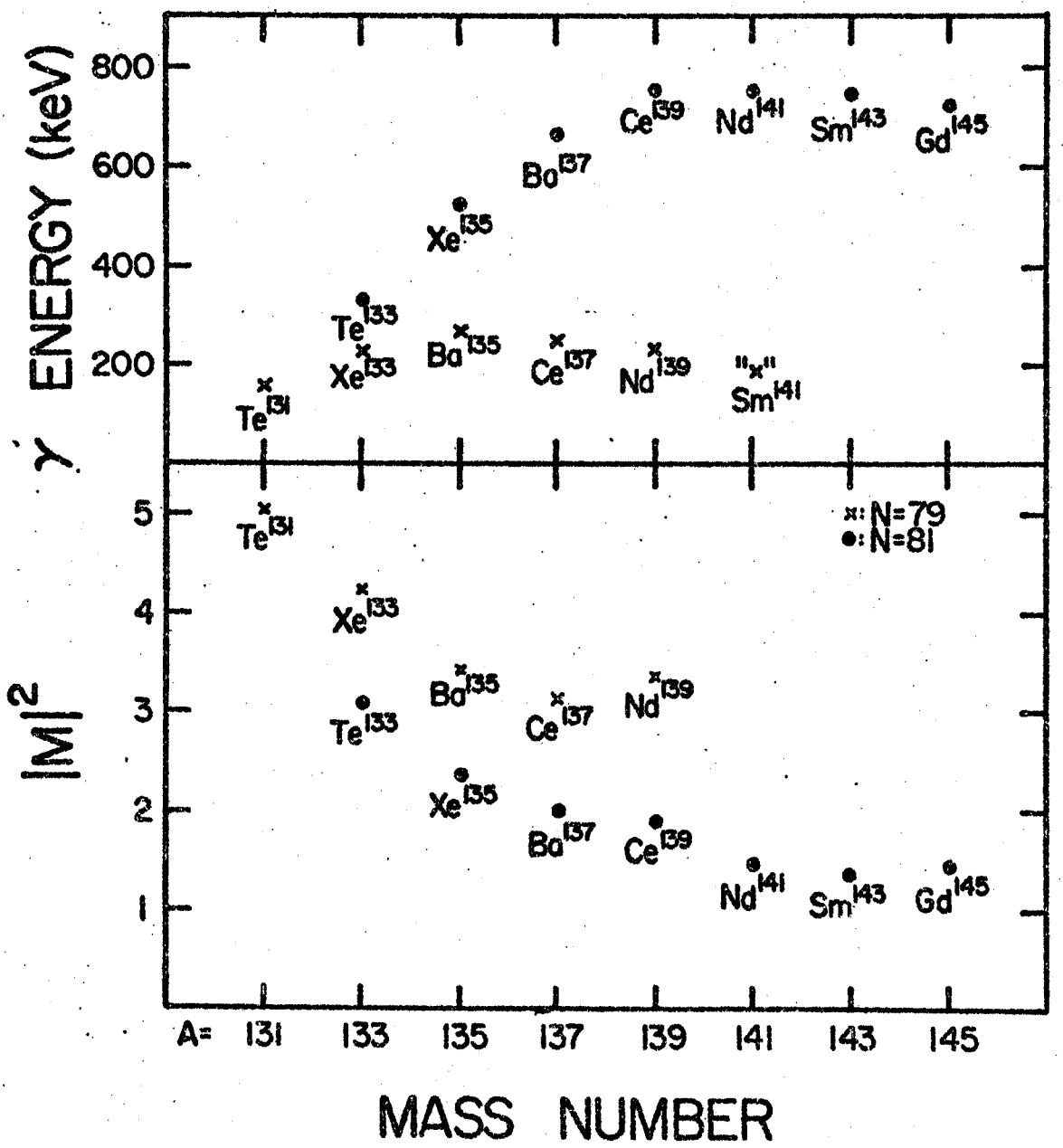

Fig. 26. Upper: Energies of the metastable states in the N=79 and N=81 isotones. (The Sm^{141} point is a predicted one.)

Lower: Values of the squared radial matrix elements for the isomeric transitions in the same nuclei.

Here $T_{SP}^{(ML)}$ is the single-particle transition probability, L (=4 for $M4$'s) is the multipolarity, a (=1.2×10^{-13} cm) is the effective nuclear radius, and $S(j_i,L,j_f)$ is a statistical factor (i.e., angular momentum portion of the matrix element), which for 11/2→3/2 transitions has the value 15/11.

The resulting values obtained are consistently smaller than the approximation of a constant wave function,

$$|M|^2 = \left(\frac{3}{L+2}\right)^2 (\mu_n L)^2 = 14.6,$$

where μ_n is the magnetic moment of the neutron, but this fact should not be of concern, for $M4$ transitions are normally retarded over such estimates and one needs much more detailed information about the nuclear wave functions in order to make detailed comparisons meaningful. What is of more importance is the fact that the values of $|M|^2$ are not constant but show a definite trend in both the N=79 and N=81 nuclei. [It is unusual for $|M|^2$ not to be constant over such a series. For example, in the odd-mass neutron-deficient lead isotopes, $|M|^2$ was constant to the point that an apparent 15% discrepancy at Pb^{203} suggested that an unobserved transition was competing with the $M4$ isomeric transition, and this competing transition was later discovered (80).]

Both because collective modes of the core would not be expected to contribute appreciably to an $M4$ multipole field and because the $h_{11/2}$ states cannot be mixed readily with other states in these nuclei, these $M4$ transitions should prove a more sensitive test of, say, $d_{5/2}$ and perhaps $s_{1/2}$ admixtures in the $d_{3/2}$ states than would normally be possible from electromagnetic transition

rates. The fact that the $|M|^2$ values for the N=79 nuclei are consistently larger than those for the N=81 nuclei goes along with this, for the N=79 three-quasiparticle states would be expected to be much less pure, and only to a (good) first approximation can the transitions be characterized as proceeding from a pure $[(d_{3/2})^2 h_{11/2}]_{11/2-}$ to a pure $[d_{3/2})^3]_{3/2+}$ configuration. A more complete analysis of these $M4$ transitions, using the occupation number formalism, is presently underway (72).

3.2.5.C. --The Ground, 113.8-, and 821.9-keV States in Pr^{139}-- The ground state of Pr^{139} is fed by the $d_{3/2}$ ground state of Nd^{139}. In the present study of this decay (see below, sections 3.2.6 and 3.2.7) a log ft of 5.1 was obtained for this transition, which suggests 1/2+, 3/2+ or 5/2+ for the ground state of Pr^{139}. Any of these assignments could be consistent with the observed (16) 99% of Pr β-decay (log ft = 5.3) to the 3/2 ground state of Ce^{139}. The simple shell model, predictions by Kisslinger and Sorensen (81), and systematics of odd-mass nuclei with odd proton numbers between 51 and 63 indicate 5/2+ and 7/2+ configurations for the two lowest levels of Pr^{139}. Sixteen nuclei in this region have ground state and first-excited states well characterized (6), and in every case the assignments are 5/2+ and 7/2+ or 7/2+ and 5/2+.

The measured K and L conversion electron intensities for the 113.8-keV transition and its 2.5-ns half-life (82) are characteristic of the l-forbidden $M1$ transitions between $g_{7/2}$ and $d_{5/2}$ states. Sixteen of these also have been measured (6) in odd-proton nuclei between

Z=51 and Z=63.

No direct β-population of the 113.8-keV state was observed from either the 3/2+ or 11/2- states of Nd^{139}. This is consistent with a 7/2+ assignment for this state. The upper limit of 3% ε-decay to it from Nd^{139m} places a lower limit for the log *ft* at 7.6, although the log *ft* is expected to be appreciably higher: The ε-decay from some of the $h_{11/2}$ Te and Sn isomers to $g_{7/2}$ states in their daughter nuclei has been observed (6,9-12,14), and the log *ft*'s cluster around 9. For an estimated log *ft* = 9 for decay to the 113.8-keV state in Pr^{139}, the corresponding ε-decay is only 0.1%.

The above cumulative evidence rather strongly suggests 5/2+ and 7/2+ assignments for the ground and first-excited states in Pr^{139}, which would imply $d_{5/2}$ and $(g_{7/2})^{-1}(d_{5/2})^2$ configurations.

The measured α_K (Table 7) of the 708.1-keV transition indicated it to be an *M*2, and this, combined with the evidence of direct feeding of the 821.9-keV state by Nd^{139m} suggests this state to be 11/2-. The measured 40-ns $t_{\frac{1}{2}}$ is consistent with this assignment. The amounts of admixing in the gamma transitions were not determined, but Weisskopf single-particle estimates (23) for the $t_{\frac{1}{2}}$'s of a 708.1-keV pure *M*2 and an 821.9-keV pure *E*3 are 1.2×10^{-9} and 1.3×10^{-6} sec, respectively. Thus, the *M*2 (partial $t_{\frac{1}{2}}$ = 42 ns) appears to be retarded over the single-particle estimate; this is not particularly surprising, however, as *M*2's are customarily retarded. More interesting, the *E*3 (partial $t_{\frac{1}{2}}$ = 600 ns) appears to be enhanced over the single-particle estimate, and *E*3's also are most often retarded (83). However, there are three other known enhanced *E*3's, in La^{137},

Eu^{147}, and Eu^{149} (references 84,85, and 85 respectively), all just below or above the N=82 shell. More will be said about this in section 3.2.9 below in terms of possible octupole admixtures in the 821.9-keV state, but the dominant characteristics of this state warrant the assignment $h_{11/2}$. The log ft of 7.0 for the ε-population of this state is high but certainly within the realm of possibilities for an 11/2- → 11/2- allowed transition. It will be seen later (section 3.2.9) that the reason for this is that a multiparticle rearrangement is necessary in order for Nd^{139m} to populate this state.

3.2.5.D. --The 828.1-, 851.9-, and 1024.0-keV States-- The 828.1-keV gamma appears to be of $E2$ and/or $M1$ multipolarity, which sets limits of 1/2+ through 9/2+ on the 828.1-keV state. This state is fed strongly by the 1624.5-, 1834.1-, and 2048.8-keV states, each of which is populated directly by 11/2- Nd^{139m}, so 1/2+, 3/2+, and possibly 5/2+ can probably be eliminated. If the state were 9/2+, one might expect some direct ε-feeding (first forbidden); none was seen, but the limits are not too precise on this. This is mentioned in anticipation of the problems that will arise concerning some of the higher-lying states. A 9/2+ assignment would also suggest that the 828.1-keV transition be pure $E2$, but again the precision in α_K does not allow one to say concretely whether this transition does or does not contain some $M1$ character. An upper limit of 0.27% (of Nd^{139m} disintegrations) can be placed on the intensity of the missing 714.3-keV gamma ray to the 7/2+ 113.8-keV

gamma ray to the 7/2+ 113.8-keV state. The absence of this transition is slightly surprising, considering either a 7/2+ or 9/2+ assignment, but, for example, a core-coupled configuration involving the $d_{5/2}$ ground state could result in either but would explain the absence of such a transition. Both 7/2+ and 9/2+ are retained as possible assignments.

Using the same approach with the 851.9-keV state, 9/2+ was obtained as the probable assignment, with 7/2+ as a somewhat less likely alternate. Again, the 738.1-keV gamma appears to be *M*1 and/or *E*2, which sets limits of 3/2+ through 11/2+ for the state. This state is fed strongly by the 1834.1-, 1927.1-, 2174.3-, and 2196.7-keV states, each of which is populated directly by what looks like an allowed transition. In particular, the intense 982.2-keV gamma from the 1834.1-keV state -- the state with the strongest claim to being a high-spin (9/2, 11/2) odd-parity state -- is characterized as an *E*1. This permits one to narrow the assignments down to 7/2+, 9/2+, and 11/2+. 11/2+ can be ruled out on the basis of the branching ratio of the 738.1- and 851.9-keV gamma rays, for it would force the 851.9-keV gamma to be an *M*3, which has a predicted (single-particle estimate) $t_{\frac{1}{2}}$ of 1.0×10^{-6} sec, as compared with only 2.7×10^{-11} sec for a 738.1-keV *E*2. The branching ratio would also favor 9/2+ (*M*1,*E*2 vs pure *E*2) over 7/2+ (both *M*1,*E*2), but, as pointed out in connection with the 828.1-keV state, one has to know more about the internal structures of such states before other than gross decisions based on branching ratios can be made.

On the basis of the 910.2-keV gamma to the 7/2+ 113.8-keV state, a gamma ray that is at least five times as intense as the unobserved 1024.0-keV ground-state gamma ray, one can probably limit the spins of the 1024.0-keV state to a range of 2 units on either side of 7/2. Because the state competes favorably for feeding from the 1624.5-, 1834.1-, and 2048.8-keV states, which again are fed directly by 11/2- Nd^{139m}, this range is biased toward the high-spin side of 7/2. Finally, the lack of direct ε-population (upper limit ≈0.4%) suggests even parity. Conclusion: (5/2+), 7/2+, 9/2+, or 11/2+ for this state.

3.2.5.E. --The "High Odd-Parity States"-- The most intriguing aspect of this study is the population of (at least) six high-lying states in Pr^{139} by what appear to be allowed transitions from 11/2- Nd^{139m}. These six states, at 1624.5, 1834.1, 1927.1, 2048.8, 2174.3, and 2196.7 keV, are populated by ε-decay with log *ft*'s that range from 5.6 to 6.3. This would seem to imply that these states have spins of 9/2, 11/2, or 13/2, all with odd parity. Granted that log *ft* values by themselves are not always reliable indicators of the degree of forbiddeness in β-decay, still it is much more common for allowed transitions to be abnormally slow than for first-forbidden transitions to be abnormally rapid (86). Also, the decay to the presumed $h_{11/2}$ 821.9-keV state should be, superficially at least, the most straightforward of the β-transitions from Nd^{139m}, and it has a log *ft* of 7.0. Thus, these six high-lying states are favored for receiving population over the $h_{11/2}$ state, and from this point of view the ε-decay to them is undoubtedly allowed. There are other indications, as well (to be described

later), that they have odd parity. These six states also have other peculiarities, among which are the large number of low-energy inter-connecting gamma transitions and the lack of transitions to the low-lying states. In this section these states will be discussed somewhat phenomenologically, arriving only at estimates of the simplest external structures (i.e., spins and parities) consistent with our data, and the problems of detailed internal structure will be postponed to section 3.2.9 where it will be shown that they are three-quasiparticle states.

Now, although the foregoing conclusions based on gamma ray branching ratios from the lower-lying states may have been overly conservative, the sheer number of competing gamma rays from these "high odd-parity" states makes it worthwhile to determine at least whether or not useful information can be obtained by analyzing their various branchings. Therefore, the single-particle estimates for the half-lives of all the gamma rays originating from these states have been assembled in Table 8, assuming possible *E*1, *M*1, or *E*2 multipolarities. *M*2 and higher multipolarities were excluded on the basis of there being no likely mechanisms for enhancing them to the point that they could complete with the many possibilities for de-excitation by lower multipolarities. This tabulated information must be used with caution, however, for the *E*1's and *M*1's could easily be retarded, as noted before, whereas the *E*2's could be either enhanced or not enhanced, depending on the collective or non-collective nature of the states involved. Also, because some common internal structure is expected among these states,

Table 8. Weisskopf single-particle estimates for gamma rays depopulating the "high odd-parity state" in Pr^{139}.

State energy (keV)	γ-ray energy (keV)	Relative intensity[a] (1%)	Single-particle estimate[b] for $t_{\frac{1}{2}}$ (sec) (corrected for conversion)		
			*E*1	*M*1	*E*2
1624.5	101.3	6.5	1.1(-13)	1.6(-11)	3.8(-07)
	254.9	20	9.5(-15)	1.4(-12)	5.1(-09)
	601	6.5	7.8(-16)	1.1(-13	7.6(-11)
	796.6	61	3.4(-16)	4.9(-14)	1.9(-11)
	802.4	≡100	3.3(-16)	4.8(-14)	1.8(-11)
1834.1	209.7	9.0	1.6(-14)	2.3(-12)	1.3(-08)
	810.1	23	3.2(-16)	4.7(-14)	1.7(-11)
	982.2	≡100	1.8(-16)	2.6(-14)	6.6(-12)
	1006.1	12	1.7(-16)	2.4(-14)	5.8(-12)
	1011.9	10	1.7(-16)	2.4(-14)	5.7(-12)
1927.1	92.9	89	8.2(-14)	1.2(-11)	3.3(-07)
	302.7	14	5.8(-15)	8.4(-13)	2.2(-09)
	403.9	86	2.5(-15)	3.7(-13)	5.4(-10)
	1075.1	≡100	1.4(-16)	2.0(-14)	4.2(-12)
	1105.2	77	1.3(-16)	1.8(-14)	3.6(-12)
2048.8	214.6	33	1.5(-14)	2.2(-12)	1.1(-08)
	424.3	39	2.2(-15)	3.2(-13)	4.3(-10)
	1024.6	72	1.6(-16)	2.3(-13)	5.3(-12)
	1220.9	≡100	9.5(-17)	1.4(-14)	2.2(-12)
	1226.9	83	9.3(-17)	1.3(-14)	2.2(-12)
2174.3	340.4	18	4.2(-15)	6.0(-13)	1.3(-09)
	1322.4	46	7.4(-17)	1.1(-14)	1.5(-12)
	2060.4	≡100	2.0(-17)	2.8(-15)	1.6(-13)
2196.7	147.9	57	3.7(-14)	5.4(-12)	5.9(-08)
	362.6	≡100	3.5(-15)	5.0(-13)	9.2(-10)
	572.1	26	9.1(-16)	1.3(-13)	9.7(-11)
	673.5	39	5.6(-16)	8.0(-14)	4.3(-11)
	1344.8	22	7.1(-17)	1.0(-14)	1.4(-12)
	1374.7	30	6.6(-17)	9.5(-15)	1.2(-12)

[a]The strongest γ-ray from each level is arbitrarily given a relative intensity of 100% and the others are compared with this.

[b]References 78 and 79 as treated in reference 23.

differences between *M*1 and *E*2 transition rates may not be predictable; therefore, the most useful information will be expected to come from comparing transitions that lead to states not in the group of six.

The "prototype" state at 1834.1 keV receives 37.4% of the ε-decay, with log *ft* = 5.6, and the argument for its being 9/2-, 11/2-, or 13/2- is clearly stronger than for any of the other states. Of the five gamma rays that de-excite it, the intense 982.2-keV gamma to the 851.9-keV state seems rather unambiguously to be an *E*1 (Table 7, Figure 25). This is additional evidence for odd parity, as 9/2+ or possibly 7/2+ was previously assigned to the 851.9-keV state. The 9/2+ assignment would imply either 9/2- or 11/2- for the 1834.1-keV state, while the 7/2+ assignment would limit it to 9/2-.

At this point only the consistency of the other gamma rays can be checked with these assignments. The 1006.1-keV gamma to the (7/2+, 9/2+) 828.1-keV state presumably is a parity-changing transition like the 982.2-keV gamma whereas the 1011.9-keV gamma to the 11/2- 821.9-keV state is not. The simplest explanation is for the 1011.9-keV gamma to be *M*1 and the 1006.1-keV gamma to be *E*1. The pronounced difference in the rates of the 982.2- and 1006.1-keV "*E*1" gamma rays must be attributed to internal structures of the states. It will be seen later that there are strong implications that the transitions out of the "high odd-parity" multiplet are rather highly hindered, so small admixtures in the states involved could have strong effects on the transition rates. The

9/2- and 11/2- assignments remain for the 1834.1-keV state, where the latter spin is recalled to be incompatible with 7/2+ for the 828.1-keV state.

The relatively intense 810.1-keV gamma ray would also appear to be an *E*1 transition, allowing the 5/2+ possibility to be removed for the 1024.0-keV state. The *M*1 and/or *E*2 assignment (Table 7, Figure 25) for the 209.7-keV gamma adds nothing new, but it is noted that the 1624.5-keV state must be quite similar to the 1834.1-keV state for this transition to be so enhanced.

Arguments for the 1927.1-keV state, which receives 12.8% of the ε-population, follow along similar lines. In particular, the 92.9-keV transition must be a collectively-enhanced *M*1 and/or *E*2, making the 1927.1- and 1834.1-keV states quite similar in origin. The 1105.2-keV gamma to the 821.9-keV state may be *M*1, and the 1075.1-keV gamma to the 851.9-keV state may be *E*1, all of which is consistent with 9/2- or 11/2- (equally probable) for the 1927.1-keV state. An educated guess for the 403.9-keV gamma is *E*1, which would imply positive parity for the 1523.2-keV state.

The 2196.7-keV state also appears to be very closely related to the 1834.1-keV state, viz., by the strong 362.6-keV gamma. Arguments parallel those above, resulting in 9/2- or 11/2- as possible choices.

The 1624.5- and 2048.8-keV states are similar in that both favor depopulating to the 828.1- rather than the 851.9-keV state. In each case what would appear to be an *M*1 transition to the 11/2- 821.9-keV state competes most favorably with an apparent *E*1 to the

828.1-keV state. Arguments for odd parity are also weakest for these two states (log ft = 6.3 for ε-decay to each), but the de-excitation pattern would be no easier to interpret if high-spin, even-parity states were assumed. Thus, 9/2(-) or 11/2(-) were tentatively chosen as possible assignments. It is perhaps worth noting that, if these assignments are correct and the six "high odd-parity" states are indeed closely related, there seems to be an interesting gradation in properties, with the 1834.1-keV state standing toward the middle, being the only state directly connected to all the others by gamma transitions. One example of this gradation is the strong transition between the 1927.1- and 1834.1-keV states, between the 1834.1- and 1624.5-keV states, and (less strong) between the 1624.5- and 1369.6-keV states -- this contrasts with the weak transition between the 1927.1- and 1624.5-keV states and the absence of a transition (upper limit ≈0.2% of the parent disintegrations) between the 1927.1- and 1369.6-keV states. [This sort of behavior ought to aid in sorting the states when shell-model calculations are done on the three-quasiparticle configuration proposed here for these states.]

The 2174.3-keV state stands somewhat apart from the other five in that it is the only one to de-excite directly to the lowest states in Pr^{139} and to miss populating several of the other five with quite intense gamma rays. Its large ε-population (log ft = 5.9) does, however, indicate 9/2-, 11/2-, or 13/2-. And its 2060.4-keV gamma to the 7/2+ 113.8-keV state, 1322.4-keV gamma to the (9/2+, 7/2+) 851.9-keV state, and lack of a transition (1352.4-keV gamma

intensity ≤0.3% of all parent decays) to the 11/2- 821.9-keV state favor the 9/2- assignment. The presence of the 2060.4-keV gamma ray also implies, if it is a three-quasiparticle state, that this state includes some $\pi g_{7/2}$ character in its composition, being thus less "pure" than the other five.

3.2.5.F. --The Remaining States-- The only remaining states in Pr^{139} excited by Nd^{139m} ε-decay that were known with enough assurance to be placed in the decay scheme are the 1369.6- and 1523.2-keV states. The 1369.6-keV state receives 1.3% of the ε-decay, with log ft = 7.3. Thus, one cannot decide between allowed and first-forbidden non-unique decay, and the assignment can be 9/2±, 11/2±, or 13/2±. Even less can be said about the 1523.2-keV state, which receives no direct population from Nd^{139m}. On the basis of the strength of the 101.3-keV gamma from the 1624.5-keV state, a weak argument can be made for spins between 7/2 and 13/2 with perhaps even parity.

3.2.6. Experimental Results for Nd^{139g}

3.2.6.A. --Gamma Ray Singles Spectra-- A gamma ray singles spectrum of Nd^{139g+m} taken with the 7-cm^3 Ge(Li) detector described in section 3.2.3.A is shown in Figures 27a and 27b. This spectrum represents the sum of six runs taken ≈30 min after the end of ≈45-sec proton bombardments. The duration of each of these runs was ≈20 min. Spectra were recorded periodically as the sources aged in order to identify activities with different half-lives and to follow the Nd^{139g} as it reached equilibrium with Nd^{139m}. Most of the gamma ray intensity, even this soon after the bombardments, originates from

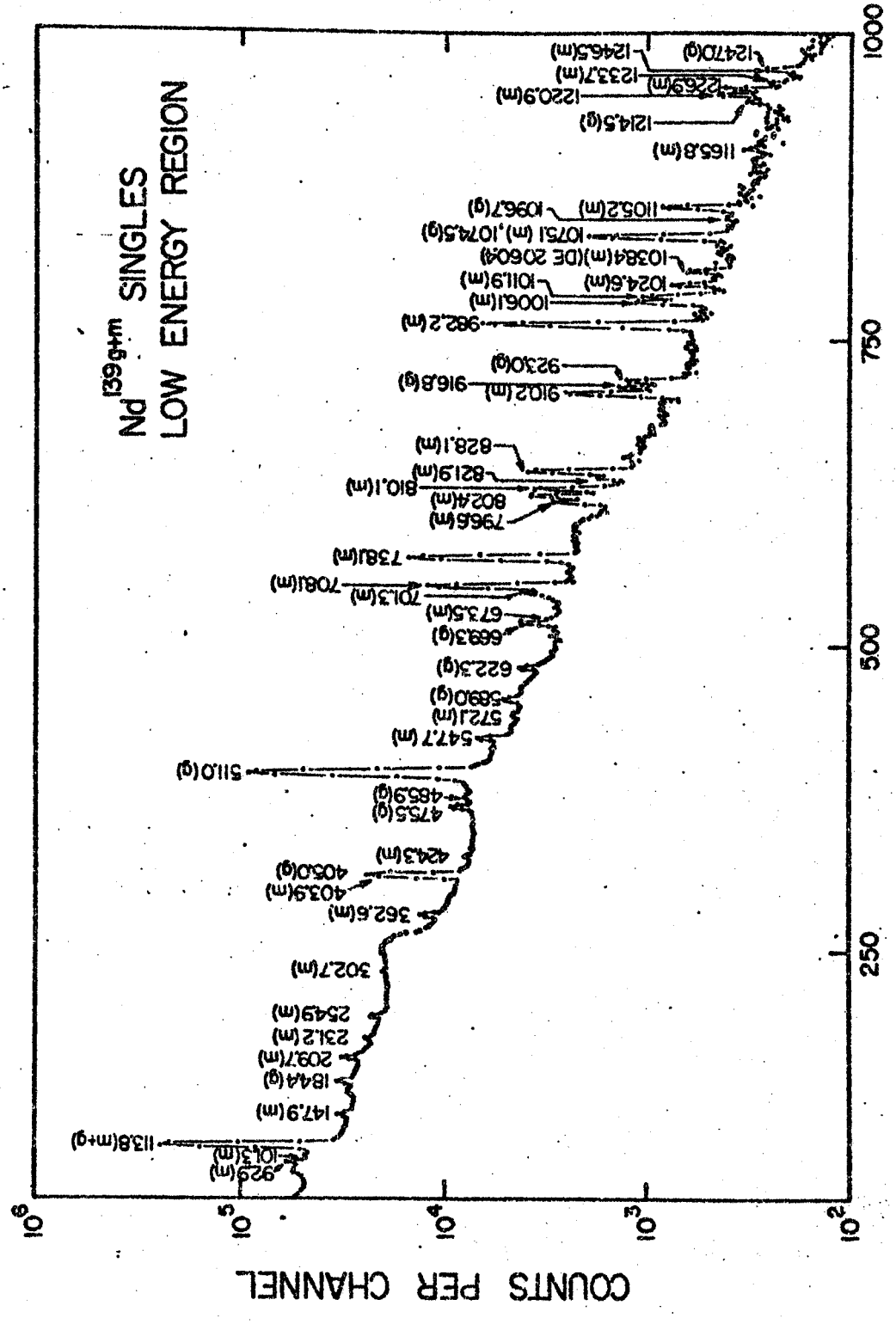

Fig. 27a. Nd^{139g+m} singles γ-ray spectrum taken with a 7-cm^3 Ge(Li) detector -- low-energy portion. This spectrum is the sum of six ≈20-min runs taken ≈30-min after the end of 45-sec proton bombardments. In this way the Nd^{139g} contribution was maximized both with respect to short-lived contaminants and with respect to Nd^{139m}.

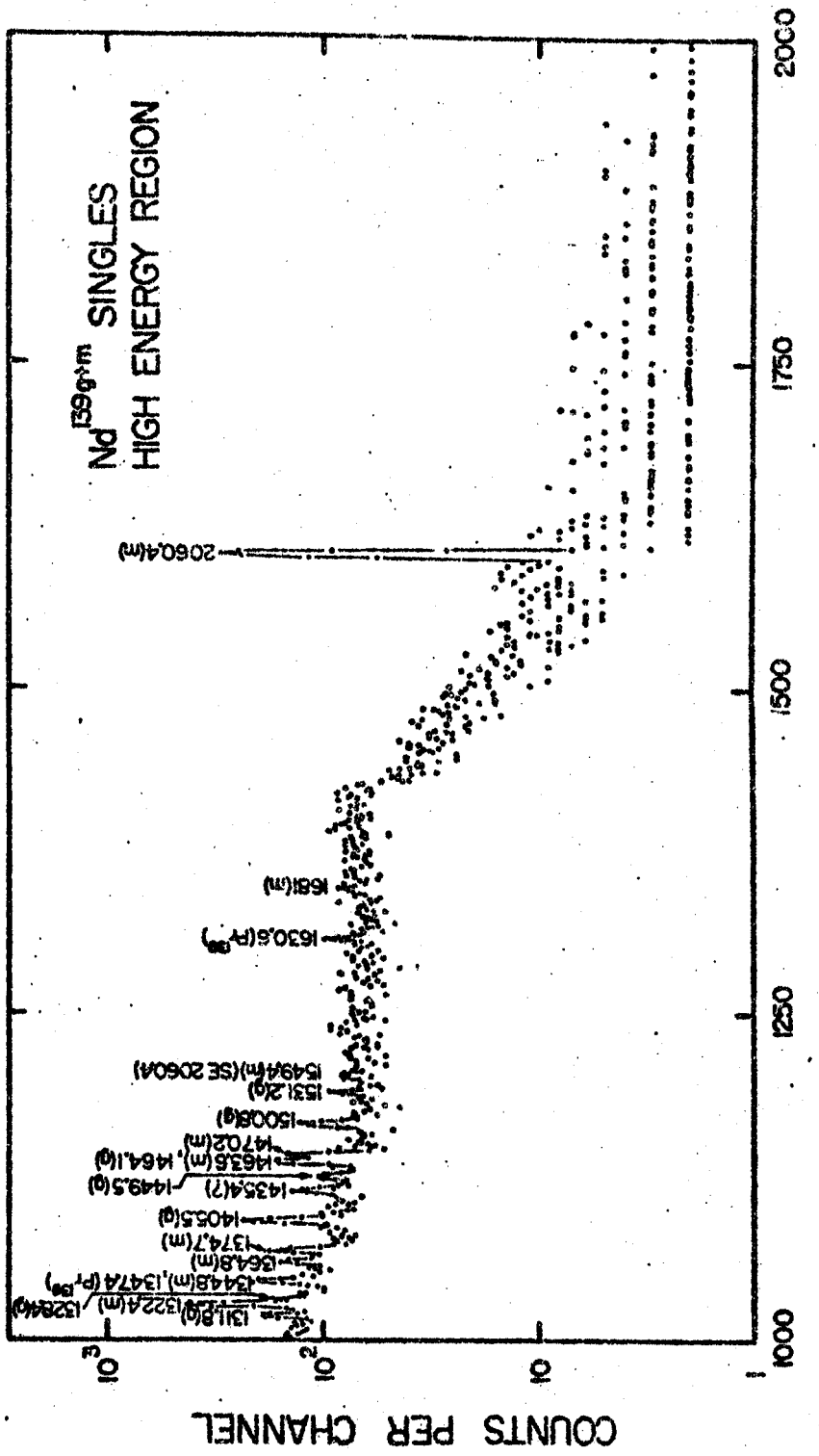

Fig. 27b. Nd^{139g+m} singles γ-ray spectrum taken with a 7-cm^3 Ge(Li) detector — high energy portion.

Nd^{139m} decay, for some 88% of Nd^{139g} beta decay proceeds directly to the ground state of Pr^{139}.

A list of the energies and relative intensities of the gamma rays identified with the decay of Nd^{139g} is given in Table 9. These were measured as described in section 3.2.3.A except that the now well-determined Nd^{139m} gamma ray energies were used as internal calibration standards. Of the 21 gamma rays listed in Table 9, only the 405.0-keV gamma has been reported previously (61).

A basic cause of experimental difficulties encountered in the study of Nd^{139g} decay is that the annihilation photons are an order of magnitude more intense than any of the gamma rays following its decay. This means that even the low activity of 5.5-h Nd^{139m} produced by the 45-sec bombardments significantly masks the 30-min Nd^{139g} gamma rays shown in Figures 27a and 27b.

As mentioned briefly in section 3.2.2, an attempt was made to populate Nd^{139g} selectively apart from Nd^{139m} by using the $Pr^{141}(\tau,5n)Pm^{139}\xrightarrow{\beta^+,\varepsilon}Nd^{139g}$ reaction. It was expected that the ground state of Pm^{139} would be a 5/2+ state and would populate 3/2+ Nd^{139g} in preference to 11/2- Nd^{139m}, thus producing a cleaner spectrum. The attempt was a partial success because the Nd^{139g}/Nd^{139m} isomer ratio was indeed increased by an order of magnitude. However, the presence of many other short- and long-lived contaminants from competing reactions nullified any net advantage of this method for producing clean Nd^{139g} sources. One would need to use this reaction in conjunction with a rapid ion-exchange separation (not yet feasible but perhaps available within a few years) for it to be

Table 9. Energies and relative intensities of gamma rays observed in Nd^{139g} spectra.

Measured γ-ray energy (keV)	Relative γ-ray intensity[a]	Measured γ-ray energy (keV)	Relative γ-ray intensity[a]
113.8±0.2	10.1±10[b]	1074.5±0.5	11.9± 1
184.4±0.4	4.2± 0.4	1096.7±1.0	0.9± 0.4
405.0±0.4	36.4± 3.0[c]	1214.5±0.4	2.2± 0.3
475.5±0.4	7.9± 0.6	1247.0± 1.0	0.6± 0.3
485.9±0.8	2.8± 0.7	1311.8±0.6	2.0± 0.7
511.0 (γ±)	360 ±50[d,e]	1328.4±0.6	1.1± 0.3
589.0±0.5	5.3± 0.6	1405.5±0.7	3.3± 0.5
622.3±0.3	6.4± 1.0	1449.5±0.7	0.8± 0.3
669.3±0.5	8.3± 2	1464.1±0.5	2.3± 0.4
916.8±0.4	8.5± 0.6	1500.8±0.8	2.0± 0.5
923.0±0.4	6.9± 0.8	1531.2±1.0	1.1± 0.4

[a]Relative to 100 for the intensity of the 738.1-keV γ-ray in Nd^{139m} ≈30 min after the end of ≈45 sec proton bombardments.

[b]Based on the sum of γ-intensity feeding the 113.8-keV level as indicated in the decay scheme (Figure 24) because most of the 113.8-keV γ-intensity originates from population by the 5.5-h Nd^{139m}, even 30 min after Nd^{139m+g} is produced.

[c]Result after the 403.9-keV component of the 403.9-, 405.0-keV doublet is subtracted out on the basis of the Nd^{139m} relative intensities (see Table 3).

[d]Approximately 98% of the annihilation photons come from Nd^{139g} decay ≈30 min after the production of Nd^{139m+g}.

[e]From the decay scheme an upper limit of 16.1 can be placed on the intensity of a hypothetical 511.8-keV γ-ray depopulating the 916.8-keV state.

really clean. It did, however, verify the relative intensities of most of the Nd^{139g} gamma rays.

3.2.6.B. --Gamma Gamma Coincidence Studies-- by analogy with the decay scheme of $d_{3/2}$ Nd^{141} (seen in Figure 8), it was expected that a number of states would be present, which, upon receiving direct β-population, would de-excite directly to the Pr^{139} ground state. For this reason the 8-in. × 8-in. NaI(Tl) split annulus (19) and a 3-in. × 3-in. NaI(Tl) detector was used in an anti-coincidence experiment with the 7-cm^3 Ge(Li) detector; the geometry was as described in section 3.2.3.B. Again, the single-channel analyzer for the NaI(Tl) detectors was set so that the gate would be active for all gamma rays above 100 keV. The resulting anti-coincidence spectrum is shown in Figure 28, and the resulting intensities of the Nd^{139g} gamma rays (relative to 100 for the 738.1-keV Nd^{139m} gamma ray) are listed in Table 10. Seven states in Pr^{139} were indicated by these results.

In order to complement the anti-coincidence data, a coincidence spectrum was obtained using the same apparatus. The gate from the NaI(Tl) detectors was open for gamma rays above 350 keV. This "integral" coincidence spectrum is shown in Figure 29A, and the relative intensities derived from it are also included in Table 10. As expected, they verify the results of the anti-coincidence data.

The high intensity of the 405.0-keV gamma suggests the presence of a state in Pr^{139} at this energy. Four energy sums also

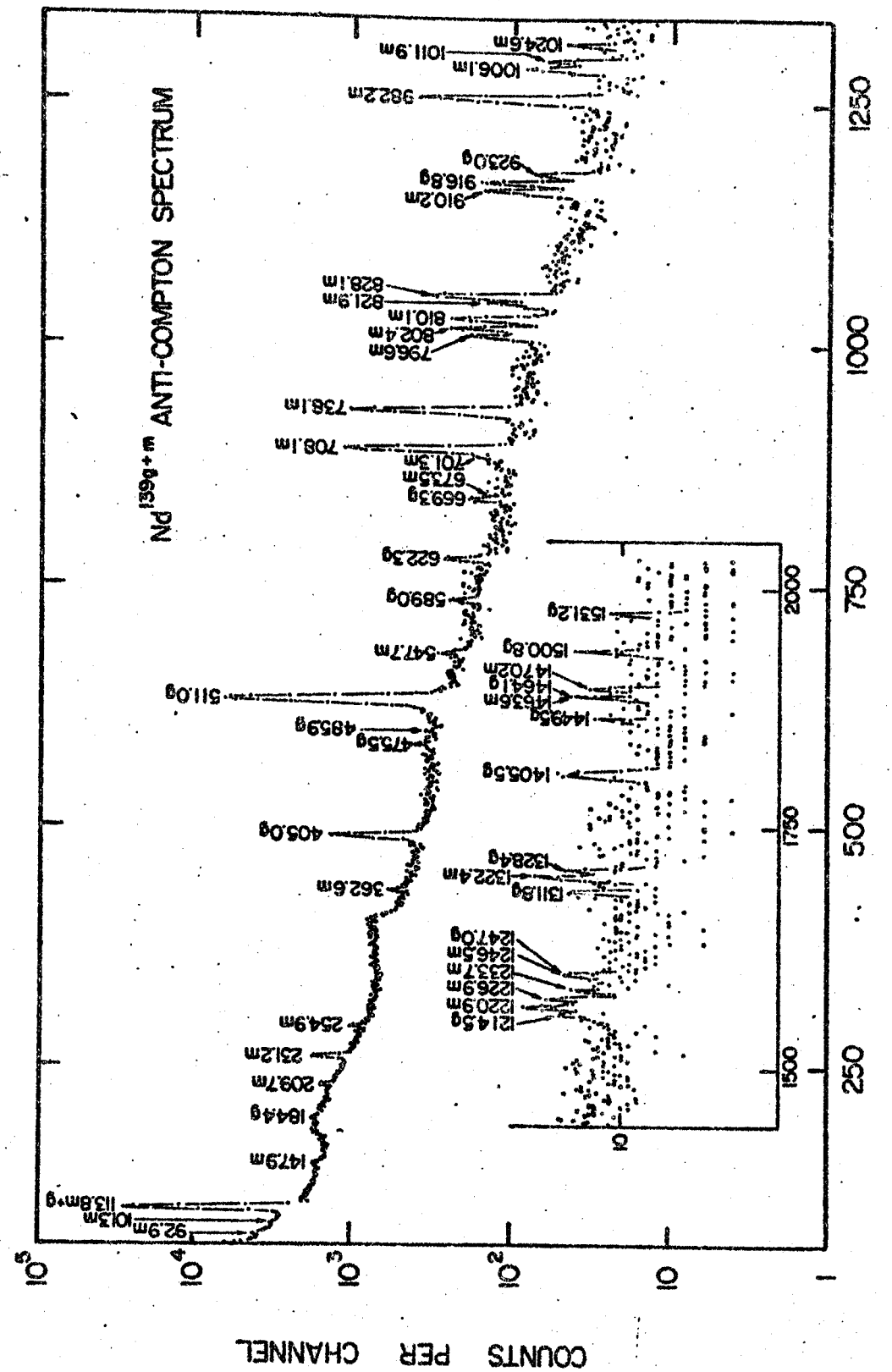

Fig. 28. Nd^{139g+m} anti-coincidence spectrum. (Cf. Figure 10.)

Table 10. Relative intensities of photons in the decay of Nd^{139g} observed in several γ-γ coincidence experiments.

E_γ (keV)	Relative intensity						
	Fig. 27 Singles[a]	Fig. 28 Anticoincidence	Fig. 29 Integral coincidence	Fig. 29 405-keV coincidence	Fig. 30 113.8-keV coincidence	Fig. 31 2-d Integral coincidence	Fig. 31 2-d 405-keV coincidence
113.8	10.1	<24	---	---	---	<160	<231
184.4	4.2	<0.3	5.8[d]	---	---	4.8[d]	27[d]
405.0	36.4	<9.8	<49[d]	18	<17	35[d]	44
475.5	7.9	0.7	8.1[d]	5.2	11	6.3[d]	---
485.9	2.8	0.5	2.7[d]	4.0[d]	<3	1.8[d]	24[d]
511.0[b]	360	120	304	127	360	78	287
(511.8?	<16.1?)	---	---	---	---	---	---
589.0	5.3	1.6	4.8	<9.8	<5	---	---
622.3	6.4	2.8	0.8	<8	<5	<2	---
669.3	8.3	1.8	1.4	18	<6	8[d]	61[d]
916.8	8.5	5.1[c]	0.3	1.9	<4	<1	---
923.0	6.9	1.0	0.8[d]	17[d]	5	3[d]	41[d]
1074.5	11.9	8[c]	<1	<11	<13	<15	---
1096.7	0.9	<0.9	0.7	2	---	---	---
1214.5	2.2	0.5	<1	2	5	---	---
1247.0	0.6	<0.6	<0.6	<6.5	---	---	---
1311.8	2.0	0.8	<0.3	<3	---	---	---

Table 10. (continued)

1328.4	1.1	0.5[c]	<0.3	<10	---	---	---
1405.5	3.3	2.3[c]	0.1	<3	---	---	---
1449.5	0.8	0.55[c]	0.1	<3	---	---	---
1464.1	2.3	<1.0	<0.6	<3	---	---	---
1500.8	2.0	1.2[c]	<0.2	<3	---	---	---
1531.2	1.1	0.4	<0.4	<3	---	---	---

[a]Intensities relative to 100 for the intensity of the 738.1-keV γ in Nd^{139m} ≈30 min after the end of 45-sec proton bombardments.

[b]Largely composed of annihilation photons, but an admixture of 511.8-keV γ's with an intensity of ≤16, using the scale of Table 7, has not been ruled out. This possibility is discussed in section 3.2.7.

[c]Evidence seen here for primarily ε-fed ground-state transition.

[d]Evidence seen here for γ-γ coincidence event.

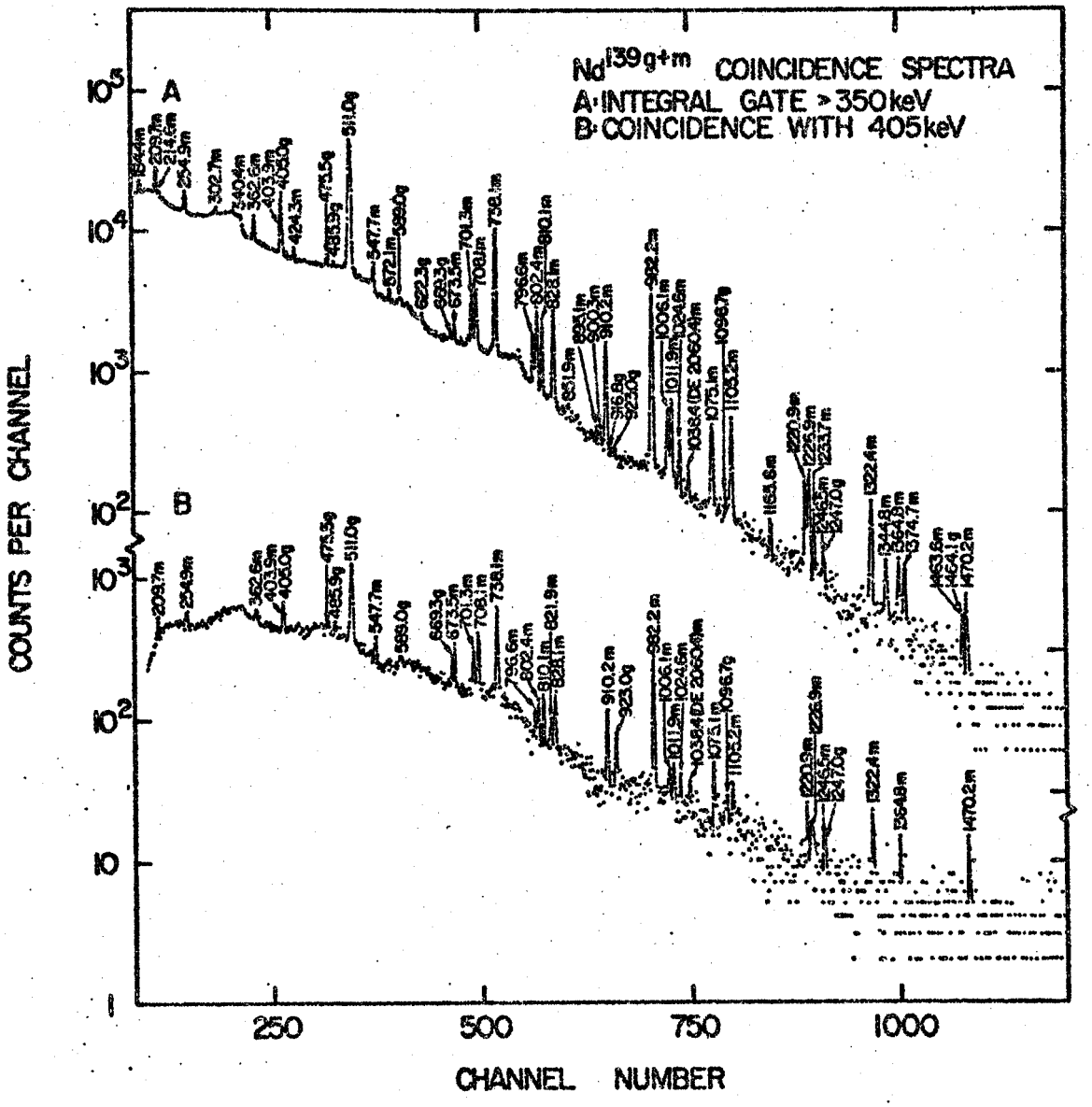

Fig. 29. A) Nd^{139g+m} integral coincidence spectrum. This spectrum was recorded by a 7-cm^3 Ge(Li) detector with the 8-in. × 8-in. NaI(Tl) split annulus set to accept all γ-rays above 350 keV.

B) The annulus gate was set on the 405-keV energy region.

indicate possible gamma ray cascades involving this transition. To obtain evidence supporting these cascades, the NaI(Tl) annulus detector was gated on the 380-430-keV region and the coincident spectrum seen by the 7-cm^3 Ge(Li) detector was displayed. The resolving time (2τ) of the coincidence circuit was ≈100 ns. This spectrum is shown in Figure 29B, and the relative intensities of the Nd^{139g} gamma rays are included in Table 10, where the ones that are thought to be in coincidence with the 405.0-keV gamma are so indicated.

The same coincidence spectrometer was then gated on the 113.8-keV gamma. The measured relative intensities from the spectrum seen in Figure 30 are also listed in Table 10. This experiment verified the energy-sum indication that the 113.8-keV gamma is in cascade with the 475.5- and 1214.5-keV gamma rays.

Confirmations of several of the coincidences described above and new evidence for a 405.0-184.4-keV cascade were obtained with a 3-in. × 3-in. NaI(Tl), 7-cm^3 Ge(Li) two-parameter (mega-channel) spectrometer employing dual 4096-channel ADC's. These data are summarized in Table 10. Following each coincident event, the channel numbers representing the photon energies were stored in a dedicated buffer in the SDS Sigma 7 computer. When the buffer filled, its contents were written on magnetic tape. It was then possible to recover the coincidence information in slices in order to construct useful spectra. In Figure 31A, the integral Nd^{139g+m} coincidence spectrum obtained on the Ge(Li) side is shown, and in Figure 31B, the results of gating on the 405-keV region of the

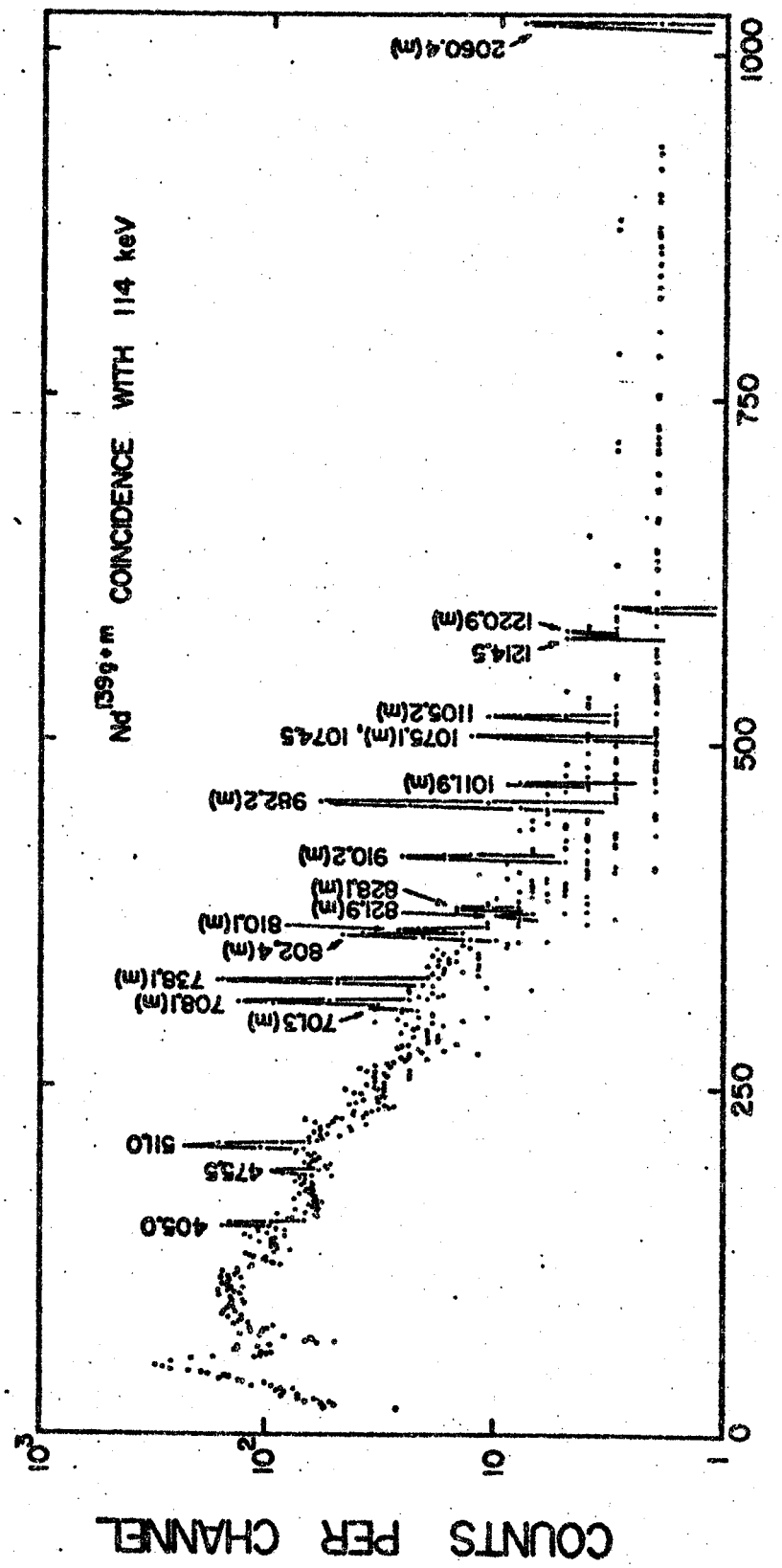

Fig. 30. Spectrum of Nd^{139g+m} γ-rays in coincidence with the 113.8-keV γ. The gate detector was the 8-in. × 8-in. NaI(Tl) split annulus, and the signal detector was the 7-cm^3 Ge(Li) detector.

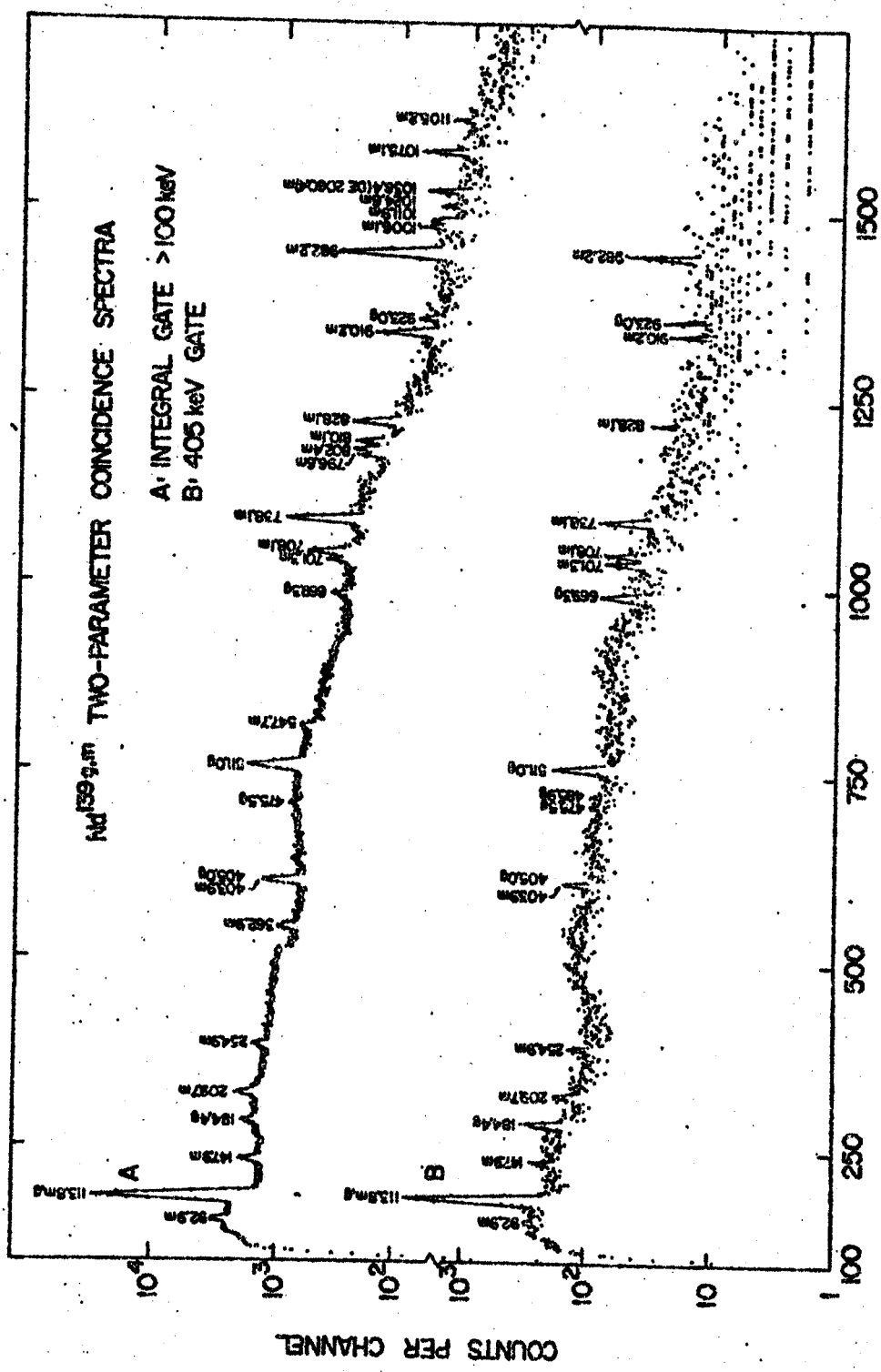

Fig. 31. Slices from a two-dimensional (megachannel) γ-ray spectrum for Nd^{139g+m}.
A) Integral gate of all γ-rays above 100 keV.
B) 405-keV gate. See the text for details.

NaI(Tl) side and displaying the resulting Ge(Li) spectrum are shown.

3.2.7. Nd^{139g} Decay Scheme

The decay scheme for Nd^{139g} that was deduced from the measurements was presented in Figure 24 for comparison with the Nd^{139m} decay scheme. Again, all transition energies and excited state energies are given in keV and the β^+/ε ratios are calculated values (47). All of the (total) transition intensities are given in percent of the Nd^{139g} disintegrations.

None of the ten excited states proposed here has been reported previously in published Nd^{139g} decay-scheme studies. The only one of these states for which there is evidence of population from Nd^{139m} decay (i.e., β-decay) is the 113.8-keV state. The 113.8-keV gamma was seen to have a 30-min decay component in addition to its dominant 5.5-h component. It was also observed to be in cascade with the 475.5- and 1214.5-keV gamma rays accompanying Nd^{139g} decay.

It was mentioned earlier that the high intensity of the 405.0-keV gamma indicates the probability of a state in Pr^{139} at 405.0 keV. This placement was confirmed by coincidences of four gamma rays (five, if a tentative 511.8-keV gamma is included) with the 405.0-keV gamma. In the process of constructing the decay scheme, it is assumed that the imbalance of gamma ray intensities leaving and entering the 405.0-keV state is removed entirely by β-feeding of this state. However, the possibility that a 511.8-keV transition from a level at 916.8 keV to this state is present

(≤2.5%) but obscured by the intense annihilation photons cannot be ruled out.

Higher-lying states at 589.2, 1074.4, 1328.2, and 1501.2 keV are suggested by energy sums and relative photon intensities and confirmed by coincidence and anti-coincidence information. The states at 916.8, 1311.8, 1405.5, and 1449.5 keV were placed on the basis of the enhancement (reduction) of the 916.8-, 1311.8-, 1405.5-, and 1449.5-keV gammas in anti-coincidence (coincidence) experiments as seen in Figures 28-31 and Table 10.

The Q_ε = 2800 keV is a calculated value (69), which ought to be good to within several hundred keV. There have been several attempts to measure the β^+ end points, but at this time their precision is not particularly good. Several measurements of the (total) annihilation photon relative intensity component due to Nd^{139g} were used in order to calculate the 88% β-branching to the ground state. In the $Nd^{139m+g} \rightarrow Pr^{139} \rightarrow Ce^{139}$ decay chain, Nd^{139g} accounts for ~3% of the annihilation photon intensity at ~30-min after the 45-sec bombardments.

Four unplaced gamma rays identified with Nd^{139g} decay were observed with energies (relative intensities) of 622.3 (6.4), 1247.0 (0.6), 1464.1 (2.3), and 1531.2 keV (1.1). The sum of these intensities yields 8.3% of the observed Nd^{139g} gamma ray intensity and 1.5% of the observed Nd^{139g} total disintegrations. Some properties of these rays can be deduced from Tables 9 and 10. The relatively strong 622.3-keV gamma perhaps suggests placing a state at 622.3 keV, but in view of the lack of any supporting evidence, it is omitted

from the decay scheme. The log ft for population of such a state would be ≥6.8.

3.2.8. Spin and Parity Assignments from Nd^{139g} Decay

Spin and parity assignments to the lowest two levels have been discussed in section 3.2.5.C in connection with the decay of Nd^{139m}. The 63% ε, 27% β^+ decay to the ground state is quite consistent with a $\pi d_{5/2} \rightarrow \nu d_{3/2}$ transition, and the log ft = 5.1 is remarkably close to that found for the analogous transition in Nd^{141} decay shown in Figure 8 (log ft = 5.3).

It is difficult to set a precise upper limit on direct β-decay to the 7/2+ 113.8-keV state because of the intense 113.8-keV gamma ray component from Nd^{139m} decay. An upper limit of 0.03% of the parent disintegrations, with log ft >8.8, was placed on the analogous and much cleaner $Nd^{141g} \rightarrow Pr^{141g}$ β-transition. For Nd^{139g} decay, of course, such precision is out of the question, but the fact that no indication of direct β-population is seen is clearly consistent with a $(d_{5/2})^2(g_{7/2})^{-1}$ configuration, as discussed before.

The remaining nine levels all are populated by β^+/ε-decay from 3/2+ Nd^{139g} with log ft's ranging from 5.6 to 7.2. These all fit quite nicely in the range expected for allowed decay, and, although one cannot rule out first-forbidden decay on the basis of these alone, no indication is seen that any states other than the 1/2+, 3/2+ or 5/2+ states are populated directly by Nd^{139g}. In fact, all the log ft values are slightly smaller than those listed

in Figure 8 for the analogous transitions in Nd^{141} decay. For some of the states, especially those exhibiting gamma ray branching, the assignments may be narrowed further:

The states at 405.0 and 916.8 keV are tentatively assigned 1/2+ or 3/2+ because they both decay to the 5/2+ ground state and miss the 7/2+ 113.8-keV state. The 916.8-keV state may or may not decay also to the 405.0-keV state via the unobserved 511.8-keV transition, which just might have appreciable intensity, but this fact is more concerned with the internal structure of (both) states than with their spin and parity -- although the presence of the transition would lend further support to the assignments proposed here. Solely on the prediction of the shell model that the $s_{1/2}$ state ought to lie between the $h_{11/2}$ state and the $d_{5/2}$ and $g_{7/2}$ states, one is tempted to identify the 405.0-keV state with it. There is no supporting evidence, however, and one must ask why the $s_{1/2}$ state should be populated so easily here when it has not been seen in either Nd^{141} decay (see section 3.1) or Ce^{143} decay (87) to the next heavier Pr isotopes, which otherwise show much the same single-particle state positions (within a few hundred keV). It will be seen that gamma ray branchings to this state tend to support the 3/2+ rather than the 1/2+ assignment.

Next the states that decay through the 7/2+ 113.8-keV state are considered, namely those at 589.2- and 1328.2-keV. The mere presence of the 475.5- and 1328.4-keV gammas rules out the 1/2+ possibility for these states. Both assignments can be tentatively nar-

rowed down to 5/2+ with the aid of the gamma ray branchings.

For the 589.2-keV state, a 3/2+ assignment would lead to single-particle estimates (23) of the relative intensities of the 589.0/475.5/184.4-keV gammas (*M*1/*E*2/*M*1, with possible *E*2 admixing in the *M*1's) of 1/0.005/0.04. A 5/2+ assignment (all *M*1's would lead to roughly 1/0.5/0.06. Although considerable *E*2 enhancement is to be expected (because of the softness of this nucleus to vibrations) and *M*1's might be somewhat retarded, the latter ratio is clearly preferable when compared with the experimental ratio, 1/1.5/0.75. The 405.0- and 589.2-keV states may well be core-coupled states involving the $d_{5/2}$ ground state. That they lie so low is not too surprising, for Pr^{139} (two neutrons fewer than 82) (87), which, being again somewhat soft to vibrational excitations, appears to have core-coupled states at this same energy. A 5/2+ assignment for the 589.2-keV state would exclude a 1/2+ assignment for the 405.0-keV state.

Quite similar reasoning holds for the 1328.2-keV state, except that it lies high enough that one can deduce little about its internal makeup. The corresponding single-particle predictions for the relative intensities of the 1328.4/1214.5/923.0-keV gammas are 1/0.005/0.3 and 1/0.8/0.3 for 3/2+ and 5/2+ assignments, respectively. Although neither can be called a satisfactory fit (experimental ratios are 1/1.5/5.5), the latter is in the ball park. Considering the obvious enhancement of the gamma rays to the 405.0-keV state from both the 1328.2- and 589.2-keV states, one is tempted

to look for the 739.0-keV gamma between the latter two. Unfortunately, it could be as intense as 0.7% and have escaped detection because of the presence of the intense 738.1-keV gamma from Nd^{139m} decay.

The states at 1074.4 and 1501.2 keV are tentatively assigned 1/2+ or 3/2+ because they hit the ground state but miss the 7/2+ 113.8-keV state in their depopulation. This is indeed tentative, however, and one must know more about the internal structure of these states before definite assignments can be made. It would be quite possible, for example, to postulate a hypothetical 5/2+ state consisting of a $d_{5/2}$ quasiparticle coupled to a 2+ phonon excitation that would clearly populate the ground state to the exclusion of the 113.8-keV state.

The remaining states, at 1311.8, 1405.5, and 1449.5 keV, which were placed on the basis of their ground-state transitions alone, might have their assignments narrowed down to 3/2+ or 5/2+; however, the population is quite weak for all three, with even parity even being somewhat in doubt, so they are left as 1/2, 3/2, 5/2(+).

3.2.9. Discussion

A total of at least twenty-three states in Pr^{139}, practically none of which had been reported before, were observed from the combined decays of Nd^{139m} and Nd^{139g}. These states apparently can be classified in three quite distinct categories: 1) single-quasiparticle states, 2) single-quasiparticle states coupled to various vibrational configurations, and 3) three-quasiparticle states. The conclusions drawn can be most definite about the states in the first

category and, because of an unusual feature in the β-decay properties of Nd^{139m}, the third category. As this is an experimental report, the discussions that follow will remain empirical, but some directions are proposed, both experimental and theoretical, that might be taken for further clarification of the properties of this most interesting nucleus.

3.2.9.A. --Single-Particle States-- Again, the term "single-particle" states is used here to label those states with primarily single-quasiparticle amplitudes in their wave functions. These range from the more or less pure states near the ground to highly fractionated and complicated states at higher energies, and when these states are spoken of in simple shell-model terms, this is not to imply that they are really pure shell-model states.

On the neutron-deficient side of N=82 in the lanthanide region, practically nothing has been done in the way of even qualitative calculations of the positions of nuclear states -- even the pairing-plus-quadrupole force calculations of Kisslinger and Sorensen (81) give out at Nd^{141}. This means that empirical data must be used for the most part, although the large number of states excited in Pr^{139} in this study makes this more practicable than usual. Thus, in Figures 32 and 33 respectively, the known states in the light odd-mass Pr isotopes and in the odd-mass N=79 isotones are plotted. Here the nuclides are beginning to get far enough from β-stability that no scattering reactions have been performed to excite states, so the number of states recorded is very much a function of Q_ε.

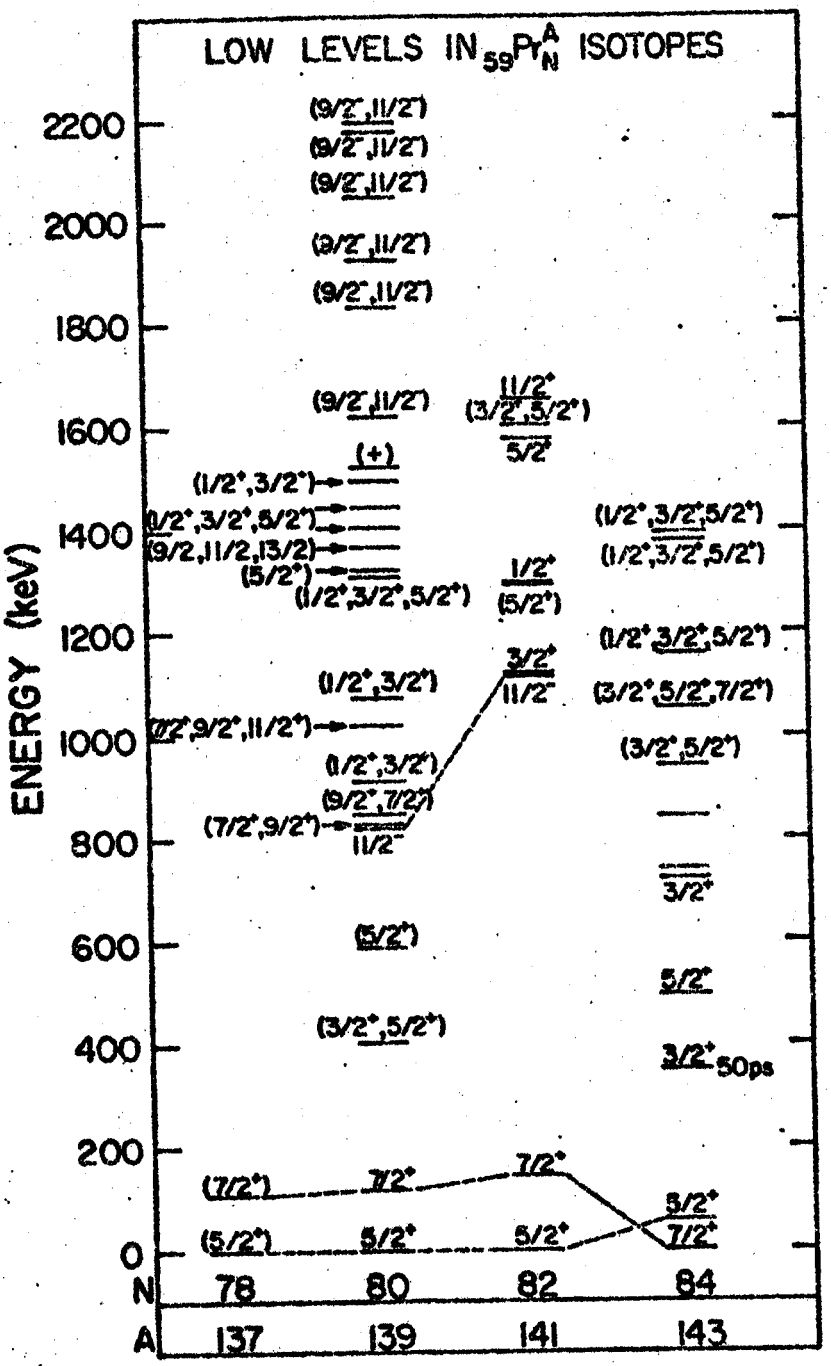

Fig. 32. Experimental levels in odd-mass Pr isotopes, demonstrating the effects of changing neutron number on the positions of the states. Unambiguously related states are connected by the dashed lines. References: Pr^{137}, ref.70; Pr^{139}, this section of this study; Pr^{141}, section 3.1 and Chapter 4 of this study and refs. 88, 89, 90; and Pr^{143}, ref. 87.

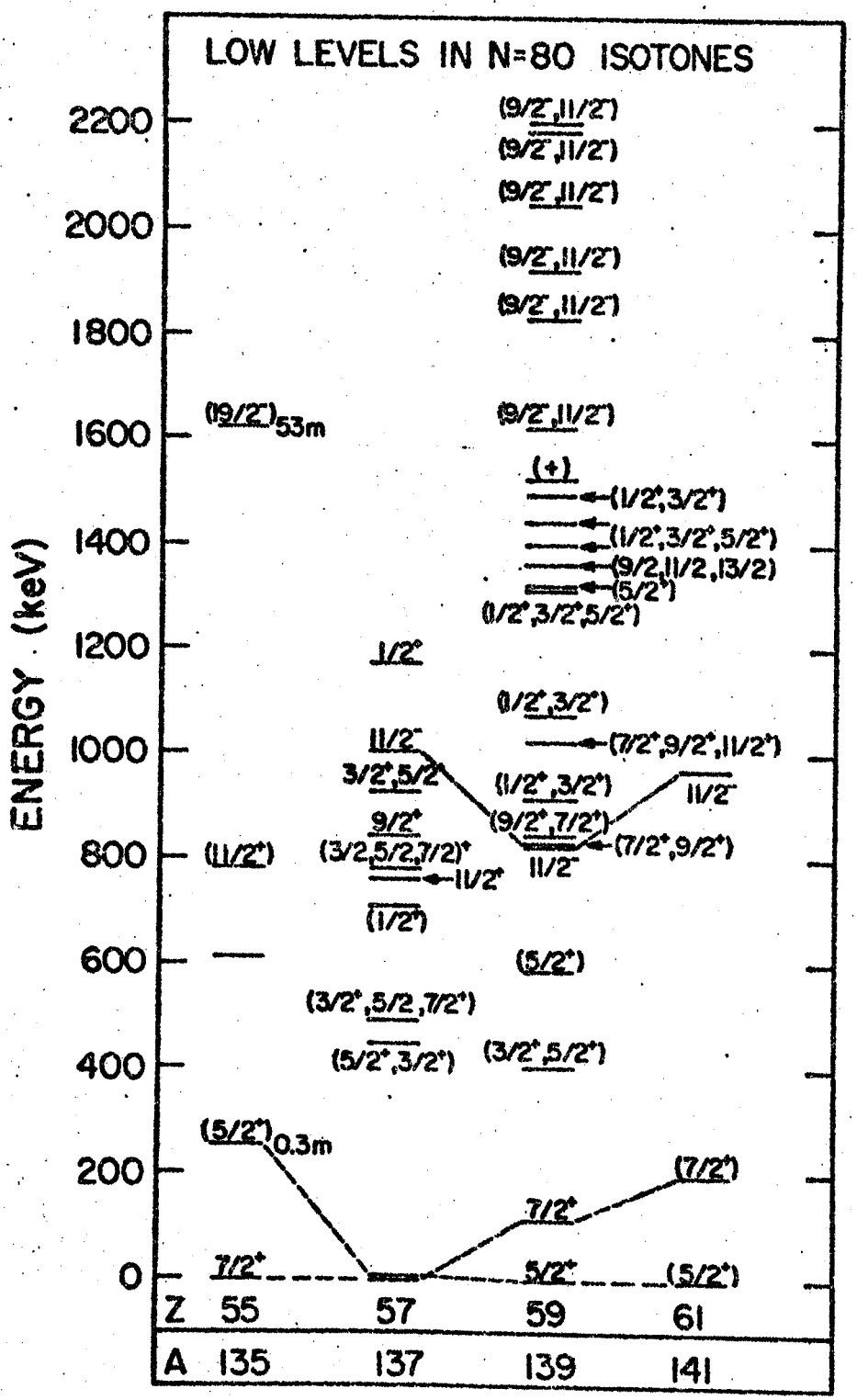

Fig. 33. Experimental levels in odd-mass N=80 isotones, demonstrating the effects of changing neutron number on the positions of the states. Unambiguously related states are connected by the dashed lines. References: Cs^{135}, refs. 91 and 92; La^{137}, section 3.3 of this study; Pr^{139}, this section of this study; and Pm^{141}, refs. 61 and 77.

Evidences of all the available single-proton states between Z=50 and Z=82 are probably seen in Pr^{139}. The most clearcut single-quasiparticle states are those at 0, 113.8, and 821.9 keV. The ground state undoubtedly consists primarily of a single $d_{5/2}$ proton outside a closed $g_{7/2}$ subshell, and the 113.8-keV state simply promotes a $g_{7/2}$ proton, resulting in a $(d_{5/2})^2(g_{7/2})^{-1}$ configuration. As mentioned previously, the retarded *M*1 transition between them is characteristic of the ℓ-forbidden *M*1's between $g_{7/2}$ and $d_{5/2}$ states in a wide variety of nuclei in this region. The relatively small spacing between the first two states is consistent with trends in both proton and neutron numbers in neighboring nuclei, for the 7/2+ and 5/2+ states cross over between Pr^{141} and Pr^{143} and also between La^{137} and Pr^{139}.

The 821.9-keV state shows evidence of being a single $h_{11/2}$ proton outside the closed $g_{7/2}$ subshell. As mentioned in section 3.2.5.C, the *M*2 transition from this state to the 113.8-keV state is retarded, while the *E*3 to the ground state is enhanced over single-particle estimates. Van Hise, Chilosi, and Stone (84) suggest that a similarly enhanced *E*3 transition in La^{137} could be explained in terms of a coupling of the $d_{5/2}$ proton to a 3- octupole vibration, resulting in a nearby 11/2- state that could be mixed into this state. Superficially, one might ask why it is not also possible to admix a similar 11/2- state, this time based on the $g_{7/2}$ proton, into this state, thereby enhancing the *M*2 as well as the *E*3 transition. As it turns out, one cannot really test either hypothesis, for the positions of possible octupole

states are unknown. With the above shell-model assignments, however, the $E3$ is the better single-particle transition, involving principally the de-excitation only of a proton from the $h_{11/2}$ to the $d_{5/2}$ orbit. The $M2$, conversely, involves breaking the $g_{7/2}$ subshell in addition, so its retardation is suggested by these simple arguments.

The positions of the $d_{3/2}$ and $s_{1/2}$ states are not so clear, but they are probably fragmented and contribute to several states above 1 MeV. The state at 405.0 keV (and at 589.2 keV, for that matter, if the spin assignments proposed here are incorrect) is not likely to be either of these single-particle states. In the more rigid Pr^{141}, other than the $g_{7/2}$ and $d_{5/2}$ states, there are no single-particle states below 1114 keV that were populated either by Nd^{141} decay (described in section 3.1) or by (τ,d) (88) or (d,τ) (89) scattering. Of the number of levels just above 1 MeV that were possible contenders, it was not possible to identify specific levels with either the $d_{3/2}$ or $s_{1/2}$ states because of uncertainties related to the vibrational character of that nucleus. Pr^{139} is much easier to deform than Pr^{141}, and thus many more low-lying states are expected, but there is no reason to expect either the $d_{3/2}$ or $s_{1/2}$ states to drop drastically in energy, so they may be partly associated with a number of the higher levels.

3.2.9.B. --Three-Quasiparticle States-- In section 3.2.5.E arguments were presented to the effect that the six states at 1624.5 1834.1, 1927.1, 2048.8, 2174.3, and 2196.7 keV appear to be high-

spin, odd-parity (9/2- or 11/2-) states. The only straightforward explanation that has been found to explain their enhanced ε-population relative to the 821.9-keV state plus the many low-energy gamma transitions among them and the lack of direct transitions down to the ground or 113.8-keV states is that these six states are part of a three-quasiparticle multiplet having the configuration $(\pi d_{5/2})(\nu d_{3/2})^{-1}(\nu h_{11/2})^{-1}$. The particle transitions postulated here are outlined in Figure 34.

In the extreme single-particle approximation, ${}_{60}Nd^{139}_{79}g$ can be represented as three $d_{3/2}$ neutron holes in the N=82 shell (i.e., a single neutron in the $d_{3/2}$ orbit) and eight $g_{7/2}$ (closed subshell) and two $d_{5/2}$ protons above Z=50. Due to the isomeric properties discussed in section 3.2.5.B, Nd^{139m} ought to differ only in the promotion of an $h_{11/2}$ neutron into the $d_{3/2}$ level, resulting in eleven $h_{11/2}$ and two $d_{3/2}$ neutrons. The only change involved in the decay of Nd^{139g} to the ground state of Pr^{139} is the conversion of a $d_{5/2}$ proton into a $d_{3/2}$ neutron. This accounts for the low log ft value of 5.1 for this transition.

The analogous transition from Nd^{139m}, i.e., $\pi d_{5/2} \rightarrow \nu d_{3/2}$, however, results in the three-particle configuration $(\pi d_{5/2})(\nu d_{3/2})^{-1}(\nu h_{11/2})^{-1}$. Hence, the apparent abnormally large population to these states is in fact the expected mode of decay. The 821.9-keV 11/2-state, on the other hand, should have the configuration $(\pi h_{11/2})(\nu d_{3/2})^2$, so decay to it would require converting one $d_{5/2}$ proton into an $h_{11/2}$ neutron, either in one step or perhaps

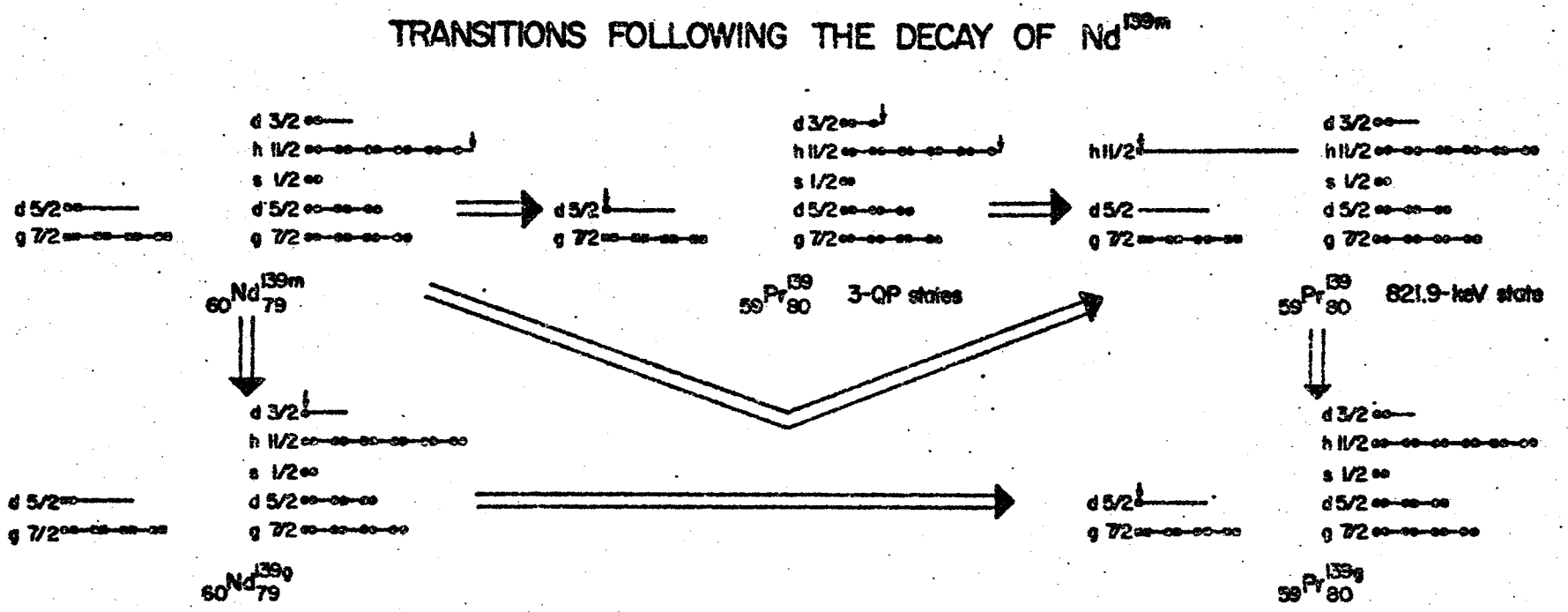

Fig. 34. Symbolic shell-model representations of some important transitions between Nd^{139} and Pr^{139} states. A stylized picture of the proton (squares) and neutron (circles) states between 50 and 82 nucleons, has been given. The arrows point to the nucleons or holes of prime interest in each state.

through an intermediate $d_{3/2}$ neutron state, and a simultaneous promotion of the remaining $d_{5/2}$ proton to the $h_{11/2}$ state. The resulting relatively large log ft of 7.0 is thus not unexpected.

Although the above interpretation qualitatively explains most of the gamma ray branchings between members of the negative-parity multiplet, there are several places involving very highly hindered transitions where it runs into difficulties. This is taken to mean that small admixtures in the states are very important in determining these transition rates. However, it is instructive to consider specifically one of the more extreme examples -- the 1011.9-keV gamma (2.9%) from the 1834.1-keV state to the 11/2- 821.9-keV state as compared with the unobserved (<0.5%) 1834.1-keV gamma to the 5/2+ ground state. With an 11/2- assignment for the 1834.1-keV state one would not expect to see the 1834.1-keV gamma, but with a 9/2- assignment the arguments are not so clear. Single-particle estimates (23) for the $t_{\frac{1}{2}}$'s of the 1011.9- ($M1$) and 1834.1-keV ($M2$ or $E3$) gammas are 2.4×10^{-14} and 8×10^{-12} or 4×10^{-9} sec, respectively. According to the above description, the missing $M2$ or $E3$ would involve an apparently very simple $\nu d_{3/2}\rightarrow\nu h_{11/2}$ transition (the $M2$ would be ℓ-forbidden); there may also be some hindrance from uncoupling and recoupling the states. On the other hand, the observed 1011.9-keV $M1$ gamma requires the simultaneous changes $\nu d_{3/2}\rightarrow\nu h_{11/2}$ and $\pi d_{5/2}\rightarrow\pi h_{11/2}$, each of which is doubly ℓ-forbidden. However, ℓ-forbiddeness loses much of its meaning in multiparticle transitions and would depend on the relative

phases of the transforming states; also core polarization in multiparticle states tends to obscure the ℓ selection rules (93). However, multiparticle gamma decay is formally absolutely forbidden, and, although there are known cases where such transitions take place at enhanced rates (e.g., the 63-keV $E1$ gamma in Bk^{250} following Es^{254} α-decay (94)), these are not common. When such involved rearrangements are compared, the single-particle estimates lose all meaning, and minute admixtures could easily be the deciding factors.

In this multiplet of three-quasiparticle states there are two different and potentially very rewarding sources of information: 1) The enhanced transitions between the various members of the multiplet. These should give information about the gross features of the states and should allow one to perform calculations on states at several MeV that normally can be done only near the ground state. 2) The very retarded transitions to states not in the multiplet. These should allow one to determine some of the admixtures in the states and also something more about the structures of many of the lower-lying states.

Relatively few three-quasiparticle states are known. The mechanism proposed here for populating three-quasiparticle multiplets has rather stringent requirements which are listed in section 4.1 together with a discussion of what nuclides may satisfy these requirements.

3.2.9.C. --Vibrational States--the Remaining States-- The term "quasiparticle" was used advisedly in the previous section, for the simple shell model becomes less and less of a good approximation for states at these energies. Thus, the states and the transition rates will need to be calculated from the occupation-number approach. When this is done, it is expected that much more information will also be forthcoming about the remaining states in Pr^{139}, most of which are probably core-coupled vibrational states. At this time it would be especially interesting to know more about the nature of the 828.1- and 851.9-keV states, which receive considerable population from the three-quasiparticle states. Assuming that our interpretation of the latter is correct, the 828.1- and 851.9-keV states would seem to be constructed from the $d_{5/2}$ ground state coupled to a 2+ quadrupole vibration. That they receive so much population could be explained partly by their receiving it in default of other states being available (cf. the gamma ray branching discussion in the previous section) and perhaps partly by the fact that the three-quasiparticle states undoubtedly contain vibrational admixtures. After all, from one viewpoint three-quasiparticle states and single-quasiparticle-plus-core states are only extreme examples of the same thing.

3.2.9.D. --Shell Model Calculations-- Calculations are presently being performed by Dr. R. Muthukrishnan using the shell model to predict the state energies in Pr^{139}. The preliminary calculations look very promising, especially for the negative parity states.

3.3. Decay Schemes of Ba^{133m}, Ba^{131m}, Ce^{137m}, and Ce^{137g}

The study reported here consists of three parts which are introduced and described separately. Each of the activities was produced by bombardments of the respective targets with protons from the Michigan State University variable-energy sector-focused cyclotron.

3.3.1. Instrumentation

The apparatus used for counting included a 7-cm^3 Ge(Li) detector, room-temperature FET preamplifiers, low-noise RC linear amplifiers with pole-zero compensation, and 1024 or 4096 channel pulse-height analyzers.

Gamma ray energy measurements were accomplished by counting "unknown" radioactive sources together with judiciously chosen calibration sources entered in Table 11. A background correction was made for each peak by fitting a linear equation to several channels above and below the peak and then subtracting. A least-squares fit of the peak energies and centroids was made to a quadratic curve from which energies corresponding to the centroids of the unknown peaks were determined. The energies of weak gamma rays, which would be obscured by the calibration standards, were determined by using the previously determined stronger gamma rays as internal standards.

The energies assigned are mean values taken from a number of different measurements recorded at different times and with

Table 11. Gamma rays used as energy standards.

Nuclide	Gamma Ray Energy (keV)	Reference
Am^{241}	59.543±0.015	a
Co^{57}	121.97 ±0.05	a
Co^{57}	136.33 ±0.04	a
Ce^{139}	165.84 ±0.03	a
Tl^{208}	238.61 ±0.01	a
Cs^{137}	661.595±0.976	b
Tl^{208}	583.139±0.023	c
Co^{60}	1173.226±0.040	c
Co^{60}	1332.483±0.046	c
Na^{24}	1368.526±0.044	c
Tl^{208} (D.E.)	1592.46 ±0.10	c

[a]Reference 39.

[b]Reference 40.

[c]Reference 44.

different system gains. The uncertainties in energies are based on the reproducibilities both of the standard energies and the "unknown" energies from the calibration curves, the sizes of the full-energy peaks above the background, and the quoted errors of the standard energies listed in Table 11.

The relative gamma ray intensities are also averages from a number of runs and were obtained using experimentally determined efficiency curves (cf. section 3.1). Associated with these intensities are statistical uncertainties that include estimated uncertainties in the underlying backgrounds.

3.3.2. Experimental Results for 38.9-h Ba^{133m}

3.3.2.A. --Introduction-- The decay of the ground state of Ba^{133} has been well characterized by many authors (see reference 95 and op. cit. therein). No evidence for direct feeding of high spin states of Cs^{133} by electron capture of Ba^{133m} was reported in a recent study (96) of this metastable state. Ba^{133m} has 775-keV available for electron capture (96-98) and has a 38.9 hour half-life (99). It would seem to be a rather sensitive probe of any low-lying high-spin states which might be present in Cs^{133}. In this study evidence has been found for such a transition.

3.3.2.B. --Source Preparation-- The Ba^{133m} activity was produced by bombardment of natural $CsNo_3$ (CP-grade) with protons. Bombardments were carried out for approximately 30-min with 0.4-μA of 14-MeV protons. Chemical separations were performed. $SrCl_2$, RbCl, and $BaCl_2$ carriers were added to an aqueous solution

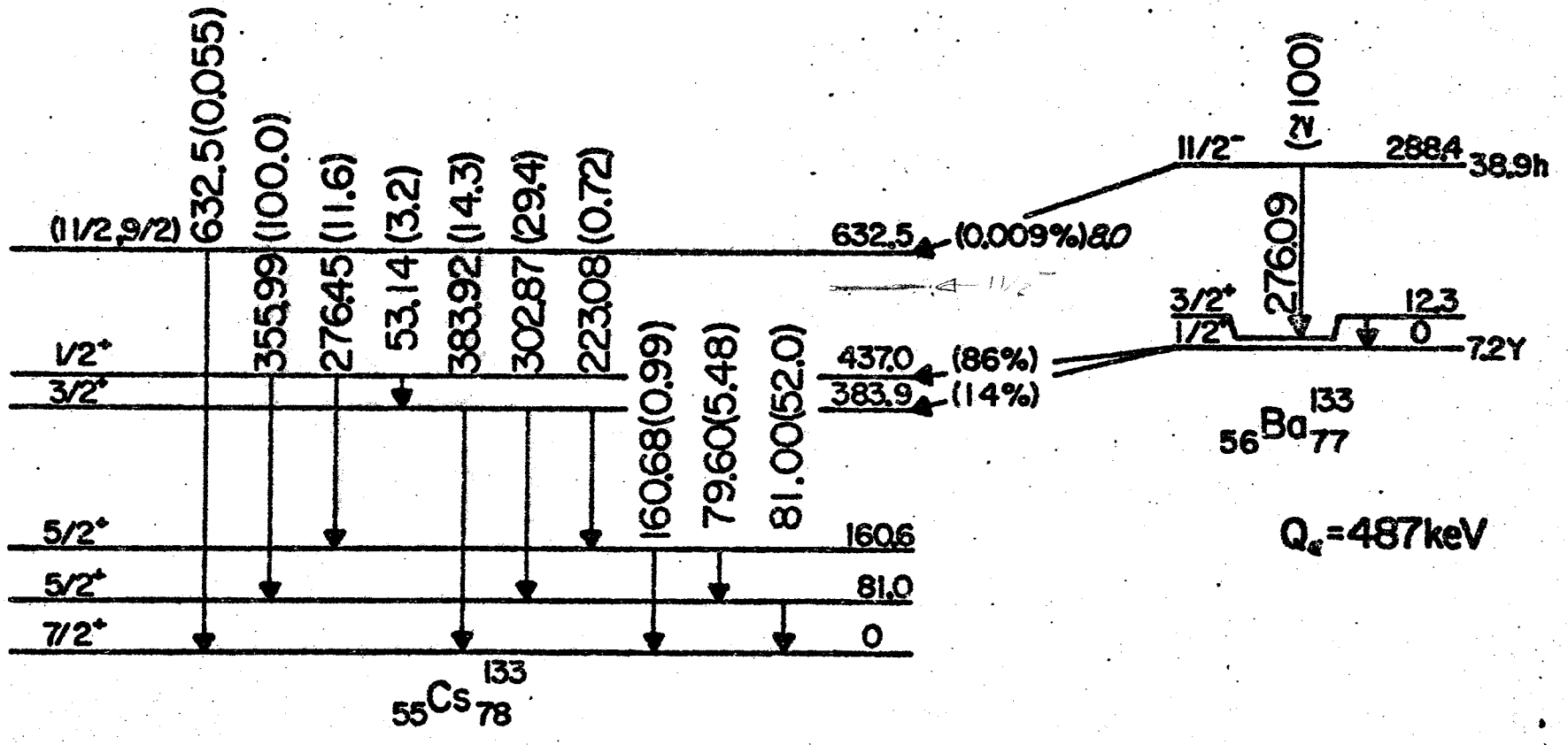

Fig. 36. Decay schemes of Ba^{133m} and Ba^{133g}. All energies are given in keV. The disintegration energy is taken from reference 97 and γ-ray intensities and energies accompanying Ba^{133g} decay are taken from reference 41. The Ba^{133m} decay scheme includes the two-transition cascade to the Ba^{133} ground state proposed by Thun et al., (96) and a new direct ε-feeding of a high spin state in Cs^{133}.

of $CsNO_3$ and then chilled. Chilled red fuming HNO_3 was then added to co-precipitate Sr and Ba. The precipitate was then redissolved in dilute HCl and, following this, HCl gas was bubbled through the chilled solution to precipitate Ba alone. Among the contaminant activities isolated from the Ba^{133m} acticity by the chemical separation were Sr^{85m} (70-min, 233-keV) (6), Sr^{87m} (2.8-h, 387-keV) (6), and Cs^{132} (6.5-d, 667.65- and 629.8-keV) (101). The remaining transitions of these contaminants were too weak to be seen.

3.3.2.C. --Gamma-Ray Spectrum-- A Ba^{133m+g} singles gamma ray spectrum is shown in Figure 35. This spectrum was taken after chemical separations were performed as described earlier. The competing gamma rays were easily identified by their well-known energies, relative intensities, and half-lived (41,95,102). The decay of the 276 keV peak was carefully followed for 8 half-lives of Ba^{133m}. This information together with a comparison of the 355.99-keV gamma ray intensity with the branching ratio of the 276.45- and 355.99-keV gamma rays from the 437.0-keV level of Cs^{133} (from ref-95, I(276.45-keV γ)/I(355.99-keV γ) = 0.116) suggest that only 0.1% of the area of the peak at 276-keV seen in Figure 35 belongs to Ba^{133g}. Hence this peak is actually a doublet. By careful comparison of the 276.45±0.08-keV Ba^{133g} gamma ray (95) and *276-keV Ba^{133m} gamma ray in alternate calibrations of photopeak centroids it was possible to determine that the Ba^{133m} gamma ray has 0.36±0.12-keV less energy than the 276.45±0.08-keV Ba^{133g} gamma ray (95). Therefore an energy of 276.09±0.15-keV is assigned to the isomeric tran-

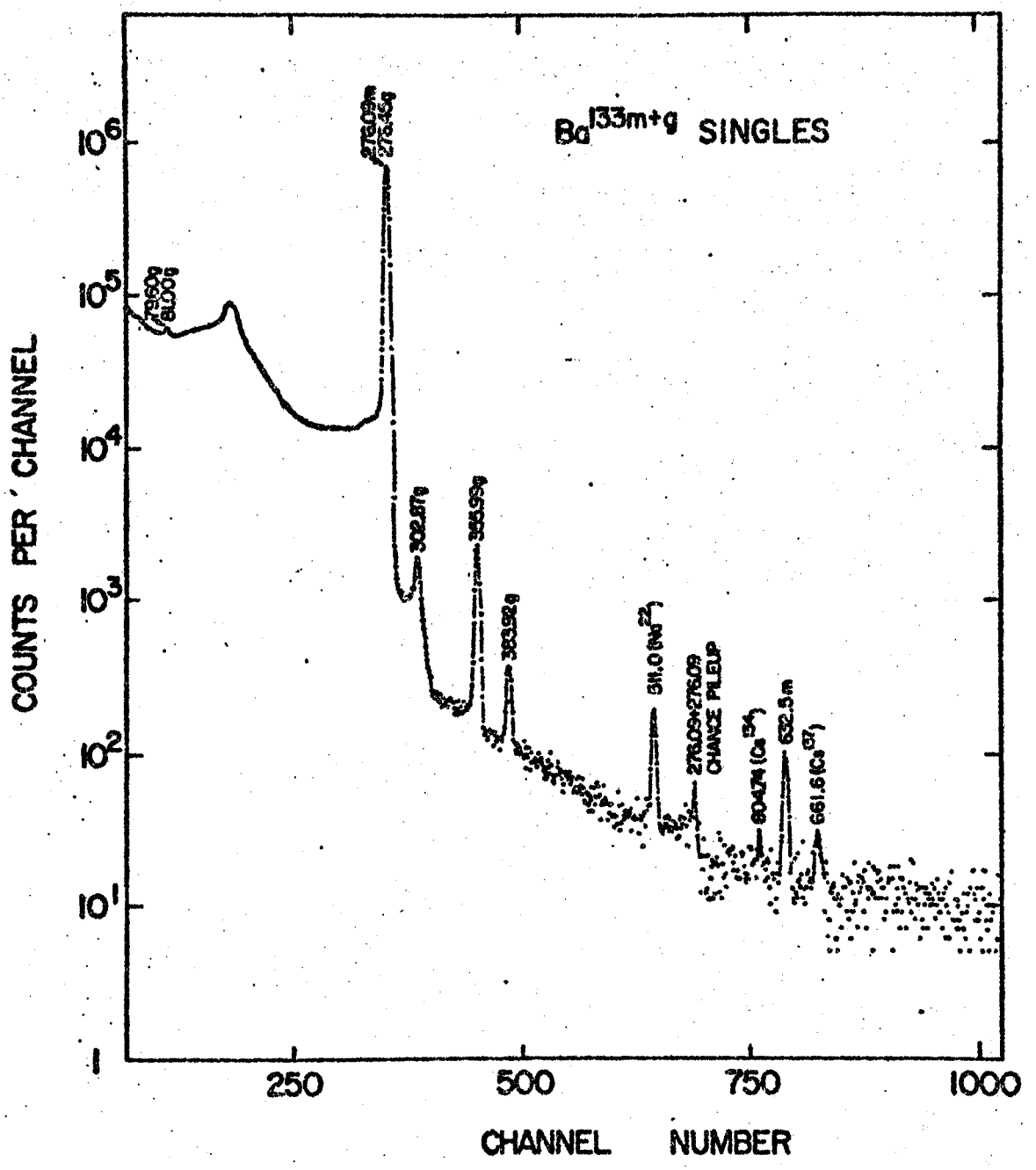

Fig. 35. Ba^{133m+g} singles γ-ray spectrum taken with a 7-cm^3 Ge(Li) detector. This run was started 46-h after the end of a 2-h activation and lasted 4-h. Only 0.1% of the area of the peak at 276-keV belongs to Ba^{133g}. The 632.5±0.5 keV γ-ray intensity was measured to be 0.055±0.010% of the 276.09-keV isomeric transition γ-ray.

sition in Ba^{133m}.

The 632.5-keV gamma ray was observed to decay with the same 38.9-h half-life as did the 276.09-keV isomeric Ba^{133m} transition. Both decays were carefully followed for four half-lives of the Ba^{133m} parent. Repeated chemical separations did not change the relative intensities of these two gamma rays. Therefore, the 632.5-keV gamma ray is indicated to belong to the decay of Ba^{133m}. The intensity of the new 632.5±0.5-keV gamma ray was measured to be 0.055±0.010% of the 276.09-keV isomeric transition gamma ray intensity. The relatively large uncertainty is due to the long counting time required to obtain adequate statistics for the weak photopeak and the small gain shifts that inevitably occurred during these times. This long counting time also made coincidence measurements impractical.

Because of the very high intensity of the 276.09-keV isomeric transition in Ba^{133m} and the necessity of a reasonable counting rate, some chance pileup of these gamma rays occured as seen in Figure 35. The characteristic shape of the "peak" at ≈552-keV and the dependence of its relative intensity and apparent half-life on the counting rate and absorber employed identified it to be a chance pileup of pairs of intense 276.09-keV gamma rays. The possibility that the peak at 632.5-keV is due to a chance sum of the 276.45- and 355.99-keV gamma rays was ruled out because such a pileup peak is calculated to be more than two orders of magnitude smaller than the 276 + 276-keV chance pileup peak seen in Figure 35.

3.3.2.D. --Ba^{133m+g} Decay Scheme and Discussion-- The Ba^{133g} decay scheme has been studied extensively (6,95) and the currently accepted one is shown in Figure 36. The disintegration energy is taken from reference 97 and the other energies and gamma ray intensities accompanying Ba^{133g} decay are taken from reference 95. The gamma ray energy and intensity values were consistent with these measurements and verify this decay scheme. Energy level systematics in the region suggest that the 81-keV level is the 5/2+ single particle level (see Chapter IV) but any difference in the character of the two 5/2+ levels is not strongly suggested by the gamma ray transition rates (95).

The Ba^{133m} decay scheme seen in Figure 36 includes the two-transition cascade to the Ba^{133} ground state proposed by Thun et al. (96), except that the 276.09±0.15-keV transition energy measured in the present study replaces the 275.7-keV energy in the earlier decay scheme (96). Thus, the energy available for electron-capture from Ba^{133m} is 288.4±0.2-keV larger than the corresponding energy from Ba^{133g}. From this information and the 487±2-keV disintegration energy (97) of Ba^{133g}, it follows that the energy available for Ba^{133m} electron-capture would support a cascade of the 632.5-keV gamma ray with any other transition below approximately 142-keV.

No evidence was observed for Ba^{133m} gamma rays within ±150-keV of 632.5-keV. From the data, an upper limit of 5% (10%) of the 632.5-keV gamma ray intensity was placed on the intensity of any higher (lower) energy Ba^{133m} gamma ray within the 632.5±150 keV interval.

The two energetically allowed alternative placements of the 632.5-keV gamma ray appear to be from a possible 713.5-keV level to the 5/2+ first excited state and from a possible 632.5-keV level to the 7/2+ ground state. These alternatives suggest very different gamma ray branching ratios to the ground and first-excited states. Comparisons with branching ratios in similar nuclei strongly suggest that the new gamma ray depopulates a 632.5-keV state in Cs^{133}. In particular, 19 high spin (9/2 or 11/2) excited states are found in odd proton (odd A) nuclei reported in this region (6,10,13-15,103) which gamma decay to both of the $7/2^+$ and $5/2^+$ ground and first excited states, respectively. If, for each of these high spin states, R is defined to be the ratio (intensity of the gamma ray feeding the $7/2^+$ state)/(intensity of the gamma ray feeding the $5/2^+$ state), it is found that $R>4.9$ for 17 of these 19 states. For the other two excited states (both $9/2^+$), $R = 0.23$ and 0.39. $R<0.05$ (>10) is suggested by the data of the present study for branching from a 713.5-(632.5-) keV state of Cs^{133} so the latter alternative is proposed as being more likely.

The 276.09-keV Ba^{133m} isomeric transition $K+L+M$ conversion coefficient of 4.80±0.30 obtained from measurements by Thun et al. (96) was used in determining a 0.009±0.003% branching ratio to the 632.5-keV state in Cs^{133}. The log $ft = 8.0$ is comparable with the other high spin states in this region populated by 11/2- isomers (6,10,13-15,103). This log ft suggests that allowed, first-forbidden, or unique first-forbidden beta transitions are possible but

systematics and gamma feeding ratios suggested that the latter alternative is quite unlikely.

A study of the gamma rays following inelastic neutron scattering in Cs^{133} has recently been reported (104) which includes $(n,n'\gamma)$ cross-section and threshhold evidence for excited states of Cs^{133} at 632.8±1, 706.2±1, and 768.4±1 keV. The 632.8-keV state was seen there to populate only the 7/2+ ground state. This evidence confirms the proposed placement of the gamma ray with an energy which was measured in the present study to be 632.5±0.5 keV. The upper limit of 5% of the 632-keV gamma ray intensity which has been placed on any higher energy Ba^{133m} gamma ray places a lower limit of ≈9.0 on the log *ft* for Ba^{133m} decay to the 706- or 768-keV state.

3.3.3. Experimental Results for Ba^{131m}

3.3.3.A. --Introduction-- An earlier study of the 14.6 min isomer of Ba^{131} suggests three possible alternatives for the $Ba^{131m} \rightarrow Ba^{131g}$ cascade spin sequence (100). In the same study, a search was conducted with scintillation detectors for possible missing transitions and direct feeding of high spin states in Cs^{131}. Although none were found, low-lying high-spin states in Cs^{133} have been discovered recently with the aid of Ge(Li) detectors as described in the previous section. In the present investigation, a search was conducted for possible missing transitions in Ba^{131m} and for direct electron capture feeding of low-lying high spin states in Cs^{131}. In the process, the Ba^{131m} decay scheme is confirmed which includes

more precise energies and shows essential agreement with the earlier scintillation study (100).

3.3.3.B. --Source Preparation-- The 14.6-min Ba^{131m} activity was produced by proton bombardments of Natural $CsNO_3$ (CP-grade). A 34-MeV proton beam irradiated the targets for 5-min durations with 2-μA of beam current. No chemical separations were performed.

3.3.3.C. --Gamma Ray Spectra-- The decay of the ground state of Ba^{131} has been well characterized recently (105-108). In Figure 37 is shown a singles gamma ray spectrum of Ba^{131g} decay taken in the course of the present study. The energies are taken from references 101 and 108. Data for the singles spectra were taken with the gamma ray spectrometer described earlier. The gamma ray energies and relative intensities were determined as outlined there. These data confirmed the Ge(Li) data of Karlsson (107) and verified the identification of the Ba^{131g} component of the Ba^{131m+g} spectra.

A Ba^{131m+g} singles gamma spectrum taken ≈30-min after a 5-min bombardment with the proton beam is shown in Figure 38. From this, and other similar spectra, the energies of the 78.5±0.2 and 108.0±0.3-keV gamma rays were determined following Ba^{131m} decay. The Ba^{131g} and Cs^{132} decay energies are taken from references 108 and 101 respectively. As seen in Table 12, these values are in good agreement with the scintillation results of Horen, Kelly, and Yaffe (100). The 108.0-keV state in Ba^{131} has recently been observed following La^{131} decay (109) and its energy was measured to be 108.1±0.5-keV in agreement with the measurement reported here. An upper limit of

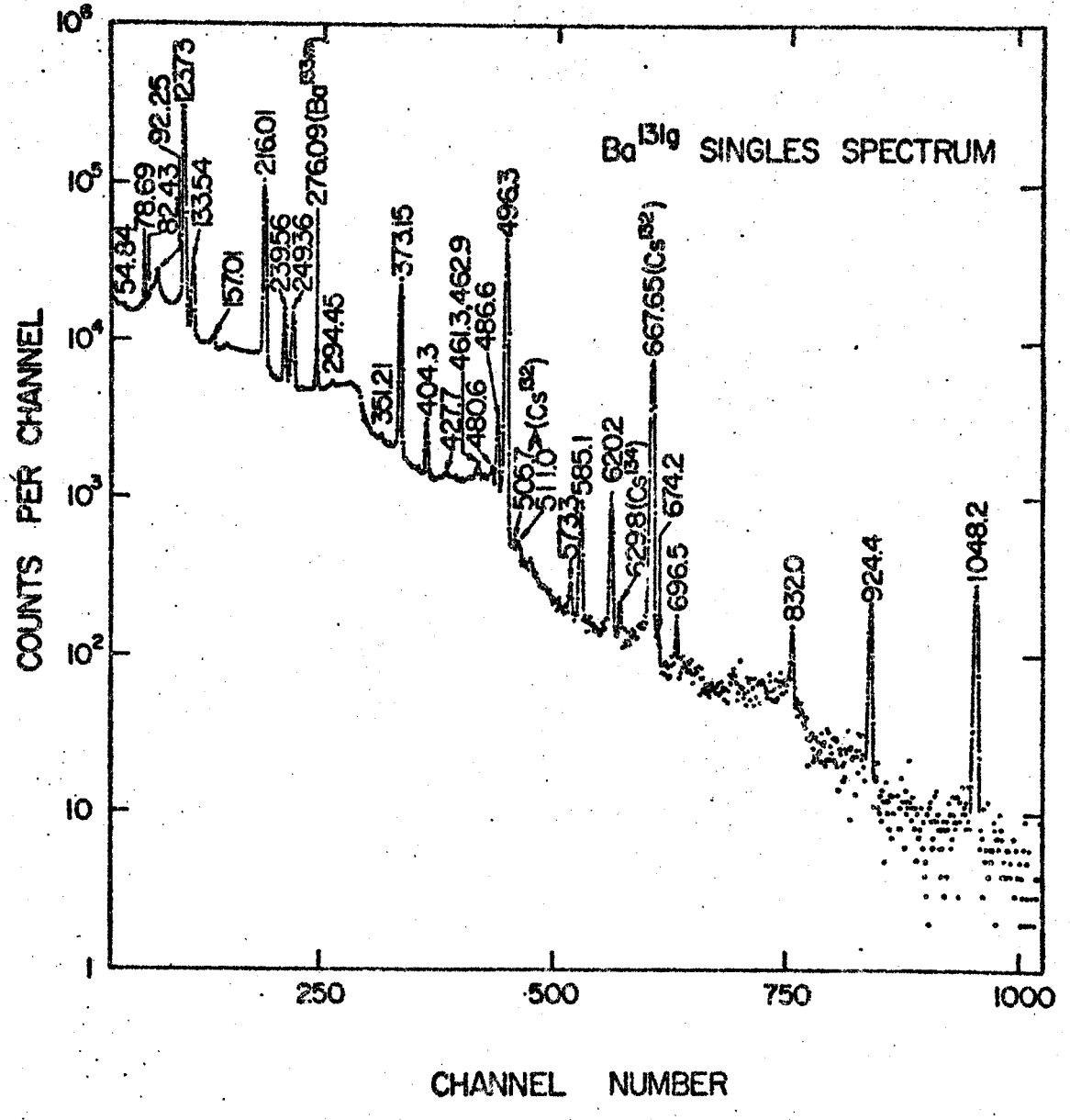

Fig. 37. Ba^{131g} singles spectrum taken with a 7-cm^3 Ge(Li) detector. The energies shown here are taken from references 107 and 108. This spectrum was one of several taken to aid in the identification of the Ba^{131g} component of the Ba^{131m+g} spectra.

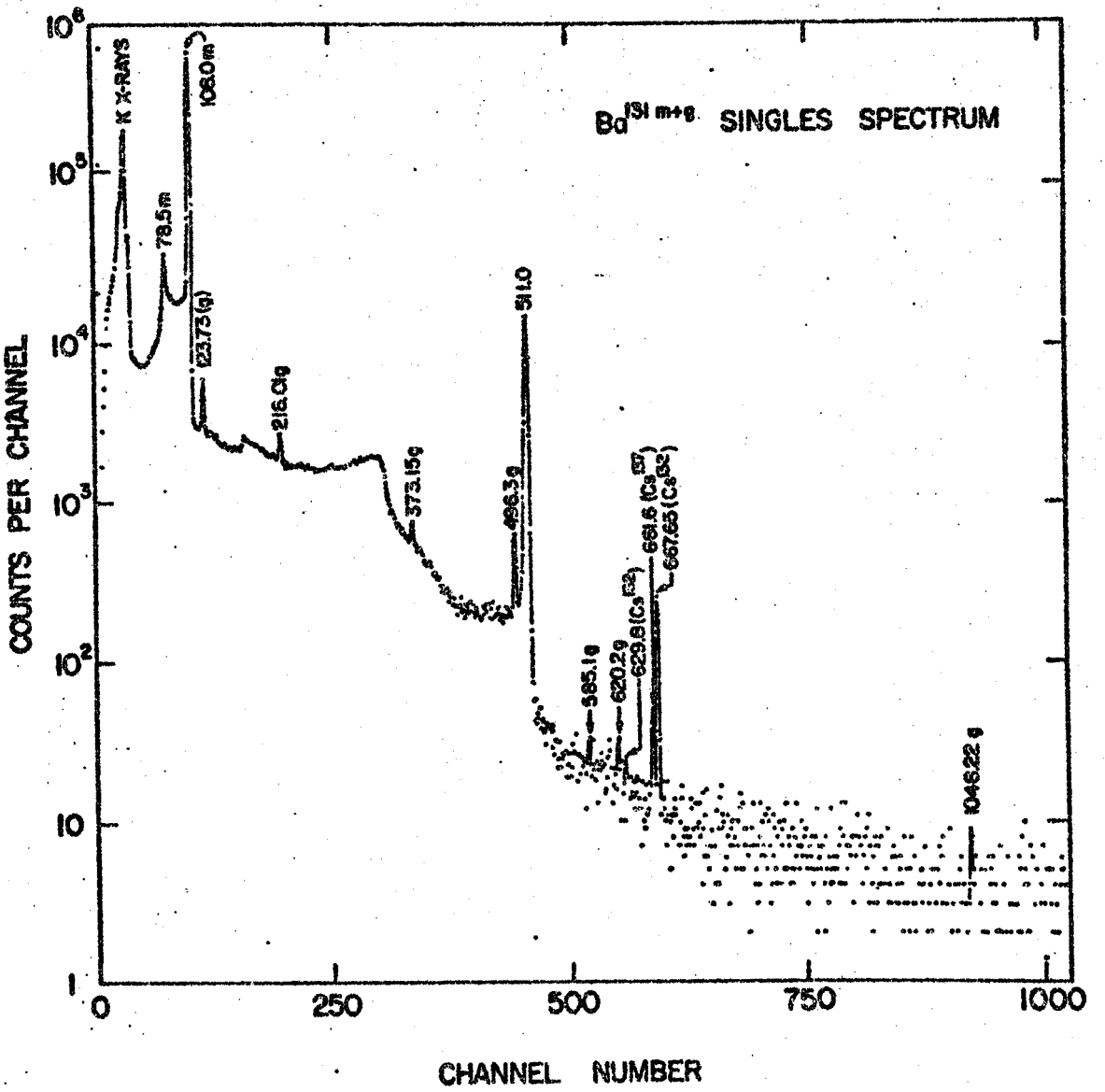

Fig. 38. Ba^{131m+g} singles spectrum taken ≈30-min after a 5-min bombardment with the proton beam. The energies of 78.5±0.2 and 108.0±0.3 keV are in good agreement with the scintillation results of Horen, Kelly, and Yaffe (100).

0.1% of the Ba^{131m} disintegrations was placed on the feeding to high spin states of Cs^{131} with energies >60-keV, in agreement with an earlier study (110) which used a differnet method. The same upper limit applies to other possible transtions in Ba^{131} following the decay of Ba^{131m}.

3.3.3.D. --Ba^{131m} Decay Scheme and Discussion-- In Figure 39 is the Ba^{131m} decay scheme suggested in reference 100 and confirmed by the present measurements. All odd-mass odd-*N* nuclei with mass numbers between 113 and 143, having fewer than 82 neutrons, and directly measured ground state spins, have 1/2+ or 3/2+ ground states. The shell model also suggests that Ba^{131g} has a spin of 1/2+ or 3/2+. From the systematics of differences between low-lying 1/2+ and 3/2+ states in odd-mass Ba, Xe, and Te isotopes seen in Figure 40, the Ba^{131g} spin is suggested to be 1/2+. This trend is in agreement with the absence of observed beta-decay to the measured 5/2+ ground state of Cs^{131} from Ba^{131g}.

The multipolarities of the 108.0- and 78.5-keV transitions respectively were measured to be *M*1+*E*2 and *E*3 respectively by Horen, Kelly, and Yaffe (100). From these multipolarities, and since no other transitions have been identified, the 9/2- → 3/2+ → 1/2+ decay sequence shown in Figure 39 is tentatively proposed. This 9/2- level can be explained in shell model terms as a projection of three $h_{11/2}$ holes as proposed by Horen et al. (100).

Recently Kisslinger (111) has suggested that, in this region, one of the 9/2- states derived from coupling three quasiparticles in the 11/2- level may be expected at an energy significantly lower than

Table 12. Ba^{131m} gamma ray data.

Energy (keV)		Intensity (relative)	
Present Study	Horen, et al.[a]	Present Study	Horen, et al.[a]
78.5±0.2	78±5	2.1±0.5	2.4±1.2
108.0±0.3	107±3	≡100	≡100

[a]Reference 100.

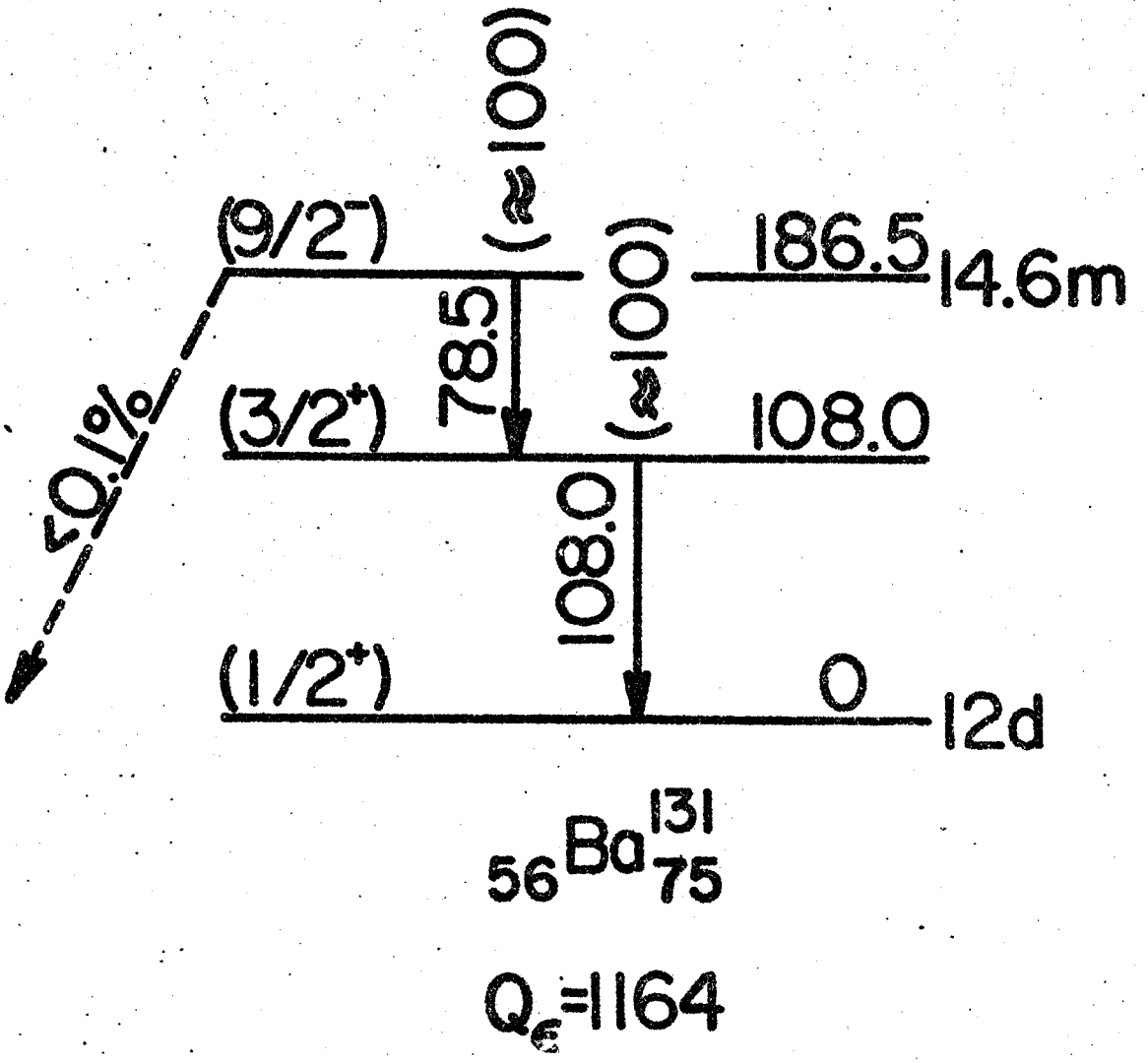

Fig. 39. Decay scheme of Ba^{131m} suggested by Horen et al. (100) and confirmed by our measurements. The energies are in keV and the tentative spins proposed are discussed in the text.

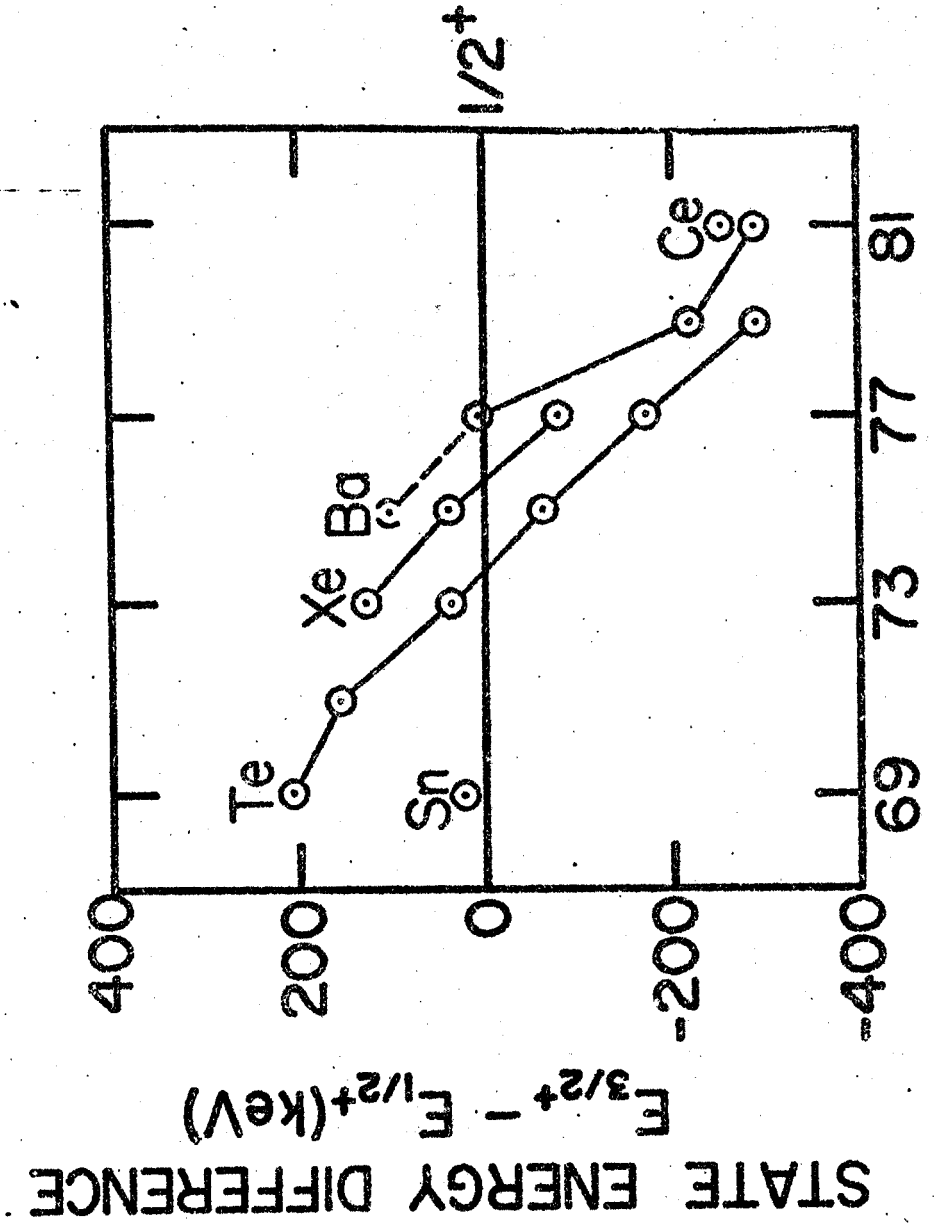

Fig. 40. Systematics of the energy level separations between low-lying $1/2^+$ and $3/2^+$ states in odd mass Sn, Te, Xe, Ba, and Ce isotopes (6). These trends clearly suggest that the ground state spin of $_{56}Ba^{131}_{75}$ is $1/2^+$ rather then $3/2^+$. Connecting lines have been drawn to guide the eye.

the other (single quasiparticle plus phonon) odd-parity levels, so it "intrudes" among the low-lying states. The 9/2- state at 321-keV in Te^{125} has been proposed (112) as an example. Possibly the Ba^{131} isomer may be another example.

A Nilsson-type 9/2- level arising from the oblate equilibrium deformation has been predicted by Kumar and Baranger (113) and suggested by W. G. Winn and D. D. Clark (114) for the Ba^{131m} case. Similar explanations have been proposed (114) for the Xe^{125} and Xe^{127} isomers. The available data on the 9/2- and 11/2- isomeric states in other Ba, Xe, and Te isotopes are not yet sufficient to permit meaningful extrapolations to Ba^{131m}.

3.3.4. Experimental Results for Ce^{137m+g}

3.3.4.A. --Introduction-- The decays of 9.0-h Ce^{137g} and 34.4-h Ce^{137m} have been examined in some detail in one earlier unpublished study with Ge(Li) detectors (76). The present work was doen independently and complements the earlier study which added eight states to the decay schemes. The present work differs from the earlier study in regard to a few key photon intensities and log *ft* values. It is noted that in recent compilation of decay schemes (6) a different parent for one of these eight new states is listed.

3.3.4.B. --Source Preparation-- The 9.0-h Ce^{137g} and 34.4-h Ce^{137m} activities were produced by the relatively clean $(p,3n)$ reaction on 99.99% pure natural La_3O_2 with 25-MeV protons. A 0.5-μA

beam was employed for a duration of ~90-min. The only competing reaction products with comparable half-lives were Ba^{135m} (28.7-h, did not hamper the investigation significantly. No chemical separations were performed.

3.3.4.C. --Gamma Ray Spectra-- In Figure 41 is shown the low energy region of the Ce^{137m+g} spectrum recorded with the 7-cm^3 Ge(Li) detector. The duration of this counting interval was 15.5 hours and it was initiated 12 hours after the end of a 1-hour bombardment. The 254.3-keV gamma ray seen here is ≥300 times as intense as 12 of the 19 other gamma rays measured following the onset of transient equilibrium. Thus the weak gamma ray full-energy peaks can be concealed easily by competing reactions.

In Figure 42 is shown the high energy region of the Ce^{137m+g} spectrum. The run used for this spectrum also had a 15.5 hour duration but it was initiated 45 hours after the end of a one hour bombardment, near the onset of transient equilibrium. The energies and relative intensities of the gamma rays observed in Figures 41 and 42 are listed in Table 13 along with results of an earlier study (76). All of the relative gamma intensities reported here are based on measurements taken while the Ce^{137m} and Ce^{137g} parents were in transient equilibrium (≥80 hours after their production). From the variation of the gamma ray intensities with time soon after bombardments, it was possible to distinguish the states populated by the 34.4-h Ce^{137m} and 9.0-h Ce^{137g} parents.

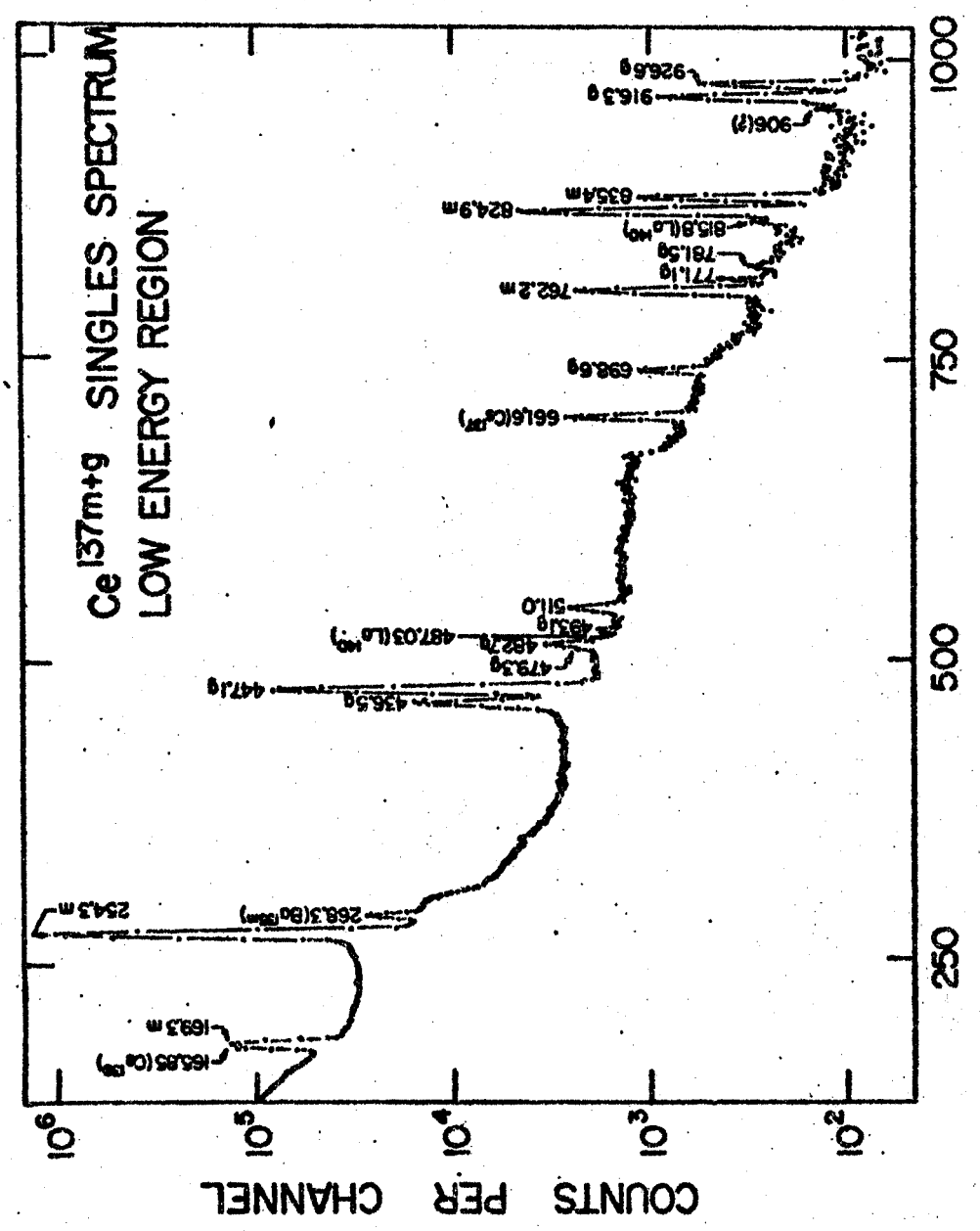

Fig. 41. Ce^{137m+g} singles γ-ray spectrum recorded with a 7-cm^3 Ge(Li) detector — low-energy portion. The duration of this run was 15.5-h and it was started 12-h after the end of a 1-h bombardment. The 254.3-keV γ-ray seen here is ≈300 times as intense as 12 of the 19 other γ-rays measured after the onset of transient equilibrium.

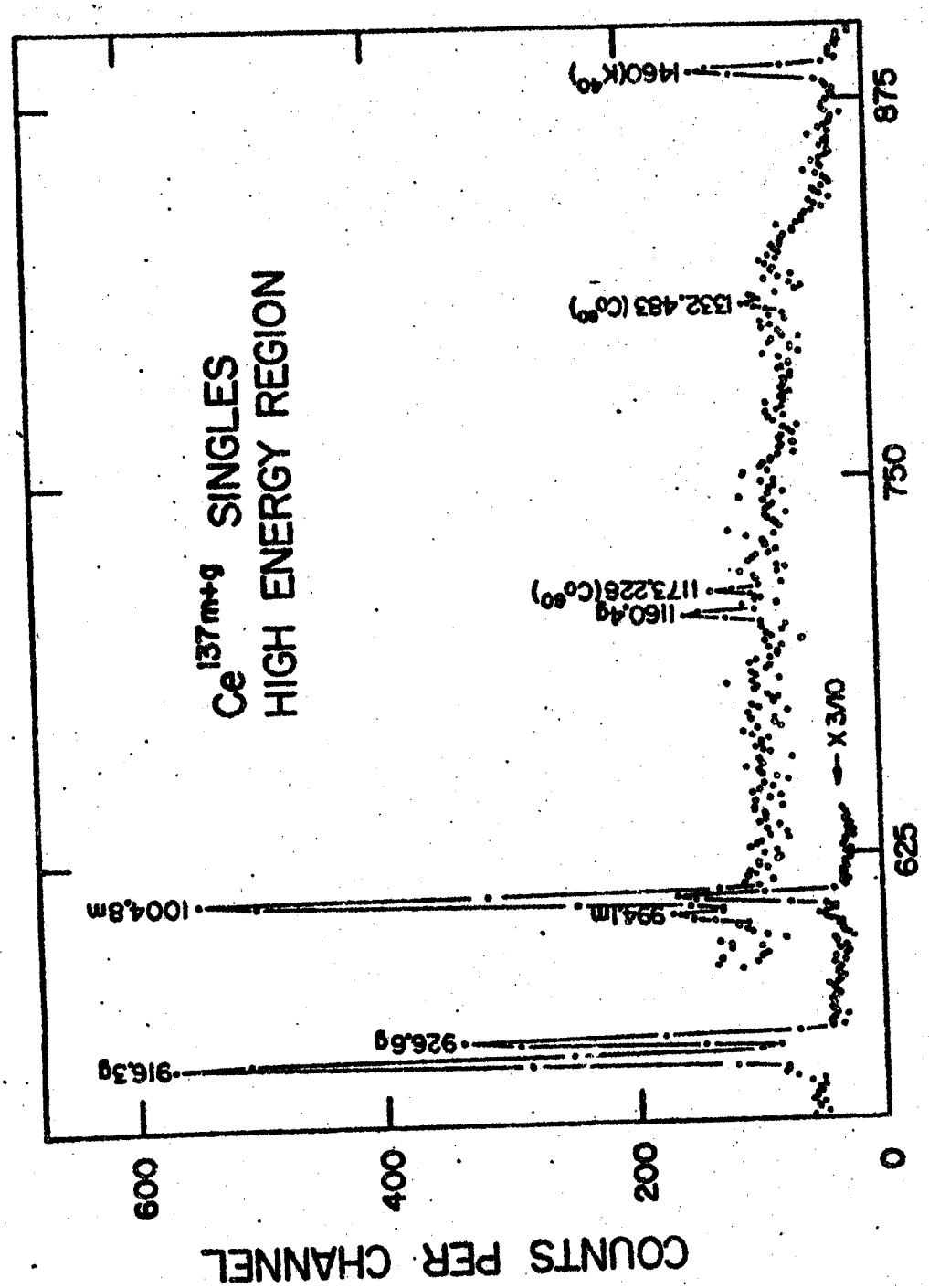

Fig. 42. Ce^{137m+g} singles spectrum — high-energy portion. The run used for this spectrum also had a 15.5-h duration but it was initiated 45 hours after the end of a one hour bombardment, near the onset of transient equilibrium.

Although energy differences and other considerations clearly indicate a state in La^{137} at 10.5-keV fed by eight gamma rays, the total conversion coefficient (115) of 130 for the 10.5-keV transition, the difficulty in measuring such low energy photons or electrons, the low intensity of the other gamma rays, and the long half-life of the parent decays makes coincidence experiments with this transition impractical at present.

3.3.4.D. --Ce^{137m+g} Decay Scheme and Discussion-- The decay scheme that was deduced from the foregoing measurements is shown in Figure 43. Transition energies and excited-state energies are given in keV, the disintegration energy for electron-capture is a calculated value (69). The β^+/ε ratio for decay to the La^{137} 10.5-keV state is also a calculated value, using the method of Zweifel (47). Spins and parities of the states are taken from reference 76 and op. cit. therin. Each assignment is consistent with the log *ft* values calculated from the data taken in the present study.

The decay scheme and conclusions regarding Ce^{137m+g} decay and La^{137} states proposed here essentially confirm the unpublished report of Frankel (76). The measurements reported here were obtained independently and the 25% reduction factor due to transient equilibrium was included in the Ce^{137g} gamma intensities involved in the calculations of the β^+ and ε_K-feeding and log *ft* values. It was also noted that the 1160.4-keV gamma ray was seen to follow Ce^{137g} decay rather than (as listed in a recent decay

Table 13. Ce^{137m+g} photon data.

Energy (keV)		Intensity (relative)		Parent[a]
Present Study	Frankel[b]	Present Study[c]	Frankel[d]	
10.5±0.4[e]	10.0	---	---	*g*
169.3±0.5	168	15 ±5	8.3	*m*
254.3±0.3	255.8	600 ±40	202	*m*
433.3±1.0	433.0	2 ± 1		*g*
436.5±0.5	436.1	16.5 ±0.8	16.2	*g*
447.1±0.3	446.5	≡100	≡100	*g*
479.3±1.0	479.0	0.5 ±0.2		*g*
482.7±0.5	481.5	2.0 ±0.4	3.2	*g*
493.1±0.5	492.5	0.4 ±0.2	0.6	*g*
511.0 (annihil)	511.0 (annihil)	≤1.8[f]	1.2	
698.6±0.3	698.0	1.6 ±0.4	2.4	*g*
762.2±0.4	762.1	8.1 ±0.8	13.5	*m*
771.1±0.5	771.1	0.3 ±0.1	0.8	*g*
781.5±0.6	781.5	0.10±0.03	0.32	*g*
824.9±0.3	825.0	19 ±2	33.5	*m*
835.4±0.4	835.8	4.2 ±0.6	7.3	*m*
916.3±0.3	915.8	3.0 ±0.3	5.5	*g*
926.6±0.3	925.8	1.7 ±0.4	3.2	*g*
994.1±0.4	994.1	≤0.14	0.12	*m*
1004.8±0.3	1004.0	1.1 ±0.3	1.70	*m*
1160.4±0.6	1160.3	0.08±0.03	0.16	*g*

[a] *g*≡9.0-h Ce^{137g} parent and *m*≡34.4-h Ce^{137m} parent. The assignments given in reference 76 and these made in the present study agreed in every case.

[b] Reference 76. Uncertainties listed as within 1 keV.

[c] All relative γ intensities are measured after transient equilibrium has been reached (≲80 hours after bombardment).

[d] Reference 76.

[e] From six energy differences. The range of the differences was 0.4 keV.

[f] Due to the presence of contaminants, we were not able to definitely identify this minimum value of annihilation photon intensity as entirely belonging to Ce^{137g} decay.

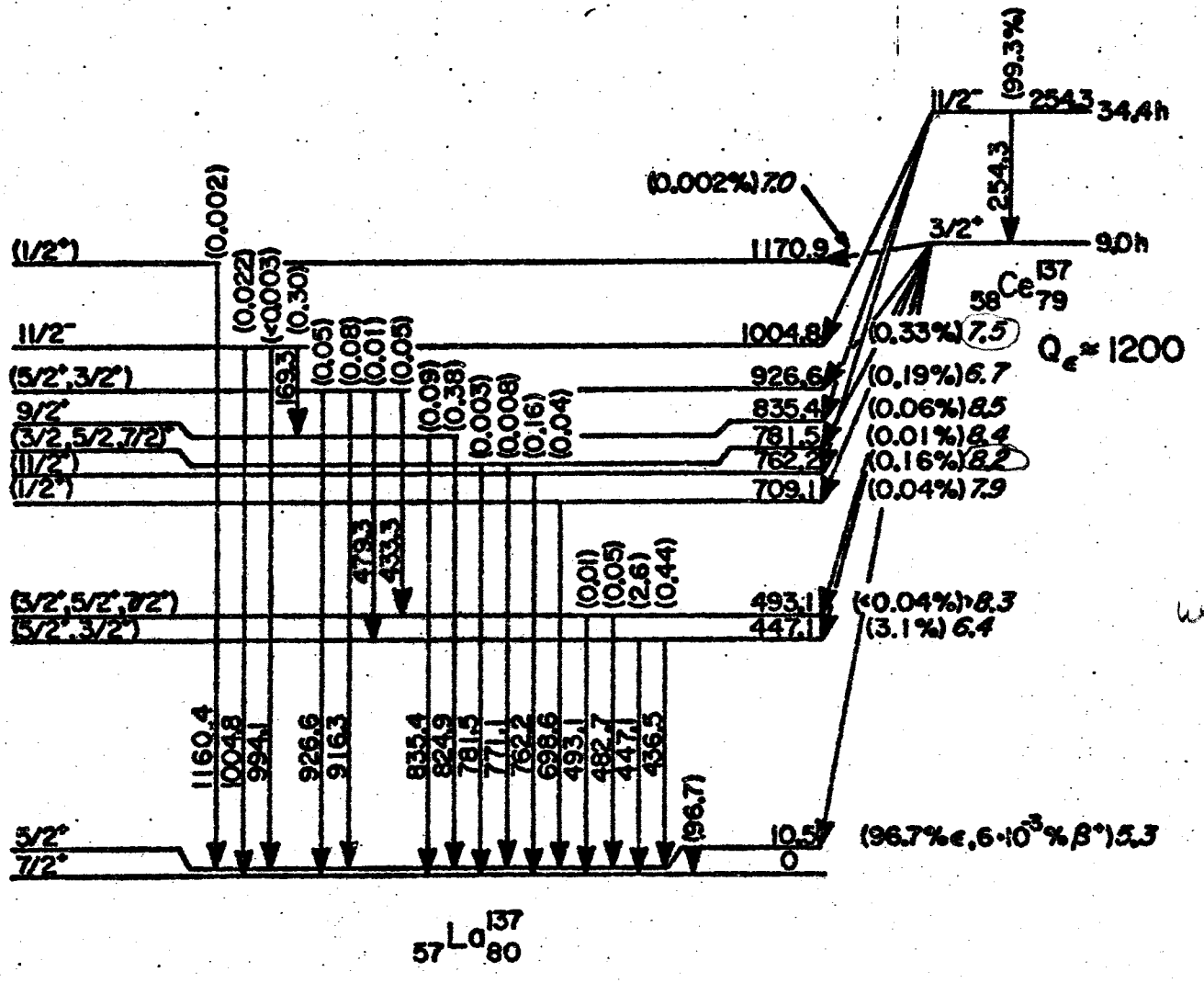

153

which to 1⁺
" " gs
Icc? ⇒ limit on spin
M1 → ΔJ = 1
→ 5/2⁺

Fig. 43. Decay schemes of Ce^{137m} and Ce^{137g}. Transition energies and excited-state energies are given in keV and the disintegration energy for electron-capture is a calculated value (69). The β^+/ε ratio for decay to the 10.5-keV state is also a calculated value, using the method of Zweifel (47). Spins and parities of the states are taken from reference 6 and op.cit. therein.

scheme compilation (6)), Ce^{137m} decay. Comparisons of the experimental levels with the calculations of Kisslinger and Sorenson (1) are recorded in reference 76. Fair agreement is seen.

The decay schemes of Ce^{137m} and Ce^{137g} are distinctly different. No evidence of common transitions was observed. The 7/2+ and 5/2+ assignments for the ground and first-excited states of $_{57}La^{137}_{80}$ would appear to suggest $(\pi g_{7/2})^{-1}$ and $(\pi d_{5/2})(\pi g_{7/2})^{-2}$ shell model configurations respectively. The close proximity of these two levels, separated by only 10.5-keV, is consistent with the energy level systematics of the $Z = 57$, $N = 80$ region for odd-proton even-neutron nuclei (see Chapter IV). The ground state spin assignments of odd-proton even-neutron nuclei for $51 \leq Z \leq 59$ nuclides are in general 5/2+ for low and 7/2+ for high mass number nuclides of a given Z. The crossover point is between $A = 127$ and 129 for $Z = 53$, between $A = 131$ and 133 for $Z = 55$, and between $A = 141$ and 143 for $Z = 59$. This trend also suggests that these two states might be expected nearly to coincide in $_{57}La^{137}$.

A recent study (see section 3.2 and reference 115) of $_{59}Pr^{139}_{80}$ levels populated by $_{60}Nd^{139m+g}_{79}$ β^+/ε decay suggest a resemblance between the $_{58}Ce^{137m+g}_{79}$ and $_{60}Nd^{139m+g}_{79}$ decay patterns. The log ft of the dominant 3/2+ $Nd^{139g} \rightarrow$ 5/2+ Pr^{139g} transition is 5.1 and for the 3/2+ $Ce^{137g} \rightarrow$ 5/2+ 10.5-keV La^{137} state transition, log $ft = 5.3$. Both the (5/2+) 589.2-keV state of Pr^{139} and the 5/2+,3/2+ 447.1-keV state of La^{139} predominately populate the lowest 7/2+ state in their respective nuclides and are populated by their 3/2+

parents with log *ft* values of 6.4 These may be corresponding 5/2+ states but the situation is somewhat less clear for the other low spin states in Pr^{139} and La^{137}. Eight other low spin states in Pr^{139} are populated by Nd^{139g} β^+/ε decay with log *ft* values ranging 5.9 to 7.2. Five other low spin states in La^{137} have log *ft* values ranging from 6.7 to 8.3. The larger log *ft* values for the $Ce^{137g} \rightarrow La^{137}$ β^+/ε transitions may be due to the initial shell configurations in the decays. In particular, Nd^{139g} has $(\pi g_{7/2})^8(\pi d_{5/2})^2(\nu d_{3/2})$ which is more favorable for a $(\pi d_{5/2}) \rightarrow (\nu d_{3/2})$ transition than the probable $(\pi g_{7/2})^8(\nu d_{3/2})$ configuration of Ce^{137g}.

Ce^{137m} decay also resembles Nd^{139m} decay in several ways. These $h_{11/2} \rightarrow d_{3/2}$ isomeric transitions have "experimental" matrix elements (see section 3.2) differing by <10% and they fit into the smooth trend of both energies and matrix elements seen in Te^{131}_{79}, Xe^{133}_{79}, Ba^{135}_{79}, Ce^{137}_{79}, and Nd^{139}_{79}. The 99.3% isomeric transitions seen in Ce^{137m} decay differs considerably with the corresponding 12.7% in Nd^{139m} due to the accessibility of six three-quasiparticle states (see section 3.2 and reference 115) in Pr^{139}. These latter states range from 1624.5- to 2196.7-keV in Pr^{139} while only ≈1450-keV is available for elctron-capture in the decay of Ce^{137m}.

The 11/2- state at 1004.8-keV in La^{137} has been reported to have an enhanced *E*3 (≥8) to the 5/2+ 10.5-keV state (84) and an (*M*2,*E*3) transition to 7/2+ ground state (76). In Pr^{139} a 40±2 ns 11/2- state at 821.9-keV has an *E*3 enhancement of ≈2.2 to the 5/2+ ground state (see section 3.2). In Eu^{147} and Eu^{149}, *E*3 enhance-

ments have also been seen for transitions depopulating low-lying 11/2- states (85). It may be suggested that the 713, 962, 1114, and 1439 keV states of Eu^{145}, Pm^{143}, Pr^{141}, and Ce^{139} (all 11/2-) may also have enhanced *E*3 transitions to their lowest 5/2+ states. In the $N = 50$-126 region, the four known cases of *E*3 enhancement (in Pr^{139}_{80}, Ce^{137}_{80}, Eu^{147}_{84}, and Eu^{149}_{86}) listed in section 3.2 and references 84 and 85 (25 measured retarded *E*3 transitions were also listed in this region) all are quite near the $N = 82$ shell.

CHAPTER IV

DISCUSSION OF RESULTS AND SYSTEMATICS

Descriptions of characteristics of the states investigated are included in the previous chapter along with some comparisons with neighboring nuclei and current nuclear models. One of the most interesting and significant results of this study was the observation of the population by Nd^{139m} of a multiplet of six high-lying, high-spin, odd-parity states in Pr^{139}. These states are interpreted to be three-quasiparticle states and are discussed in Chapter III in some detail. Here these studies are related to other nuclides in the region. This thesis then concludes with a brief survey of experimental energy level systematics in the neutron deficient odd mass, odd proton ($50 \leq Z \leq 62$) region.

4.1. Three-Quasiparticle Multiplets in Other Nuclides

Well-characterized three-particle states in nuclei are comparatively rare, and recognizing them most often has depended on the isomeric properties of a few high-spin states. Consequently, the excitation of a multiplet of such states in one nucleus, each state decaying to a number of lower-lying states, has many interesting theoretical implications.

It is worth noting that there are stringent requirements

for the mechanism suggested in section 3.2.9.B for populating the particular three-quasiparticle multiplets that were seen to be populated by the electron capture decay of Nd^{139m}. These include a high-spin parent nucleus, such as the $h_{11/2}$ isomer, and a sufficient decay energy to populate states well above the pairing energy gap in its daughter nucleus. Additionally, the parent nucleus must be unable to decay readily by other modes, e.g., an isomric transition, if present, must be of low-enough energy to allow the β^+/ε-decay to compete. Finally, the nucleus must have an intrinsic configuration that forces the preferred decay path to be into the three-quasiparticle states. Such arrangements would appear to be present only for β^+/ε-decay of nuclides with $N<82$. (Below $N=50$ the correct configuration occurs at Kr^{83} and Sr^{85}, but these are too close to β-stability for populating high-lying states. Below $N=126$ the configuration is projected to occur around Pu^{211}, a region that is not even particle stable.)

Below $N=82$ the appropriate configurations can be found only at $N=79$ and $N=77$, with the possibility of $N=75$, depending on the relative spacing of the $h_{11/2}$ and $s_{1/2}$ states. On the neutron-rich side of $N=79$ there are some peculiar and complex decays of 11/2- isomers, e.g., Te^{131m} decays primarily to high-spin states at 1899 and 1980 keV (14). However, these cannot be definitely described as decay to three-particle states. On the neutron-deficient side, Ce^{137m} has a possible configuration, although it lacks the $d_{5/2}$ protons, so decay would be forbidden ($\pi g_{7/2} \rightarrow \nu d_{3/2}$). However its Q_ε is small enough to preclude such decay anyway (76). This leaves

Nd^{139m} as the nucleus closest to β-stability with the requisite properties. Other possible candidates in this region among currently known nuclei are $Sm^{141(m)}$ and $Nd^{137(m?)}$. Sm^{141} is now being investigated (77).

4.2. Experimental Energy Level Systematics In the Odd Proton (Z=50-62) Odd Mass Region

Because of the small amount of experimental information available concerning the levels of the highly neutron deficient nuclei in this region, this discussion will be restricted to $_{51}Sb^{115-133}_{64-82}$, $_{53}I^{121-135}_{68-82}$, $_{55}Cs^{129-137}_{74-82}$, $_{57}La^{135-139}_{78-82}$, $_{59}Pr^{137-141}_{78-82}$, and $_{61}Pr^{141-143}_{80-82}$. Of these 31 nuclei, six are stable. These nuclides and their abundances (where ≠ 100%) are Sb^{121} (57.25%), Sb^{123} (42.75%), I^{127}, Cs^{133}, La^{139} (99.911%), and Pr^{141}. All Pm isotopes are unstable.

4.2.1. Log *ft* Values for $3/2^+$ Ground State to Lowest $5/2^+$ State Transitions.

In searching for the systematic variations of the properties of the nuclear states of this region, a start could be made with the beta decay which populates the states of interest. In section 2.3 of Chapter II a sequence of operations used for calculating log *ft* values was outlined. The difficulties encountered in determining relative intensities for β and γ transitions and the length and complexity of this process could suggest that errors might easily slip into the literature where calculation is made of

the fraction of beta decay which proceeds by the decay mode of interest. The theory from which log *ft* values are derived does not include the detailed nature of the states involved in the transitions. For these reasons, as the tools of gamma ray spectroscopy and the understanding of state configurations improve, the departures from the approximation that log *ft* values are independent of the available energy for electron capture and the number of protons of the parent may lead to new insights concerning the nature of the states involved.

As pointed out in section 3.3.5.B, there are a large number of $d_{3/2}$ ground states in the even proton, N=79,81 nuclides. The low log *ft* values for transitions between these states and the lowest-lying $d_{5/2}$ states in the adjacent odd proton isobars suggest that these states may be quite similar in nature.

Figures 44 and 45 have been constructed from references 6-15, and from Chapter III of the present study. Parent and daughter nuclei are listed along the abscissas in order of increasing Z and A. The effect of increasing numbers of nucleon pairs on the $(\nu d_{3/2})\rightarrow(\pi g_{5/2})$ and $(\pi g_{5/2})\rightarrow(\nu d_{3/2})$ transitions are shown separately. Since large fractions of the beta decay proceed in the decay modes of interest, these log *ft* values might be expected to be somewhat more accurate than usual. An error of ≈23% (≈50%) in fractional beta feeding intensity contributes an error of ≈0.1(0.3) in the log *ft*.

One of the experimental difficulties encountered during this investigation was that such large fractions of the decays of 3/2+

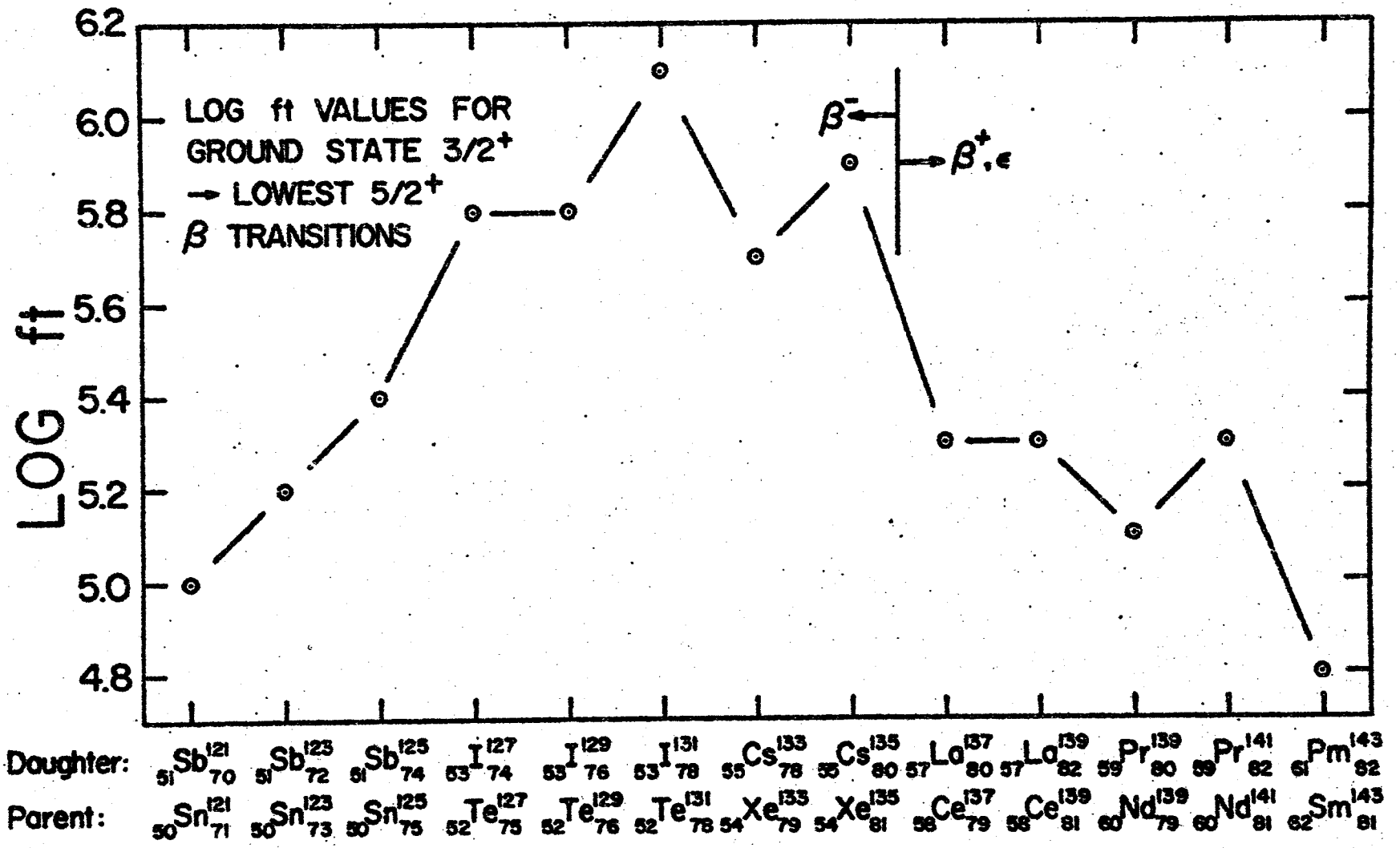

Fig. 44 Log ft values. Each corresponds to a β transitions from the $3/2^+$ ground state of an odd neutron (odd mass) parent nucleus to the lowest lying $5/2^+$ state of its odd proton (odd mass) daughter.

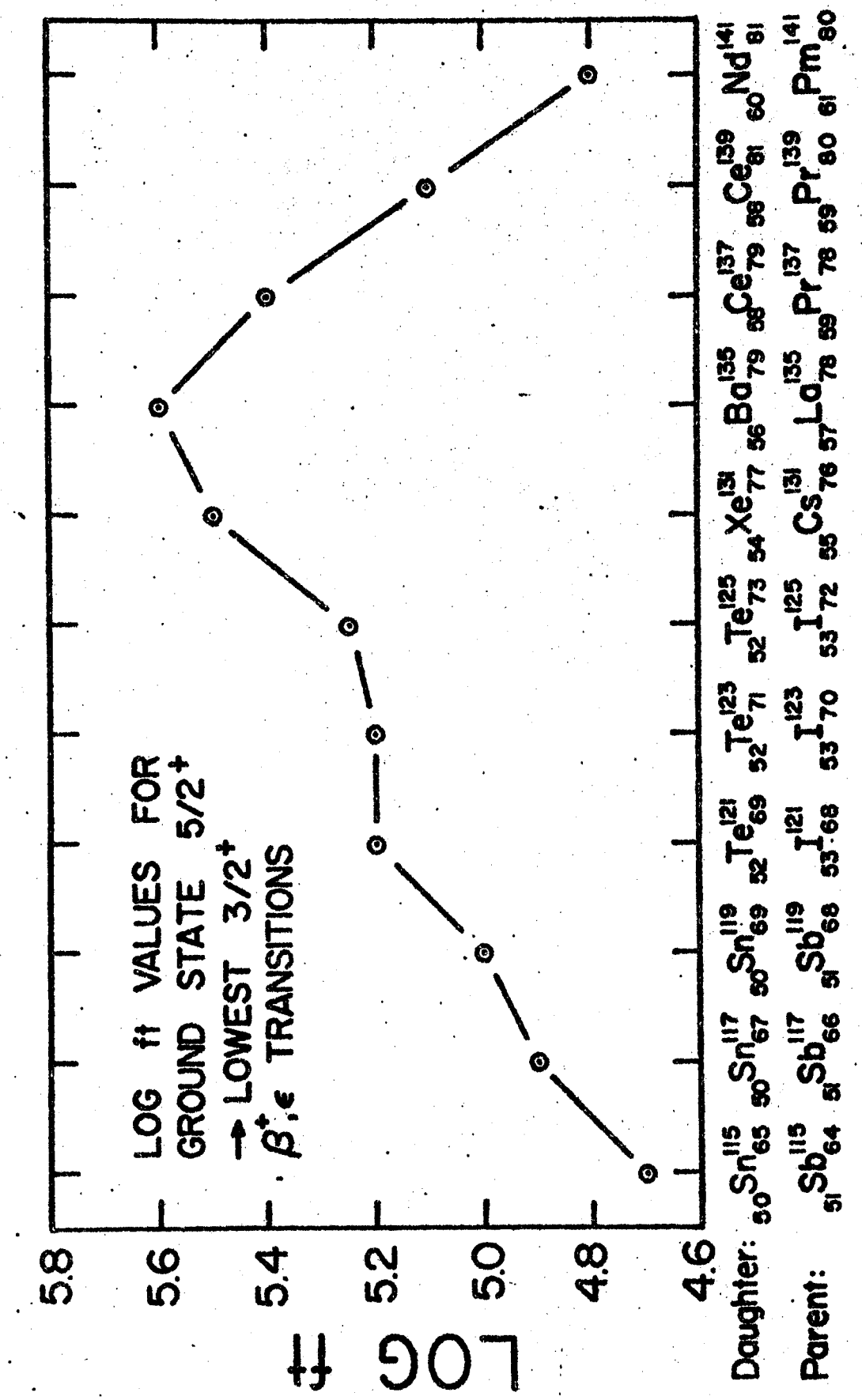

Fig. 45. Log ft values. Each corresponds to a β^+,ε-transition from the $3/2^+$ ground state of an odd proton (odd mass) parent nucleus to the lowest lying $3/2^+$ state of its odd neutron (odd mass) daughter.

$Nd^{141}g$, $Nd^{139}g$, and $Ce^{137}g$ proceeded directly to the ground or first excited state of the daughter of each. These fractions were 98.5%, 88%, and 96.7% respectively of the parent decays. In consequence, the higher-energy gamma rays were so weak that they could be obscured or concealed by the more intense gamma rays from contaminant activities even though the contaminants themselves were quite weak.

In Figure 44 the largest log *ft* values are seen relatively far from closed shells. The general pattern is relatively smooth and suggests that lower log *ft* values may be associated with beta transitions near closed shells. In Figure 45 a similar pattern is seen in the 5/2→3/2+ even proton daughter transitions, possibly at somewhat lower values of log *ft*. The relatively smooth progression of log *ft* values was interrupted by a value of 4.9 for $I^{125}\rightarrow Te^{125}$ decay from the compilation of data found in reference 6. A look at the original references disclosed that this value was out of date and that the more recently determined value (116) of 5.25 fits nicely into the relatively smooth pattern. An extrapolation of this curve to $Pm^{141}\rightarrow Nd^{141}$ decay suggests a log *ft* of 4.8 for the ε_K/β^+ decay.

Kisslinger and Sorensen (1) suggest that the effect of pairing correlations on the β-decay matrix elements may account for these trends. Their calculations for "odd-jumping" beta decays show an increase in the log *ft* values for *A* increasing from 117 to 133. ("Odd-jumping" beta transitions are accompanied by the transformation of an odd $p(n)$ into an odd $n(p)$.) For the "even-jumping" beta decays, a decrease is obtained for *A* increasing

from 137-141. ("Even-jumping" β transitions are accompanied by an even $p(n) \rightarrow$ even $n(p)$ transformation.) These latter log ft values are predicted to lie lower than the ones for the odd-jumping cases. In the more complete experimental data shown in Figures 44 and 45, the log ft values of both the odd and even-jumping transitions are seen to drop as the N=82 shell fills. These data then seem to suggest that other effects may be important.

4.2.2. Energy Systematics of the Low-Lying 7/2+, 5/2+, 3/2+, and 1/2+ States in the Region

Figure 46 shows the relative energy spacings of the low-lying 5/2+ and 7/2+ states of odd proton odd mass nuclei in the region of interest. The data are taken from references 6,7-15, 117, and from Chapter 3 of the present study.

The parabolic appearances of the Sb and I curves have been previously noted by G. Berzins (7) and L. M. Beyer (15). The pattern may be followed in Cs but the number of data points (four) is too small to yield significant evidence. The first sharp departure from the smooth trend of increased spacing as pairs of neutrons are added is seen in Pr^{139}_{80} and Pr^{141}_{82} which were discussed in Chapter III, and in La^{133}_{76} and La^{135}_{78}. This pattern change may be related to the coupling of the 59th proton in Pr^{141}_{82} to the two $d_{3/2}$ neutron holes present in Pr^{139}_{80}. The effect of the $(\pi d_{5/2})(\nu d_{3/2})^{-2}$ coupling in Pr^{139}_{80} may be to depress the 7/2+ state and/or raise the 5/2+ state energy.

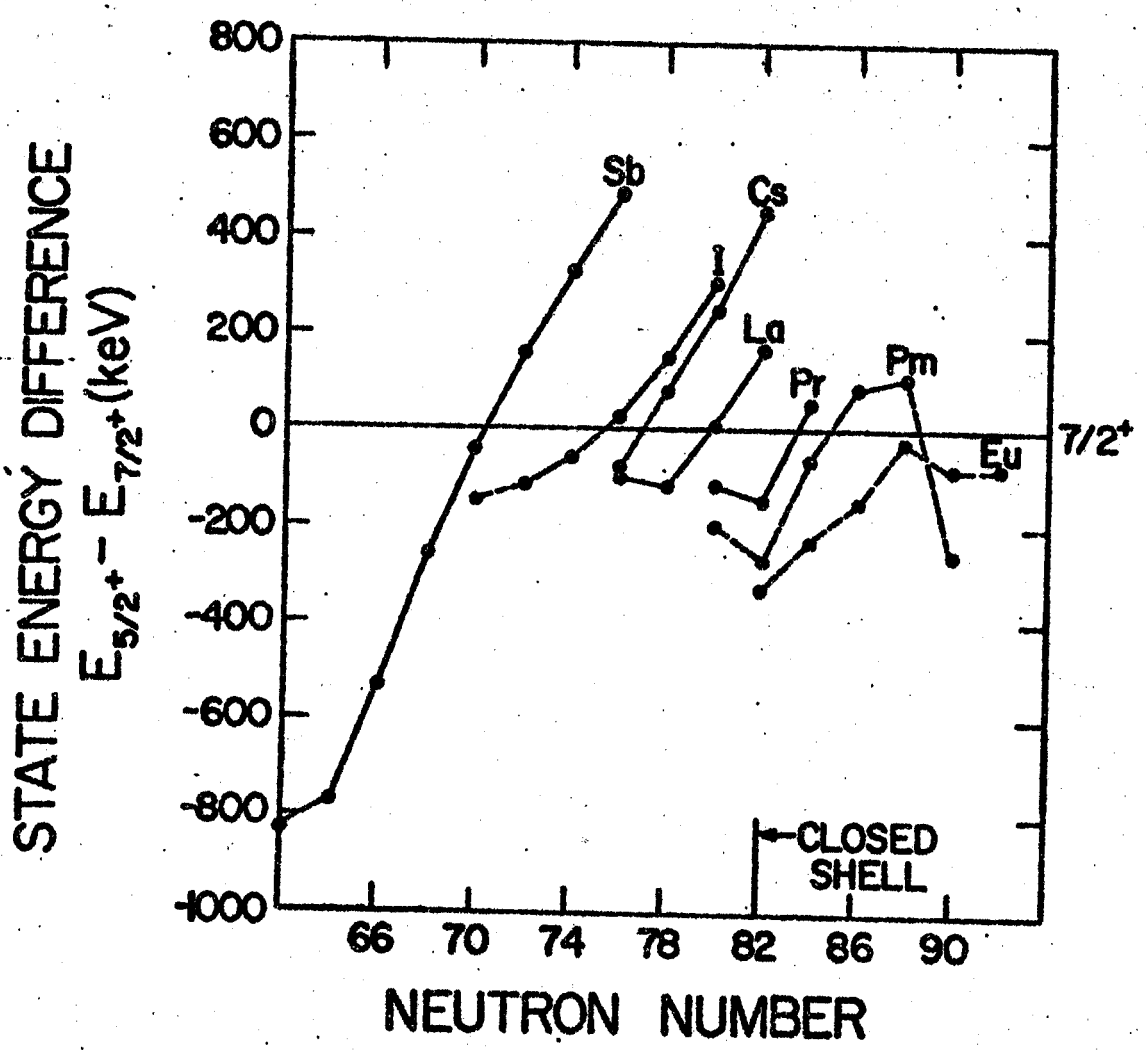

Fig. 46. Systematics of the energy level separations between low-lying $5/2^+$ and $7/2^+$ states in odd proton (odd mass) nuclei. The spin assignment of at least one of the states connected by each dashed line is tentative.

The effect of the closure of the neutron shell appears to be negligible on these states. This observation suggests that the lowest lying 7/2+ and 5/2+ states in the odd proton odd mass nuclei of the region are fairly pure quasiparticle states. Spectroscopic factors from a recent study of (He^3,d) reactions on the even Sn isotopes (117), in good agreement with the predictions of Kisslinger and Sorensen (120), also suggest relatively pure one-quasiparticle states for the lowest lying 7/2+ and 5/2+ states.

A recent study and compilation (40) of $M1$ and $E2$ transition probabilities in the region of interest includes a comparison of experimental and theoretical hindrance factors for $g_{7/2} \rightleftarrows d_{5/2}$ l-forbidden $M1$ and $E2$ transitions. These are obtained from a combination of $M1/E2$ mixing ratios and mean life measurements. The experimental $M1$ hindrance factors were noted in reference 40 to range from ≈10-100 and the $E2$ enhancements range from ≈1-100. Sorensen's pairing-plus-quadrupole force calculation gives a fair description of the $E2$ transition rates but fails to provide a satisfactory description of the $M1$ transition rates. Calculations with the shell model and configuration mixing have had more sucess in accounting for the measured $M1$ transition rates (40,121).

It is also noteworthy that Wildenthal (2) has performed a shell model calculation with six adjustable parametems for ten N=82 nuclei. The 7/2+, 5/2+ energy difference trends in the odd proton nuclides and the energy gaps (energy of the first 2+ states) in the even-even N=82 nuclides are well described by the model.

In Figure 47 the current experimental relative energy spac-

ings of 3/2+ and 7/2+ states of odd proton odd mass nuclei (6-15, 117) are displayed. A parabolic pattern is also observed for iodine as noted by L. M. Beyer (15). The remainder of the data are too sketchy to be convincing.

The current experimental relative energy spacing of the 1/2+ and 7/2+ states is shown in Figure 48 (6-15,117). Again, definite conclusions cannot be drawn from the available data although the parabolic pattern persists. Also, shell effects are apparent in Figures 47 and 48 at N=82 where large energy differences are seen. These behaviors are very similar to that seen in Figure 49 which gives the energy gaps of the adjacent even-even nuclei. The similarity of the behaviors seen in these three figures may suggest the presence of significant components of core coupling in the wave functions for the 1/2+ and 3/2+ states in these nuclei.

4.2.3. Beta Decay of 11/2- Levels to 7/2+ Low-Lying Daughter States

Seven first forbidden unique beta transitions from the 11/2- isomeric state of even proton nuclei to the lowest 1/2+ states contained in Figures 46-48 have been reported (7-15) in the region of interest. The log ft values for these seven beta transitions are 7.9, 8.7, 8.9, 9.2, 9.3, 9.6, and 9.9. During the present investigation, an upper limit of 0.1% of the intensity of the 756.5-keV isomeric gamma ray in Nd^{141} was placed on the population of the 7/2+ state at 145.4 keV in Pr^{141}. This limit, however, leads to a lower limit of only *6.5 on the log ft for this transition. Similarily,

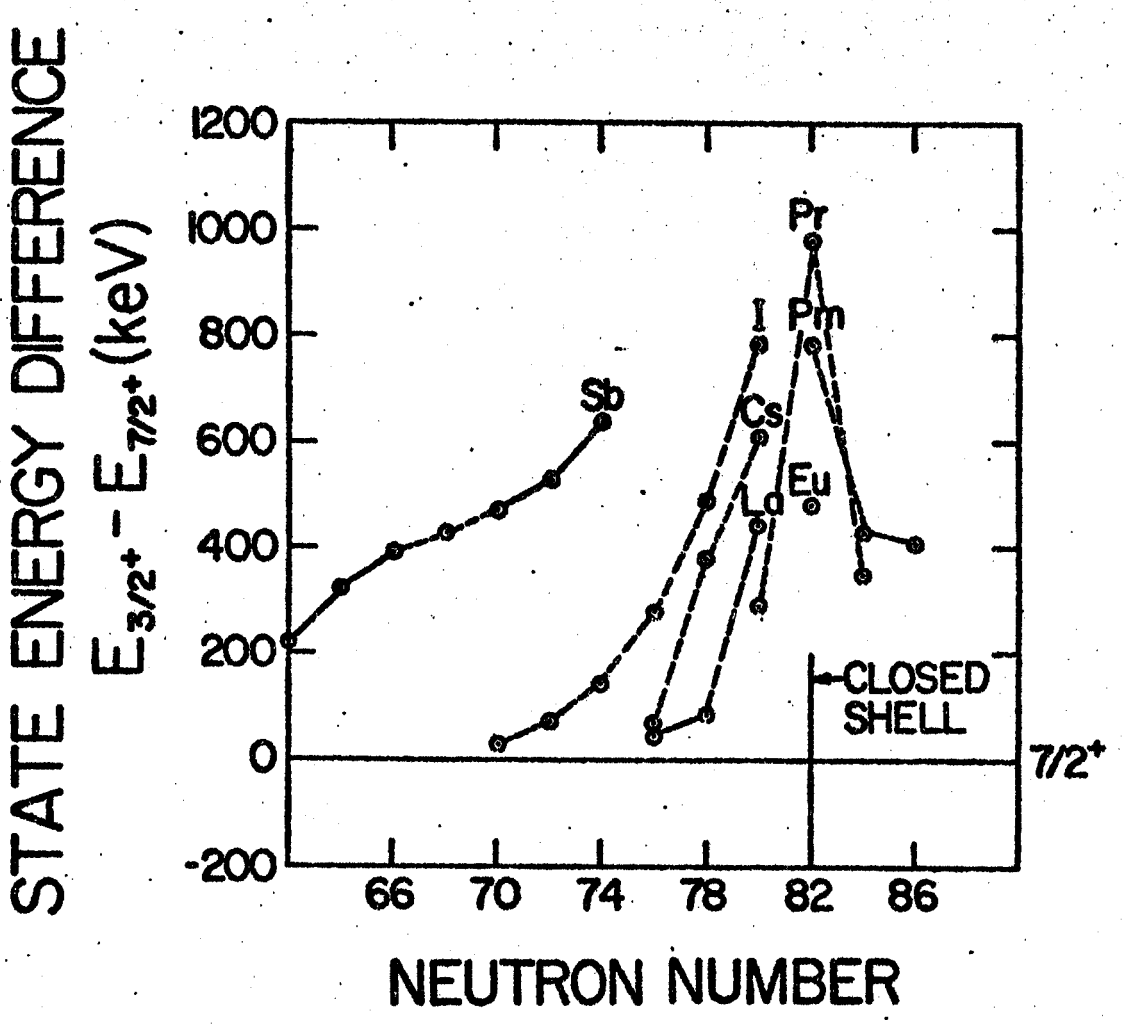

Fig. 47. Systematics of the energy level separations between low-lying $3/2^+$ and $7/2^+$ states in odd proton (odd mass) nuclei. The spin assignment of at least one of the states connected by each dashed line is tentative.

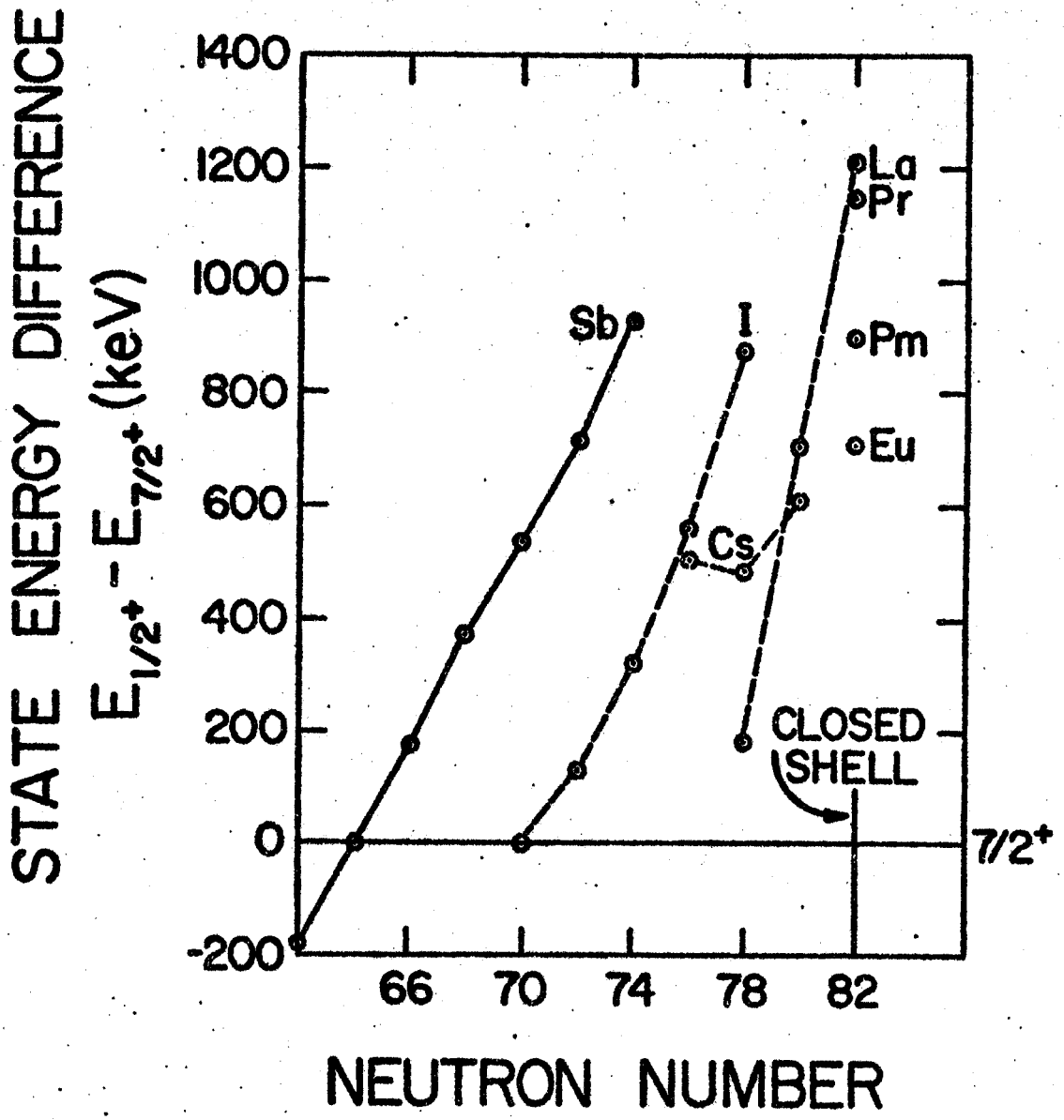

Fig. 48. Systematics of the energy level separations between low-lying $1/2^+$ and $7/2^+$ states in odd proton (odd mass) nuclei. The spin assignment of at least one of the states connected by each dashed line is tentative.

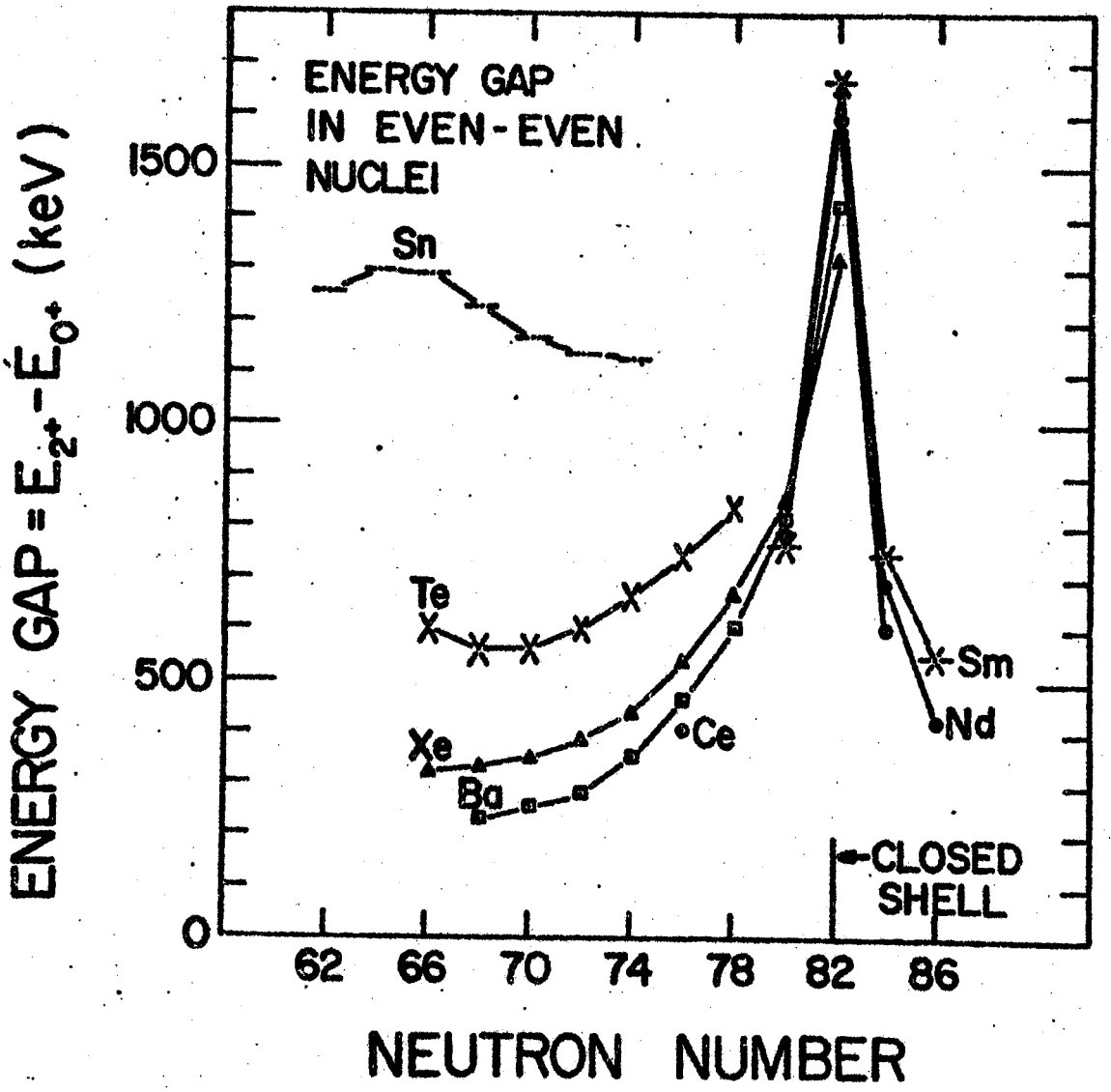

Fig. 49. Energy gaps between the lowest lying 2^+ and 0^+ states in even-even nuclei in the Z=50-62 region.

the attempts to detect direct feeding of the lowest lying 7/2+ states in the daughters were also futile in the corresponding cases for Nd^{139m}, Ce^{137m}, and Ba^{133m} decay. The range for the log *ft* values stated above (all in the 8.9±1.0 range) is consistent with the fact that the corresponding transitions were not detected in these decay schemes.

4.2.4. Characteristics of Similar 11/2- States in Odd Proton Odd Mass Nuclei

In Pr^{139}, the 40 ns delayed 11/2- state at 821.9-keV was quite important in the determination of the properties of the Nd^{139m} decay scheme as discussed in section 3.2.3.C. Table 14 lists the energies, half-lives, and *E*3 enhancement values (where available) of the nearby 11/2- states which are suggested here to be corresponding states. The effect of the *N*=82 closed shell on the energies is clearly seen but little can be said about the unusual enhancement of the *E*3 transitions (11/2- → 5/2+). The pattern of energies seen here seems to suggest that a corresponding 11/2- state may be found in Pm^{141} at circa 700 keV. As mentioned in section 4.1, the decay of Sm^{141} to Pm^{141} is presently being studied as another likely system in which three-quasiparticle states might be populated.

4.3. General Summary

Gamma ray spectroscopy has been employed to investigate the behavior of the Nd^{141m+g}, Nd^{139m+g}, Ba^{133m}, Ba^{131m}, and Ce^{137m+g} decay schemes.

Table 14. —Characteristics of similar 11/2- states in odd proton odd mass nuclei.

Nuclide	State Energy (keV)	State $t_{1/2}$ (ns)	E3 Enhancement	Reference
$_{63}Eu^{149}_{86}$	497	2400	1.4	a
$_{63}Eu^{147}_{84}$	625	710	2.1	a
$_{63}Eu^{145}_{82}$	713			b
$_{61}Pm^{143}_{82}$	962			b
$_{59}Pr^{141}_{82}$	1114			b
$_{59}Pr^{139}_{80}$	822	40	2.2	c
$_{57}La^{139}_{82}$	1420			b
$_{57}La^{137}_{80}$	1005	$\leq$0.41	$\geq$7.8	c,d

[a]Reference 85.

[b]Reference 122.

[c]Chapter III of this thesis.

[d]Reference 84.

A general overview of the apparatus and methods employed is given. A multiparameter coincidence system, used for the first time during the course of this study has been described. An outline of those aspects of nuclear decay scheme construction which could be treated in a routine way is presented. This 14-step sequence forms the basis of a useful computer program called DECAY SCHEME.

The utility of the beta, gamma method of studying properties of nuclear states has been illustrated in the present investigation which placed 56 gamma rays in decay schemes containing 22 excited states below 2200-keV in Pr^{139} alone. Six of these states were identified as three-quasiparticle states. Reaction studies are seen to be useful sources of complementary information regarding nuclear state characteristics.

Each of the odd-proton odd-mass nuclides included in the above discussion of systematics by virture of the availability of experimental data are very close to stable nuclei. As the observations described here are extended into the transition region between the spherical and deformed nuclei, two main problems are foreseen. The short half-lives of the nuclides and complexity due to numerous contaminating activities encountered will require that additional techniques be employed. Plans are underway at Michigan State to employ in-beam gamma studies in conjunction with a mass separator in order to achieve this goal.

BIBLIOGRAPHY

BIBLIOGRAPHY

1. L. S. Kisslinger and R. A. Sorensen, Rev. Mod. Phys. 35, 853 (1963).

2. B. H. Wildenthal, Phys. Rev. Lette 22, 1118 (1969).

3. A. deShalit, Phys. Rev. 122, 1530 (1961).

4. Nuclear Science Abstracts (U.S.A.E.C., Division of Technical Information).

5. Nuclear Data Sheets (The National Academy of Sciences -- National Research Council); reissued by Academic Press, 1965.

6. C. M. Lederer, J. M. Hollander, and I. Perlman, Table of Isotopes, 6th Ed., Wiley, 1966.

7. G. Berzins and W. H. Kelly, G. Graeffe, and W. B. Walters, Nucl. Phys. A104, 241 (1967).

8. G. Berzins and W. H. Kelly, Nucl. Phys. A92, 65 (1967).

9. R. L. Auble, W. H. Kelly, and H. H. Bolotin, Nucl. Phys. 58, 337 (1964).

10. R. L. Auble and W. H. Kelly, Nucl. Phys. 81, 442 (1966).

11. R. L. Auble and W. H. Kelly, Nucl. Phys. 79, 577 (1966).

12. R. L. Auble and W. H. Kelly, Nucl. Phys. 73, 25 (1965).

13. G. Berzins, L. M. Beyer, W. H. Kelly, W. B. Walters, and G. E. Gordon, Nucl. Phys. A93, 456 (1967).

14. L. M. Beyer, G. Berzins, and W. H. Kelly, Nucl. Phys. A93, 436 (1967).

15. L. M. Beyer, and W. H. Kelly, Nucl Phys. A104, 274 (1967).

16. D. B. Beery. W. H. Kelly, and Wm. C. McHarris, Phys. Rev. (to be published).

17. D. B. Beery, W. H. Kelly, and Wm. C. McHarris, (to be published).

18. This detector was manufactured by Dr. G. Berzins working with Dr. C. R. Gruhn.

19. R. L. Auble, D. B. Beery, G. Berzins, L. M. Beyer, R. C. Etherton, W. H. Kelly, and Wm. C. McHarris, Nucl. Inst. and Meth. 51, 61 (1967).

20. D. L. Bayer, private communication.

21. G. Berzins, Ph.D. Thesis, Michigan State University (1967).

22. R. L. Heath and R. J. Gehrke, IN-1218 (Dec. 1968).

23. A. H. Wapstra, G. J. Nijgh, and R. van Lieshout, Nuclear Spectroscopy Tables, North Holland Publ. Co., Amsterdam (1959).

24. Nuclear Data (edited by K. Way), A6, 1, Academic Press, New York (1969).

25. M. L. Pool and L. L. Quill, Phys. Rev. 53, 437 (1938).

26. H. L. Polak, W. Schoo, B. L. Schram, R. K. Girgis, and R. van Lieshout, Nucl. Phys. 5, 271 (1958).

27. E. W. Cybulska and L. Marquez, Nucl. Phys. 14, 117 (1959).

28. E. I. Biryukov and N. S. Shimanskaya, Izv. Akad. Nauk SSSR, ser. fiz. 27, 1402 (1963).

29. W. L. Alford, D. R. Koehler, and R. G. Polk, Nucl. Phys. 44, 439 (1963).

30. B. L. Cohen and R. E. Price, Phys. Rev. 123, 283 (1961).

31. V. A. Bukarev and V. I. Popov, Yadernaya Fiz. 1, 443 (1965).

32. D. G. Alkhazov, K. I. Erokhina, and I. Kh. Lemberg, Izv. Akad. Nauk SSSR, ser. Fiz. 29, 139 (1965).

33. D. R. Koehler and J. T. Grissom, Nucl. Phys. 84, 235 (1966).

34. G. Wilkinson and H. G. Hicks, Phys. Rev. 75, 1687 (1949).

35. R. A. James and C. D. Bingham, Phys. Rev. 117, 810 (1960).

36. K. Kotajima and H. Morinaga, Nucl. Phys. 16, 231 (1960).

37. G. R. Choppin, B. G. Harvey, and S. G. Thompson, J. Inorg. Nucl. Chem. 2, 66 (1956).

38. This 3-cm^3 detector was manufactured by Dr. R. E. Berg working with Dr. C. R. Gruhn.

39. J. B. Marion, Gamma-Ray Calibration Standards, Univ. of Maryland Technical Report 653 (1957).

40. J. S. Geiger, R. L. Graham, I. Bergstrom, and F. Brown, Nucl. Phys. 68, 352 (1965).

41. D. E. Raeside, J. J. Reidy, and M. L. Wiedenbeck, Nucl. Phys. A98, 54 (1967).

42. D. H. White and D. J. Groves, Nucl. Phys. A91, 453 (1967).

43. W. W. Black and R. L. Heath, Nucl. Phys. A90, 650 (1967).

44. G. Murray, R. L. Graham, and J. S. Geiger, Nucl. Phys. 63, 353 (1965).

45. L. Nemet, Izv. Akad. Nauk SSSR, ser. fiz. 25, 681 (1961).

46. J. S. Geiger and R. L. Graham, Can. J. Phys. 45, 2281 (1967).

47. P. F. Zweifel, Phys. Rev. 107, 329 (1957).

48. S. S. Alpert, B. Budick, E. Lipworth, and R. Marrus, Bull. Am. Phys. Soc. 7, 239 (1962).

49. P. Brix, Phys. Rev. 89, 1245 (1953); R. W. Kedzie, M. Abraham, and C. D. Jeffries, Phys. Rev. 108, 54 (1957).

50. K. P. Gopinathan, M. C. Joski, and E. A. S. Sarma, Phys. Rev. 136, B1247 (1964).

51. D. W. Martin, M. K. Brice, J. M. Cook, and S. B. Burson, Phys. Rev. 101, 182 (1955).

52. S. Ofer and A. Schwarzschild, Phys. Rev. 116, 725 (1959).

53. W. M. Curie, Nucl. Phys. 48, 561 (1963).

54. W. V. Prestwich and T. J. Kennett, Phys. Rev. 134, B485 (1964).

55. K. P. Gopinathan, Phys. Rev. 139, B1467 (1965).

56. K. Ya. Gromov, A. S. Danagulyan, L. N. Nitityuk, V. V. Murav'eva, A. A. Sorokin, M. Z. Shtal', and V. A. Shpinel', Zhur. Eksptl. i Teoret. Fiz. 47, 1644 (1964) English transl.: Soviet Phys. -- JETP 20, 1104 (1965).

57. M. L. Pool and N. L. Krisberg, Phys. Rev. 73, 1035 (1948).

58. B. J. Stover, Phys. Rev. 81, 8 (1951).

59. K. Ya. Gromov, A. S. Danagulyan, A. T. Strigachev, and V. S. Shpinel', Izv. Akad. Nauk SSSR, ser. fiz. 27, 1357 (1963).

60. J. Gilat and W. J. Tretyl, University of California Lawrence radiation Laboratory Report UCRl-17299, p. 20 (1967).

61. J. Lange, Kernforschungszentrum Karlsruhe Report KFK-519, p. 47 (1967); summarized in J. Lange, H. Munzel, and I. Leitl, Radiochimica Acta 8, 123 (1967).

62. Obtained from Allied Chemical Corp., General Chemical Div., 800 Marion Ave., River Rouge, Mich. Targets of 99.9% Pr_2O_3 obtained from K & K Laboratories, Plainview, N. Y. were also used.

63. J. D. King, N. Neff, and H. W. Taylor, Nucl. Phys. A99, 433 (1967).

64. D. de Frenne, J. Demuynck, K. Heyde, E. Jacobs, M. Dorikens, and L. Dorikens-Vanpraet, Nucl. Phys. A106, 350 (1968).

65. K. Hisatake, Y. Yoshida, K. Etoh, and T. Murata, Nucl. Phys. 56, 625 (1964).

66. R. L. Graham and J. S. Geiger, Bull. Am. Phys. Soc. 11, 11 (1966).

67. H. W. Baer, J. J. Reidy, and M. L. Wiedenbeck, Nucl. Phys. A113, 33 (1968).

68. The 59.543±0.015-keV calibration line from Am^{241} (reference 6) was included with the standards listed in Table 1 of this Chapter and those listed in Table 1 of D. B. Beery, G. Berzins, W. B. Chaffee, W. H. Kelly, and Wm. C. McHarris, Nucl. Phys. 123, 649 (1969).

69. J. H. E. Mattauch, W. Thiele, and A. H. Wapstra, Nucl. Phys. 67, 1, 32, and 73 (1965).

70. K. Gromov, V. Kalinnikov, V. Kuznetsov, N. Lebedev, G. Musiol, E. Herrmann, Zh. Shelev, B. Dzhelepov, and A. Kudryavtseva, Nucl. Phys. 73, 65 (1965).

71. L. A. Sliv and I. M. Band, in Alpha-, Beta- and Gamma-Ray Spectroscopy, ed. by K. Siegbahn (North-Holland Publ. Co., Amsterdam, 1965).

72. R. E. Eppley, Wm. C. McHarris, D. B. Beery, and W. H. Kelly, "the New Isomer Gd^{145m} and the N=81 $M4$ Transition Probabilities", to be published.

73. W. B. Walters, C. E. Bemis, and G. E. Gordon, Phys. Rev. 140, B268 (1965).

74. J. M. Ferguson, D. L. Love, and D. Sam, J. Inorg. Nucl. Chem. 24, 1 (1962).

75. S. Morinobu, T. Hirose, and K. Hisatake, Nucl. Phys. 61, 613 (1965).

76. R. B. Frankel, Ph.D. Thesis, Univ. of Calif., Berkeley, Lawrence Radiation Laboratory Report UCRL-11871 (1964).

77. R. Todd, R. E. Eppley, D. B. Beery, W. H. Kelly, and Wm. C. McHarris, in progress.

78. S. A. Moszkowski, in Alpha-, Beta-, and Gamma-Ray Spectroscopy, ed. by K. Siegbahn (North-Holland Publ. Co., Amsterdam, 1965).

79. S. A. Moszkowski, Phys. Rev. 89, 474 (1953).

80. R. E. Doebler, Wm. C. McHarris, and C. R. Gruhn, Nucl. Phys. A120, 489 (1968).

81. L. S. Kisslinger and R. A. Sorensen, Dan. Mat.-fys. Medd. 32, No. 9 (1960).

82. A. A. Sorokin, Zh. Eksperim. i Teor. Fiz. 47, 1232 (1964).

83. C. F. Perdrisat, Rev. Mod. Phys. 38, 41 (1966).

84. J. R. Van Hise, G. Chilosi, and N. J. Stone, Phys. Rev. 161, 1254 (1967).

85. E. Yu. Berlovich, V. N. Klementyev, L. V. Krasnov, M. K. Kikitin, and I. Yurski, Nucl. Phys. 23, 481 (1961).

86. C. E. Gleit, C.-W. Tang, and D. C. Coryell, Nuclear Data Sheets, NAS-NRC, 5-5-109 (1963).

87. P. R. Gregory, L. Schellenberg, Z. Sujkowski, and M. W. Johns, Can. J. Phys. 46, 2797 (1968); K. P. Gopinathan, Phys. Rev. 139, B1467 (1965).

88. B. H. Wildenthal, R. L. Auble, E. Newman, and J. A. Nolen. Bull. Am. Phys. Soc. 13, 1430 (1968).

89. H. W. Baer and J. Bardwick, Bull. Am. Phys. Soc. 13, 1430 (1968).

90. P. van der Merwe, I. J. van Heerden, W. R. McMurray, and J. G. Malan, Nucl. Phys. A124, 433 (1969).

91. L. B. Haller and B. Jung, Nucl. Phys. 52, 524 (1964).

92. S. Thulin, Ark. Fys. 9, 137 (1955).

93. M. Gmitro, J. Hendekovic, and J. Sawicki, Phys. Rev. 169, 983 (1968).

94. Wm. C. McHarris, F. S. Stephens, F. Asaro, and I. Perlman, Phys. Rev. 144, 1031 (1966).

95. D. P. Donnelly, J. J. Reidy, and M. L. Wiedenbeck, Phys. Rev. 173, 1192 (1968).

96. J. E. Thun, S. Tornkvist, F. Falk, and H. Snellman, Nucl. Phys. 67, 625 (1965).

97. H. E. Bosch, A. J. Haverfield, E. Szichman, and S. M. Abecasis, Nucl. Phys. A108, 209 (1968).

98. R. D. Hill, F. R. Metzger, Phys. Rev. 83, 455 (1953).

99. F. C. Yu and J. D. Kurbatov, Phys. Rev. 74, 34 (1948).

100. D. J. Horen, W. H. Kelly, and L. Yaffe, Phys. Rev. 129, 1712 (1963).

101. H. K. Carter, J. H. Hamilton, and J. J. Pinajian, Nucl. Phys. A115, 417 (1968).

102. J. S. Geiger, R. L. Graham, and F. Brown, Can. J. Phys. 40, 1258 (1968).

103. J. F. Wild and W. B. Walters, Nucl. Phys. A103, 601 (1967).

104. V. R. Dave, R. M. Wilenzick, and J. A. Nelson, Bull. Am. Phys. Soc. 14, 56 (1969). Private communication with the authors.

105. W. H. Kelly and D. J. Horen, Nucl. Phys. 47, 454 (1963).

106. T. Hirose and K. Histake, J. Phys. Soc. Japan 19, 1542 (1964).

107. K. Karlsson, Arkiv. Fysik 33, 47 (1966).

108. D. J. Horen, J. M. Hollander, and R. L. Graham, Phys. Rev. 135, 302 (1964).

109. A. E. Norris, G. Friedlander, and E. M. Franz, Nucl. Phys. 86, 102 (1966).

110. R. S. Tilbury and L. Yaffe, Phys. Rev. 129, 1709 (1963).

111. L. S. Kisslinger, Nucl. Phys. 78, 341 (1966).

112. N. J. Stone, R. B. Frankel, and D. A. Shirley, Phys. Rev. 172, 1243 (1968).

113. K. Kumar and M. Baranger, Phys. Rev. Lett. 12, 73 (1964).

114. W. G. Winn and D. D. Clark, NYO-3664-5, (1967).

115. Wm. C. McHarris, D. B. Beery, and W. H. Kelly, Phys. Rev. Lett. 22, 1191 (1969).

116. H. Leutz and K. Ziegler, Nucl. Phys. 50, 648 (1964).

117. M. Conjeaud, S. Harar, and Y. Cassagnou, Nucl. Phys. A117, 449 (1968).

118. K. Hesse and K. Wien, Z. Naturf. 22a, 1642 (1967).

119. K. Hesse, Z. Naturf. 23a, 1668 (1968).

120. L. S. Kisslinger and R. A. Sorensen, private communication referred to in reference 121.

121. E. Ye. Berlovich and G. M. Bukat, Izv. Akad. Nauk SSSR 28, 214 (1964).